

RICE UNIVERSITY

**Stability Analysis of a Phase Plane Control System**

By

**Michael Plummer**

A Thesis Submitted

in Partial Fulfillment of the

Requirements for the Degree

Master of Science

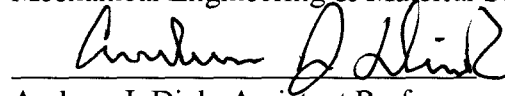
Approved, Thesis Committee:



Pol D. Spanos, Professor, L.B. Ryon  
Endowed Chair in Engineering  
Mechanical Engineering & Materials Science



Andrew J. Meade, Professor  
Mechanical Engineering & Material Science



Andrew J. Dick, Assistant Professor  
Mechanical Engineering & Materials Science



Jiann-Woei Jang, Technical Supervisor  
The Charles Stark Draper Laboratory

Houston, Texas

April, 2009

UMI Number: 1472737

All rights reserved

INFORMATION TO ALL USERS

The quality of this reproduction is dependent upon the quality of the copy submitted.

In the unlikely event that the author did not send a complete manuscript and there are missing pages, these will be noted. Also, if material had to be removed, a note will indicate the deletion.



UMI 1472737

Copyright 2010 by ProQuest LLC.

All rights reserved. This edition of the work is protected against unauthorized copying under Title 17, United States Code.



ProQuest LLC  
789 East Eisenhower Parkway  
P.O. Box 1346  
Ann Arbor, MI 48106-1346

The views expressed in this thesis are those of the author and do not reflect the official policy or position of the United States Air Force, Department of Defense, or the U.S. Government.

(this page intentionally left blank)

## Abstract

### Stability Analysis of a Phase Plane Control System

by

Michael Plummer

Many aerospace attitude control systems utilize a phase plane control scheme which includes nonlinear elements such as dead zone and ideal relay. Nonlinear control techniques such as pulse width modulation (PWM), describing functions, and absolute stability are implemented to determine stability. To evaluate phase plane control robustness, stability margin prediction methods must be developed. While PWM has been used to predict stability margins, in this research, describing functions and absolute stability are extended to predict stability margins. Time domain simulations demonstrate all techniques yield conservative gain margin results. A constrained optimization approach is also used to design flex filters for roll control. The design goal is to optimize vehicle tracking performance while maintaining adequate stability margins. Two filters are designed in this thesis; one meets PWM stability margin specifications and the other holds for Popov stability.

(this page intentionally left blank)

## Acknowledgments

I want to acknowledge and thank several individuals for supporting my research and thesis-writing efforts throughout my stay in Houston. My parents and sister have always provided endless encouragement and unceasing support. Next, I would like to thank Jimmy for patiently providing research advice, helping me present my ideas, and carefully helping me to understand dynamics and controls concepts. I must extend thanks to all my fellow Draper students who assisted me in valuable courses, difficult projects, and turbulent times. Furthermore, I owe a huge figurative debt to Dr. Spanos who kept me focused on applying academic rigor to my research issues.

## Acknowledgement

April 2009

This thesis was prepared at The Charles Stark Draper Laboratory, Inc., under NASA contract NNJ06HC37C.

Publication of this thesis does not constitute approval by Draper or the sponsoring agency of the findings or conclusions contained herein. It is published for the exchange and stimulation of ideas.

A handwritten signature in cursive script, reading "Michael Plummer".

---

(author's signature)



## Assignment

Draper Laboratory Report Number T-1635

In consideration for the research opportunity and permission to prepare my thesis by and at The Charles Stark Draper Laboratory, Inc., I hereby assign my copyright of the thesis to The Charles Stark Draper Laboratory, Inc., Cambridge, Massachusetts.

Michael Mummer

(author's signature)

13 April 2009

(date)

# Contents

<b>Acknowledgments .....</b>	<b>vi</b>
<b>List of Figures.....</b>	<b>xiii</b>
<b>List of Tables .....</b>	<b>xvii</b>
<b>List of Variables and Abbreviations .....</b>	<b>xviii</b>
<b>Chapter 1: Introduction.....</b>	<b>1</b>
1.1 Problem Motivation .....	1
1.2 Thesis Objective.....	2
1.3 Scope .....	2
1.3.1 Frozen-Time Solution.....	2
1.3.2 Roll Control Only .....	3
1.3.3 Aerodynamics Ignored .....	3
1.4 Thesis Outline .....	3
<b>Chapter 2: Spacecraft Attitude Dynamics and Control .....</b>	<b>5</b>
2.3 Spacecraft Dynamics.....	7
2.4 The Phase Plane Controller .....	7
2.4.1 Phase Plane Controller Model .....	8
2.4.2 Equivalent PD Controller.....	9
2.5 Conclusions.....	12
<b>Chapter 3: Limit Cycle Prediction.....</b>	<b>14</b>
3.1 Pulse Width Modulation (PWM) Approximation .....	14
3.1.1 PWM Discrete-Time .....	15
3.1.2 System On-Time Calculation .....	16
3.1.3 Dead Zone Scaling.....	17
3.1.4 PWM versus PWPF.....	18
3.2 Describing Functions .....	19
based on the Nyquist criterion. ....	19
3.2.1 Describing Function Theory .....	19
3.2.2 Derivation of an Odd Describing Function in General Form .....	20
3.2.3 Dead Zone Describing Function Derivation .....	22
3.2.4 Two Nonlinear Elements in Series .....	24
3.2.5 Nichols-Based Limit Cycle Prediction.....	26
3.2.6 Gain and Phase Margin Tester .....	27

3.3 PWM and Describing Function Conclusions.....	31
<b>Chapter 4: Absolute Stability .....</b>	<b>33</b>
4.1 Lur'e Problem and Background.....	33
4.2 Circle Criterion.....	35
4.3 Popov Criterion.....	39
4.4 The Siljak Transformation .....	42
4.4.1 Siljak Transformation Theory.....	42
4.5 Kharitonov's Theorem .....	48
4.6 Stability Margin Prediction .....	52
4.7 Absolute Stability Conclusions .....	55
<b>Chapter 5: Application to a Phase Plane Control System .....</b>	<b>56</b>
5.1 Flex Filter .....	56
5.2 PWM Results .....	57
5.2.1 PWM Linear Approximation .....	58
5.2.2 Nichols Chart Results .....	58
5.2.3 Flex Dynamics Results .....	60
5.3 Describing Function Results .....	61
5.3.1 Nichols-Based Intersection Analysis .....	61
5.3.2 Gain Margin Tester .....	63
5.4 Absolute Stability Results.....	65
5.4.1 Sector Requirements .....	66
5.4.2 $k_\delta$ Optimization .....	67
5.4.3 Circle Criterion and Popov Criterion Results .....	72
5.4.4 Finite Domain of Absolute Stability Determination.....	74
5.4.5 Kharitonov Theorem Results .....	76
5.5 Time Domain Simulation.....	79
5.6 Method Comparison .....	83
5.7 Analysis Conclusions .....	84
<b>Chapter 6: Filter Design for a Phase Plane Control System .....</b>	<b>85</b>
6.1 Flex Filter Optimization .....	85
6.2 PWM-Based Flex Filter .....	87
6.3 Absolute Stability-Based Flex Filter.....	91
6.3.1 Optimizing $k_\delta$ for the New Filter .....	93

6.3.2	Stability Confirmation .....	95
6.4	<i>Performance-Measuring Time Simulation</i> .....	97
6.4.1	The Monte Carlo Method .....	98
6.4.2	Random Initial Condition Generation .....	98
6.4.3	Performance Results.....	100
6.5	<i>Performance Conclusions</i> .....	105
<b>Chapter 7:</b>	<b>Closure .....</b>	<b>106</b>
<b>Bibliography</b>	<b>.....</b>	<b>110</b>

## List of Figures

Figure 2.1: Dynamics and Control Block Diagram .....	7
Figure 2.2: The Phase Plane Controller .....	9
Figure 2.3: PD-Equivalent Phase Plane Development .....	10
Figure 2.4: Sloped Portion of the Phase Plane.....	11
Figure 3.1: Phase Plane Controlled System with PWM .....	14
Figure 3.2: Discrete PWM-Actuated System.....	15
Figure 3.3: PWM System Model .....	17
Figure 3.4: Phase Plane Control System with Describing Function.....	19
Figure 3.5: Describing Function Form.....	20
Figure 3.6: Dead Zone Nonlinearity Input vs. Output.....	22
Figure 3.7: Two Nonlinear Elements in Series .....	24
Figure 3.8: Predicting Limit Cycling Through Intersections.....	27
Figure 3.9: Gain/Phase Margin Tester Block Diagram .....	28
Figure 3.10: Gain Margin Test Results.....	30
Figure 3.11: Phase Margin Test Results .....	31
Figure 4.1: Lur'e Problem System Model .....	33
Figure 4.2: Input/Output Sector Bounds.....	34
Figure 4.3: Circle Criterion (Case 1) Example .....	36

Figure 4.4: Circle Criterion (Case 2) Example .....	37
Figure 4.5: Circle Criterion (Case 3) Example .....	38
Figure 4.6: Popov Criterion Example .....	41
Figure 4.7: Loop Transformation.....	42
Figure 4.8: Siljak Transformed Input/Output .....	44
Figure 4.9: Linear $k_\delta$ Analysis.....	45
Figure 4.10: Pitch Control Transformed Nonlinearity.....	46
Figure 4.11: Time Domain Simulation for Pitch Example ( $\sigma = 5.0$ ) .....	47
Figure 4.12: Time Domain Simulation for Pitch Example ( $\sigma > 5.0$ ) .....	47
Figure 5.1: Current Flex Filter .....	57
Figure 5.2: PWM Nichols Chart .....	59
Figure 5.3: PWM SVD Plot .....	60
Figure 5.4: Describing Function Nichols Chart .....	62
Figure 5.5: Describing Function Margin Tester Results.....	64
Figure 5.6: Nonlinear Element with Sector Requirements .....	66
Figure 5.7: $k_\delta$ versus Maximum Real Eigenvalues .....	68
Figure 5.8: Siljak Transformed Input/Output Chart .....	69
Figure 5.9: Circle Criterion $k_\delta$ Graphical Optimization.....	70
Figure 5.10: Popov Criterion $k_\delta$ Graphical Optimization .....	70

Figure 5.11: Circle Criterion Plot Results.....	72
Figure 5.12: Popov Criterion Plot Results .....	73
Figure 5.13: Linear $k_\delta$ Analysis.....	74
Figure 5.14: Input/Output Plot for Finite Domain Determination.....	75
Figure 5.15: Time Domain Test for Finite Domain of Absolute Stability.....	75
Figure 5.16: Kharitonov Circle Criterion Plot .....	77
Figure 5.17: Kharitonov Popov Criterion Plot.....	78
Figure 5.18: SIMULINK Model .....	79
Figure 5.19: Gain vs. Energy (t = 120 sec) .....	81
Figure 5.20: Phase Plane Plots with Gain Added (t = 120 sec) .....	82
Figure 6.1: Unfiltered SVD Flex Response .....	86
Figure 6.2: Optimization Criteria (PWM Filter).....	88
Figure 6.3: PWM Optimized Flex Filter .....	88
Figure 6.4: PWM Nichols Chart (PWM Filter) .....	89
Figure 6.5: Filtered SVD Response (PWM Filter) .....	90
Figure 6.6: Optimization Criteria (Absolute Stability Filter) .....	92
Figure 6.7: Absolute Stability Optimized Flex Filter .....	93
Figure 6.8: Circle Criterion $k_\delta$ Graphical Optimization (Absolute Stability Filter).....	94
Figure 6.9: Popov Criterion $k_\delta$ Graphical Optimization (Absolute Stability Filter) .....	94

Figure 6.10: Popov Criterion (Absolute Stability Filter) .....	96
Figure 6.11: Filtered SVD Response (Absolute Stability Filter) .....	97
Figure 6.12: Uniformly Distributed Initial Attitude Error .....	99
Figure 6.13: Uniformly Distributed Initial Rate Error .....	100
Figure 6.14: Maximum Attitude Distribution (Current Filter) .....	101
Figure 6.15: Maximum Attitude Distribution (PWM Filter) .....	101
Figure 6.16: Maximum Attitude Distribution (Absolute Stability Filter) .....	102
Figure 6.17: Number of On-Times Distribution (Current Filter) .....	103
Figure 6.18: Number of On-Times Distribution (PWM Filter) .....	103
Figure 6.19: Number of On-Times Distribution (Absolute Stability Filter) .....	104



## List of Tables

Table 5.1: PWM Results .....	59
Table 5.2: Describing Function Nichols Chart Results .....	63
Table 5.3: Describing Function Margin Tester .....	65
Table 5.4: $k_\delta$ Graphical Optimization .....	71
Table 5.5: Absolute Stability Gain Margin Comparison .....	73
Table 5.6: Simulation Results .....	83
Table 5.7: Gain Margin Comparison [dB] .....	83
Table 6.1: Gain Margin Results (PWM Filter) .....	90
Table 6.2: $k_\delta$ Graphical Optimization (Absolute Stability Filter) .....	95
Table 6.3: Gain Margin Results (Absolute Stability Filter) .....	96
Table 6.4: Statistical Performance Comparison .....	104

## List of Variables and Abbreviations

Symbol	Definition
$A$	<i>Generic Amplitude</i>
$\Lambda$	<i>Diagonal Eigenvalue Matrix</i>
$(a, b)$	<i>Lower and Upper Limit, Uniform Distribution</i>
$\alpha$	<i>Lower Sector Bound</i>
$B_{RCS}$	<i>Thrust Direction Mapping Matrix</i>
$\beta$	<i>Upper Sector Bound</i>
$\beta_{min}$	<i>Required Upper Sector Limit</i>
$\delta$	<i>Dead Zone Width</i>
$\Delta h_c$	<i>Desired Momentum</i>
$\Delta t$	<i>Time Step</i>
$e(t)$	<i>Error Signal</i>
$\eta$	<i>Flex Displacement</i>
$f_{Rk}$	<i>Force Vector from Roll Thrust <math>k</math></i>
$G(s)$	<i>Open Loop Transfer Function</i>
$G_{tr}(s)$	<i>Siljak Transformed Open Loop Transfer Function</i>
$G_{xR}$	<i>Roll Torque about Centerline Due to All Thrusters</i>
$I_{xx}$	<i>Inertia</i>
$K$	<i>Generic Gain</i>
$k_\delta$	<i>Siljak Transformation Gain</i>
$k_D$	<i>Derivative Gain</i>
$k_P$	<i>Proportional Gain</i>

$\mu_{RKi}$	<i>Displacement Vector of the <math>i^{th}</math> Mode at Thrust <math>k</math></i>
$n$	<i>Uniform Random Variable <math>c</math> (0, 1)</i>
$N(A)$	<i>Describing Function</i>
$\sigma_{max}$	<i>Limit to Finite Domain of Absolute Stability</i>
$\Omega$	<i>Diagonal Matrix of Flex Frequencies</i>
$\omega_c$	<i>Crossover Frequency [rad/sec]</i>
$\omega_{RL}$	<i>Rate Limit</i>
$\omega_{RGA}$	<i>Sensed Rate at Rate Gyro Assembly</i>
$\Phi_\beta$	<i>Mode Shapes at Jet Locations</i>
$\Phi_\gamma$	<i>Mode Shapes in Roll at Output Node</i>
$\phi$	<i>Roll Attitude</i>
$\psi(t)$	<i>Nonlinear Element Output</i>
$\psi_{tr}(t)$	<i>Siljak Transformed Nonlinear Element Output</i>
$PD$	<i>Proportional-Derivative Control</i>
$PWM$	<i>Pulse Width Modulation</i>
$PWPF$	<i>Pulse-Width-Pulse-Frequency</i>
$RCS$	<i>Reaction Control System</i>
$r(t)$	<i>Reference Signal</i>
$\rho_{\phi i}$	<i>Rotation of the <math>i^{th}</math> Mode at the Rate Gyro</i>
$\sigma(t)$	<i>Nonlinear Element Input</i>
$T_{jets}$	<i>Jet Select Mapping Matrix</i>
$t_c$	<i>Control Cycle Time</i>
$t_{PW}$	<i>Pulse Width On-Time</i>
$\tau_c$	<i>Desired Torque</i>

$\tau_{jets}$	<i>Activated Torque</i>
$\theta$	<i>Generic Phase</i>
$u$	<i>Uniform Random Variable <math>\epsilon</math> (a, b)</i>
$u_R$	<i>Roll Command (0,1,-1)</i>
$V$	<i>Vandermonde Matrix</i>
$Z$	<i>Diagonal Matrix of Modal Damping Ratios</i>

(this page intentionally left blank)

## Chapter 1: Introduction

The objective of this thesis is to explore various analytical techniques for evaluating nonlinear controller stability and performance such as a phase plane controller developed for an aerospace system. Linearization and quasi-linearization methods such as pulse width modulation (PWM) and describing functions are reviewed as well as Lyapunov-based absolute stability techniques including the circle criterion and the Popov criterion. Stability margin techniques are reviewed for PWM and describing functions and developed for absolute stability. A constrained minimization approach is applied to design optimized flex filters. The design goal is to maximize bandwidth in order to optimize system performance while ensuring robust system stability margins.

### 1.1 Problem Motivation

The nonlinear phase plane controller , “an idealized method of treating performance optimization for classes of minimum time and/or minimum fuel problems,” has been used in aerospace systems such as the Space Shuttle and the ISS for years [1] [2]. Few techniques are currently available to evaluate nonlinear control systems such as the phase plane controller. In the past, describing functions have been implemented to linearly approximate the phase plane controller’s nonlinearities, but this process only predicted instabilities and did not provide stability margins [1] [2]. Additional nonlinear control techniques such as PWM and absolute stability have also been applied to aerospace systems to determine stability. PWM has been used for ISS attitude control and stability margin predictions while absolute stability was utilized in a concept for stabilizing the Saturn V pitch control system [3] [4] [5]. Similar to describing functions,

absolute stability has not been applied to a phase plane controlled system for the purpose of determining stability margins.

## **1.2 Thesis Objective**

There is a need for a nonlinear control technique comparison with regards to a phase plane controller. The techniques need to be compared not only to each other but also to time domain simulations. Aspects such as accuracy and conservatism must be weighed and considered throughout the analytical process. The primary goal of this thesis is to review nonlinear control techniques, establish stability margin tests for the techniques that do not currently possess stability margins, and use the knowledge gained to design performance-optimized flex filters with guaranteed asymptotic stability.

## **1.3 Scope**

This thesis seeks to provide a review and analysis of nonlinear techniques that can be applied to a phase plane controller to determine stability margins. To this end it is advantageous to limit the number of simplifications and assumptions; on the other hand, in order to concisely compare these analytical techniques, it is necessary to implement several simplifications and assumptions that limit the scope of this thesis.

### **1.3.1 Frozen-Time Solution**

All the analytical methods that will be discussed in this thesis (PWM, describing functions, the circle criterion, the Popov criterion, Kharitonov's theorem) are all frozen time techniques; therefore, all analysis for these techniques will take place in frozen time format. Frozen time analysis has proven to be effective in launch vehicles with slowly

varying parameters such as the Saturn V [6]. Because of this fact, frozen time only frozen time models will be considered in this thesis.

### **1.3.2 Roll Control Only**

Aerospace attitude control systems often consist of both gimbal control and fixed jet control where the former is used for pitch and yaw control while the latter is utilized for roll control. Pitch and yaw axes have both been thoroughly explored in previous work, so this thesis will only examine the roll axis [7].

### **1.3.3 Aerodynamics Ignored**

This thesis operates under the assumption that there will be no aerodynamic forces exerted on the system structure in the roll axis. This assumption simplifies the rigid and flex dynamics without losing very much fidelity in most aerospace systems.

## **1.4 Thesis Outline**

Subsequent to the introductory chapter, this thesis is organized as follows:

Chapter 2 discusses roll dynamics and the phase plane control system. Both the rigid dynamics and the flex dynamics are fully explored and adapted to the system. Once the dynamics have been established, a description of the phase plane controller follows.

Chapter 3 details two methods for approximating the nonlinear behavior of a phase plane controller. The first method that will be considered is PWM which involves discretization of the linear system and linear approximation of the nonlinear system by dead zone scaling. The second method outlined in Chapter 3 involves describing functions which are quasi-linearization tools that approximate nonlinear elements with



equivalent gains. Once applied, both PWM and describing functions allow for linear design methods such as Nichols and Bode to be used in system analysis.

Chapter 4 provides a background into classical absolute stability including the circle criterion and the Popov criterion, presents D. D. Siljak's method for transforming non-Hurwitz systems so that absolute stability can be applied, and concludes by discussing the Kharitonov theorem's implications for robust, absolute stability. Additionally, a technique is developed for the circle criterion and the Popov criterion for predicting gain margins.

Chapter 5 applies the techniques discussed in Chapter 3 and Chapter 4 to roll stability; furthermore, time domain simulations are accomplished in order to verify the validity of the above mentioned analytical techniques.

Chapter 6 builds on the knowledge gained in Chapter 5 and designs new flex filters optimized for performance while utilizing PWM and absolute stability as stability design constraints. The optimized filter is then compared to the current filter based on performance-measuring simulations.

Chapter 7 summarizes the findings and draws conclusions from the results of Chapter 5 and Chapter 6. The chapter also cites new developments in the nonlinear control field and suggests directions for future research.

## Chapter 2: Spacecraft Attitude Dynamics and Control

This chapter begins by discussing the spacecraft attitude dynamics which include both rigid and flex subsystems. After it is shown how the plant combines these two subsystems, the chapter will move on to the phase plane controller which will be used to stabilize the control system in the roll axis.

### 2.1 Governing Equations

The dynamics equations can be split into two subsets: rigid and flex. The equation for rigid dynamics can be seen in Equation 2.1 [8]:

$$I_{xx}\ddot{\phi} = G_{xR} \quad (2.1)$$

In Equation 2.1,  $G_{xR}$  is the torque about the centerline due to all thrusters while  $I_{xx}$  is the inertia. In order to use this equation for analysis, it is desirable to convert the equation into state-space form which can be seen in Equation 2.2:

$$\begin{bmatrix} \dot{\phi}(t) \\ \ddot{\phi}(t) \end{bmatrix} = \begin{bmatrix} 0 & 1 \\ 0 & 0 \end{bmatrix} \begin{bmatrix} \phi(t) \\ \dot{\phi}(t) \end{bmatrix} + \begin{bmatrix} 0 \\ \frac{G_{xR}}{I_{xx}} \end{bmatrix} u(t) \quad (2.2)$$

Because only rate is desired in the output, the output equation is defined as such:

$$y_1(t) = \begin{bmatrix} 0 & 1 \end{bmatrix} \begin{bmatrix} \phi(t) \\ \dot{\phi}(t) \end{bmatrix} \quad (2.3)$$

The flex dynamics equation for the can be derived from the following dynamics equations [8]:

$$(s^2 + 2\zeta_{\beta i}\omega_{\beta i}s + \omega_{\beta i}^2)\eta_{\beta i} = u_R \sum_k^{\text{thrusters}} f_{Rk}^T \mu_{Rki} \quad (2.4)$$

In Equation 2.4,  $\zeta_{\beta i}$  is the damping ratio of the  $i^{th}$  mode,  $\omega_{\beta i}$  is the flex frequency of the  $i^{th}$  mode,  $\eta_{\beta i}$  is the flex displacement of the  $i^{th}$  mode,  $u_R$  is the roll command (0,1,-1),  $f_{Rk}^T$  is the force vector from roll thrust  $k$ , and  $\mu_{Rki}$  is the displacement vector of the  $i^{th}$  mode at thrust  $k$  [8]. The state-space representation for the flex system can be seen in Figures 2.14 and 2.15 [8]:

$$\begin{bmatrix} \dot{\eta}(t) \\ \ddot{\eta}(t) \end{bmatrix} = \begin{bmatrix} 0 & I \\ -\Omega_\beta^2 & -2Z_\beta\Omega_\beta \end{bmatrix} \begin{bmatrix} \eta(t) \\ \dot{\eta}(t) \end{bmatrix} + \begin{bmatrix} 0 \\ \Phi_\beta^T B_{RCS} T_{jets} \end{bmatrix} u(t) \quad (2.5)$$

$$y_2(t) = [0 \quad \Phi_\gamma] \begin{bmatrix} \eta(t) \\ \dot{\eta}(t) \end{bmatrix} \quad (2.6)$$

In Equation 2.5,  $\Omega_\beta$  is a diagonal matrix of flex frequencies,  $Z_\beta$  is a diagonal matrix of damping ratios,  $\Phi_\beta^T$  is the mode shapes at jet locations,  $B_{RCS}$  is the thrust direction mapping matrix,  $T_{jets}$  is the jet select mapping matrix, and  $\Phi_\gamma$  is the mode shape at the output node. The final governing equation that will be discussed in this section is the sensor output equation which reflects how the flex dynamics affect the readings to which the controller responds [8].

$$\omega_{RGA} = \dot{\phi} + \sum_i^{flex} \rho_{\phi i} \eta_i s \quad (2.7)$$

In Equation 2.7,  $\omega_{RGA}$  is the sensed rate at the rate gyro assembly and  $\rho_{\phi i}$  is the rotation of the  $i^{th}$  mode at the rate gyro. Because the high-frequency flex dynamics possess the ability to make the system unstable, it is critical that a low pass filter be employed to attenuate high-frequency flex modes.

## 2.3 Spacecraft Dynamics

The rigid and bending plant dynamics are integrated with the flex filter and phase plane controller to create the roll dynamics and control system. The block diagram in Figure 2.1 outlines the dynamics and control components:



Figure 2.1: Dynamics and Control Block Diagram

The flex filter block includes a low-pass filter to attenuate high-frequency noise while at the same time allowing low-frequency dynamics to feedback into the controller. A phase plane control system regulates attitude tracking and performance. The phase plane controller is an inherently nonlinear system which necessitates the requirement for nonlinear techniques in order to predict the system's behavior.

## 2.4 The Phase Plane Controller

The phase plane controller is “an idealized method of treating performance optimization for classes of minimum time and/or minimum fuel problems” [1]. The phase plane controller offers a unique method for attitude control. In this section the ideal phase plane controller will first be explained. After the phase plane controller's behavior has been outlined, a method for creating an equivalent PD controller combined with a nonlinear element comprised of a dead zone and an ideal relay will be explored.

### 2.4.1 Phase Plane Controller Model

First, the concept behind an ideal phase plane controller will be explained. A phase plane controller responds to the vehicle dynamics in the plane defined by state errors and state rate errors. The trajectories in the phase plane can be described through Equations 2.8 and 2.9 [9].

$$\phi_2 = \phi_1 + \omega \Delta t \quad (2.8)$$

$$\dot{\phi}_2 = \dot{\phi}_1 + \alpha \Delta t \quad (2.9)$$

In the expressions above  $\omega$  is angular velocity,  $\alpha$  is angular acceleration, and  $\Delta t$  is the thruster firing time for the phase plane controller. Figure 2.2 demonstrates exactly how trajectories in the phase plane operate. For example, consider the starting point in Figure 2.2. The system applies a continuous torque until it enters the drift channel. At this point, the thrusters discontinue their firing and the system's attitude continues to increase because the system is in the upper half of the phase plane which means it has a positive rate. The rate is constant as long as there is no firing because the system cannot accelerate. Once the system crosses the negative switch line into the negative firing region, the system undergoes a negative acceleration which places the system back into the non-firing region; however, the system's attitude will continue to move towards the negative firing region until the system has been driven into the lower half of the phase plane. Once there, the system's attitude will decrease in the non-firing region until it crosses the positive switch line at which point a positive firing will occur [1].

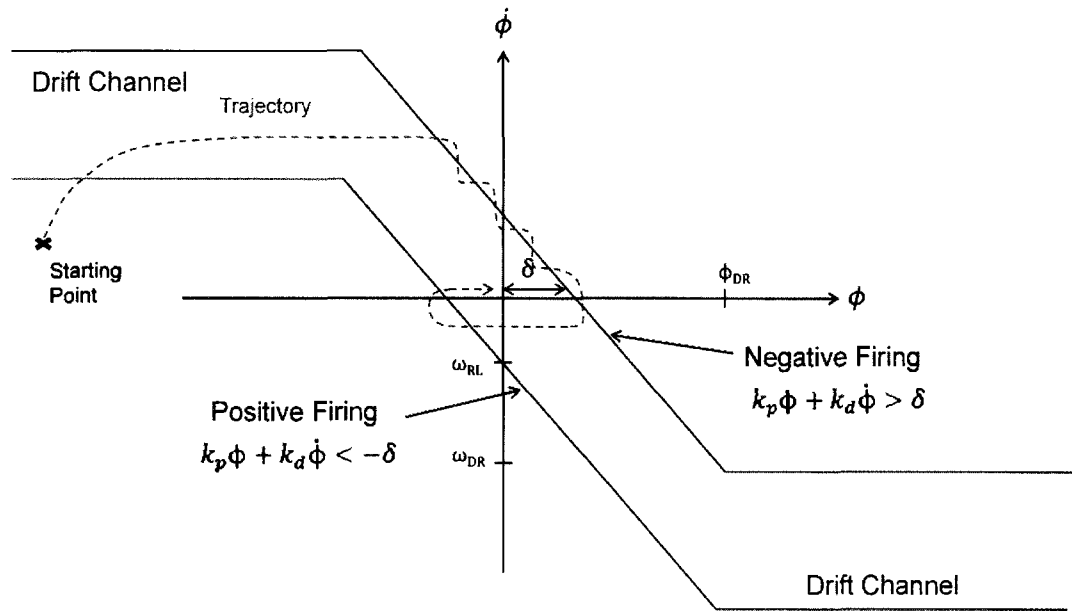
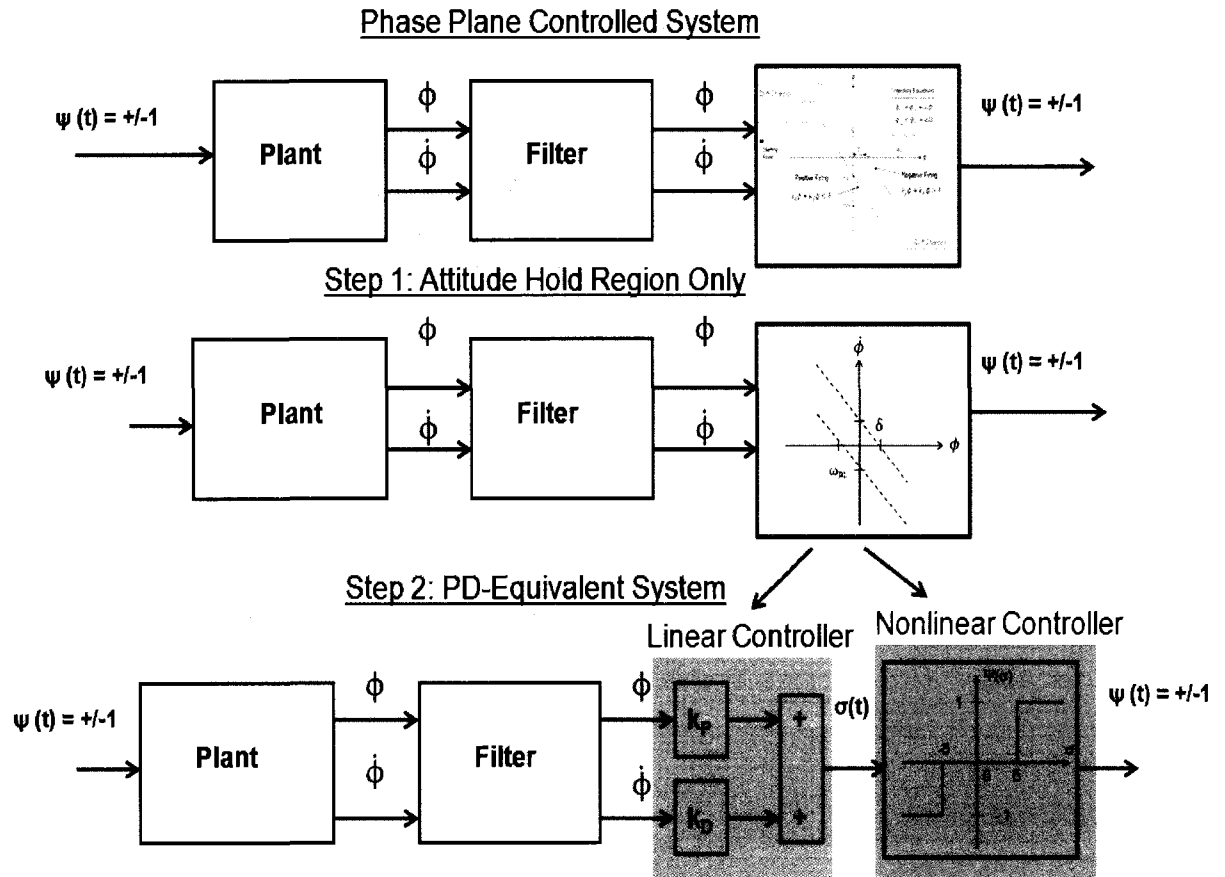


Figure 2.2: The Phase Plane Controller

The system will continue to oscillate around the origin of the phase plane in what is called a limit cycle. A common definition of a limit cycle is an oscillation of “fixed amplitude and fixed period without external excitation” [10].

#### 2.4.2 Equivalent PD Controller

In order to evaluate a nonlinear system such as a phase plane controlled system, it is necessary to transform the phase plane controller into a form where linear control techniques can be applied. This will be accomplished in a two step process. First, only the attitude hold region will be evaluated, and second, the phase plane controller will be transformed into an equivalent system consisting of a PD controller and a nonlinear element consisting of a dead zone and an ideal relay. This development can be seen in Figure 2.3:



**Figure 2.3: PD-Equivalent Phase Plane Development**

In Figure 2.3 above, step one ignores the drift channels of the phase plane controller because this thesis will focus on the sloped portion of the phase plane. Figure 2.4 below illustrates the region to be analyzed in the proceeding development [11].

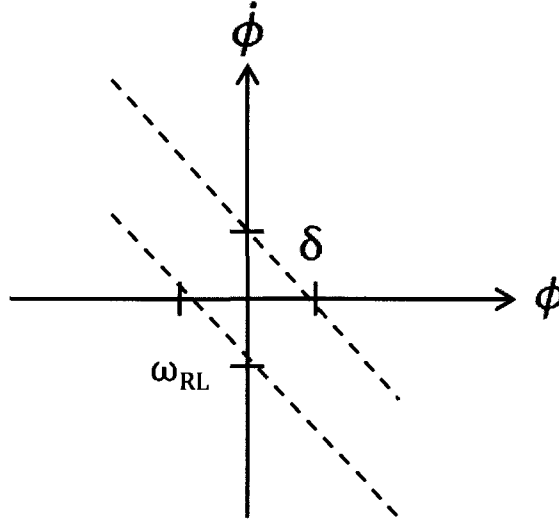


**Figure 2.4: Sloped Portion of the Phase Plane**

The two switching curves, which define the dead zone between the positive and negative firing regions, can be defined by the inequality:

$$-\left(\omega_{RL}/\delta\right)\phi - \omega_{RL} < \dot{\phi} < -\left(\omega_{RL}/\delta\right)\phi + \omega_{RL} \quad (2.10)$$

In order to progress from step two to step three in Figure 2.3, it is necessary to implement a PD controller. It is first necessary to rewrite Equation 2.10:

$$-1 < \phi/\delta + \dot{\phi}/\omega_{RL} < 1 \quad (2.11)$$

Multiplying Equation 2.11 by the dead zone,  $\delta$ , leads to Equation 2.12:

$$-\delta < \phi + \left(\delta/\omega_{RL}\right)\dot{\phi} < \delta \quad (2.12)$$

This inequality provides the following values for  $k_P$  and  $k_D$  which are the proportional and derivative gains respectively [11].



$$k_p = 1 \quad (2.13)$$

$$k_D = \delta / \omega_{RL} \quad (2.14)$$

The  $k_p$  and  $k_d$  values calculated above are instrumental in creating a practical phase plane controller that can be used with control analysis techniques. Substituting these values into Equation 2.12 yields the result for the dead zone [11].

$$-\delta < k_p \phi + k_D \dot{\phi} < \delta \quad (2.15)$$

The phase plane controller utilizes thruster firings. To model these firings, it is necessary to switch the signs from Equation 2.15 which models the dead zone. The thrusters are activated whenever either of the two inequalities becomes true [11].

$$k_p \phi + k_d \dot{\phi} < -\delta \text{ [Positive Firing]} \quad (2.16)$$

$$k_p \phi + k_d \dot{\phi} > \delta \text{ [Negative Firing]} \quad (2.17)$$

The nonlinear controller portion in step three of Figure 2.3 can be evaluated by nonlinear control analysis techniques such as PWM, describing functions and absolute stability.

## 2.5 Conclusions

The spacecraft attitude control system takes into account both rigid and flex dynamics. The phase plane controller offers an idealized model for constructing a nonlinear controller which optimizes time and fuel performance. It is possible create an equivalent phase plane controller system that functions as the ideal phase plane

controllers using a PD controller. Nonlinear control techniques for the phase plane controller will be expanded upon in the proceeding chapters.

## Chapter 3: Limit Cycle Prediction

In this chapter two methods of limit cycle prediction will be explored. The first method, PWM, will create a linear approximation for which stability criteria such as those proposed by Bode, Nichols, and Nyquist can be applied. The second topic, describing functions, approximates nonlinear behavior through a quasi-linearization process. This information can be used to predict unstable limit cycles either through Nichols Plot intersections or by applying a gain and phase margin tester.

### 3.1 Pulse Width Modulation (PWM) Approximation

PWM is a method which transforms a nonlinear system into a form in which classical control techniques can be utilized through converting the linear system into discrete-time, calculating the system on-time, and performing dead zone scaling. For PWM the nonlinear element in Figure 2.3 is replaced by dead zone scaling as can be seen in Figure 3.1:

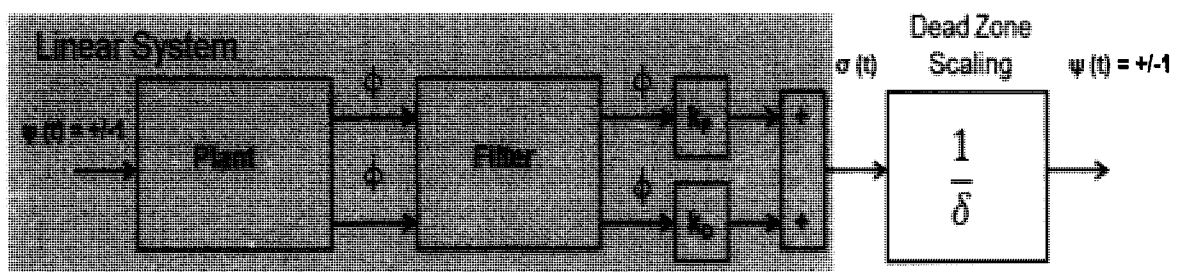


Figure 3.1: Phase Plane Controlled System with PWM

PWM discussion concludes with an explanation as to why PWM is utilized instead of pulse-width-pulse-frequency (PWPF).

### 3.1.1 PWM Discrete-Time

A PWM approach will require transforming the linear system from Figure 3.1 to a discrete-time system of the form shown in Figure 3.1 [12]:

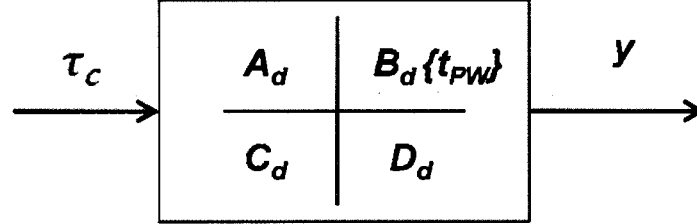


Figure 3.2: Discrete PWM-Actuated System

The state space equations appear as follows in the discrete-time domain [12]:

$$\mathbf{y}[(k+1)t_c] = \mathbf{C}_d \mathbf{x}[kt_c] + \mathbf{D}_d \tau_c[kt_c] \quad (3.1)$$

$$\mathbf{x}[(k+1)t_c] = \mathbf{A}_d \mathbf{x}[kt_c] + \mathbf{B}_d \tau_c[kt_c] \quad (3.2)$$

The discrete-time matrices  $\mathbf{A}_d$ ,  $\mathbf{B}_d$ ,  $\mathbf{C}_d$  and  $\mathbf{D}_d$  are defined in Equation 3.3-3.6 [4].

$$\mathbf{A}_d = e^{\mathbf{A}t_c} \quad (3.3)$$

$$\mathbf{B}_d = (e^{\mathbf{A}t_c}) \mathbf{V} \begin{bmatrix} \mathbf{I} & \mathbf{0} \end{bmatrix} e^{\begin{bmatrix} -\mathbf{\Lambda} t_{PW} & \mathbf{I} \\ \mathbf{0} & \mathbf{0} \end{bmatrix}} \begin{bmatrix} \mathbf{0} \\ \mathbf{I} \end{bmatrix} \mathbf{V}^{-1} \mathbf{B} t_c \quad (3.4)$$

$$\mathbf{C}_d = \mathbf{C} \mathbf{A}_d \quad (3.5)$$

$$\mathbf{D}_d = \mathbf{C} \mathbf{B}_d \quad (3.6)$$

Where  $\begin{bmatrix} \mathbf{A} & \mathbf{B} \\ \mathbf{C} & \mathbf{D} \end{bmatrix}$  is the original continuous state space representation. In the above

$\mathbf{B}_d$  matrix,  $\mathbf{V}$  is known as the Vandermonde matrix and  $\mathbf{\Lambda}$  is the diagonal eigenvalue

matrix. The Vandermonde and diagonal eigenvalue matrices are shown in Equation 3.7 and 3.8 [13] [14].

$$V = \begin{pmatrix} 1 & \dots & 1 \\ \lambda_1 & \dots & \lambda_n \\ \lambda_1^2 & \dots & \lambda_n^2 \\ \vdots & \ddots & \vdots \\ \lambda_1^{n-1} & \dots & \lambda_n^{n-1} \end{pmatrix} \quad (3.7)$$

$$\Lambda = \begin{pmatrix} \lambda_1 & 0 & 0 \\ 0 & \ddots & 0 \\ 0 & 0 & \lambda_n \end{pmatrix} \quad (3.8)$$

The above matrices can be determined through Equation 3.9 [14]:

$$A_d = V\Lambda V^{-1} \quad (3.9)$$

With the linear system properly converted to discrete-time, it is now possible to move forward with the remainder of the PWM analysis.

### 3.1.2 System On-Time Calculation

Since the system is discrete-time, it can be broken down into control cycles with period,  $t_c$ . At each cycle the PWM-based phase plane controller is updated to enhance performance for the nonlinear roll control system. The jets provide a constant torque,  $\tau_{jets}$ , when activated. It is important to remember that there is a minimum “on” time for the actuators when calculating the desired torque,  $\tau_c$ . Once the desired torque has been computed it is now desirable to calculate the total desired momentum,  $\Delta h_c$ , through Equation 3.10 [4]:

$$\Delta h_c = \tau_c t_c \quad (3.10)$$

Depending on whether or not the system is in a firing or non-firing region, the applied torque,  $\tau$ , is determined [4]:

$$\tau = \begin{cases} \tau_{jets}, & kt_c \leq t < kt_c + t_{PW} \\ 0, & kt_c + t_{PW} \leq t < (k+1)t_c \end{cases} \quad (3.11)$$

In the expression above  $k$  is the integer series  $0, 1, 2, \dots$  and  $t_{PW}$  is the pulse-width on time which comes from Equation 3.12 [4]:

$$\Delta h_c = \tau_c t_c = \tau t_{PW} \quad (3.12)$$

Based on the principle of angular momentum, Equation 3.12 can be simplified to the following equation to solve for  $t_{PW}$  [4]:

$$t_{PW} = \frac{|\tau_c|}{|\tau_{jets}|} t_c \quad (3.13)$$

The value calculated here for  $t_{PW}$  is utilized to determine the appropriate amount of  $\Delta h_c$  to be applied to the system.

### 3.1.3 Dead Zone Scaling

In order to compensate for the dead zone nonlinearity in the system, it is necessary to cut the closed loop system immediately before the dead zone nonlinearity in order to create an open loop system without the dead zone or ideal relay nonlinearities. This can be seen in Figure 3.3:

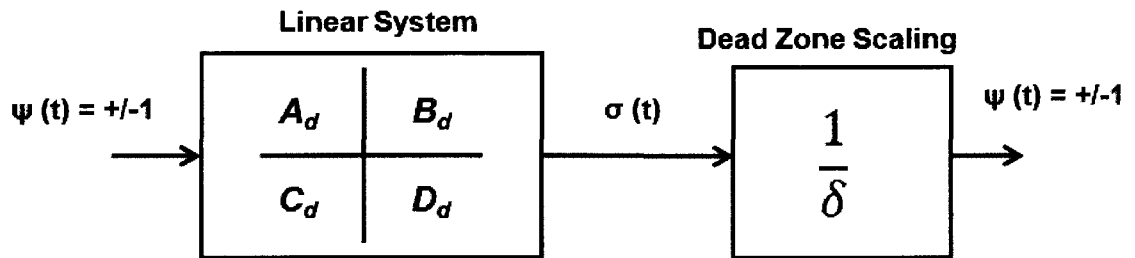


Figure 3.3: PWM System Model

This system's response is then scaled by the dead zone value in order to approximate the nonlinear behavior of the phase plane controller [3]. The small gain theorem is then applied to the new linear approximation of the nonlinear system. If the system's open loop gain is greater than or equal to unity, unstable limit cycling will occur within the system [15]. Though this method accounts for the dead zone nonlinearity, it does not make an additional approximation for the ideal relay nonlinearity. This absence can lead to inaccuracies when using the method to predict stability margins for nonlinear systems as shown in Section 4.4.

#### **3.1.4 PWM versus PWPF**

One alternative to PWM is PWPF which is a similar jet selection logic technique that "converts the torque command to the RCS jets command" [16]. For this case RCS denotes a reaction control system which is the physical control setup the roll control system utilizes. The technique has advantages over PWM because PWM utilizes short pulses which are "generally fuel-inefficient under harsh aerodynamic environments" which the system encounters in the first stage of flight [17]. Because PWPF "originates from an analog device" a "minimum pulse could be selected to be equal to the sampling time of the flight computer or an integer multiple of the sampling time [17]. This essentially means that the PWPF method offers fuel efficiency and reliability; however, the "PWPF has a potential issue of phase loss at high frequencies" which is an important problem for many systems due to the large amount of structural flex these systems experiences [17]. This flex is ultimately why PWM was selected over PWPF for this thesis.

## 3.2 Describing Functions

Describing functions are quasi-linearization tools that detect limit cycles. As discussed in Chapter 2, limit cycles are “sustained oscillations” in a nonlinear system which exists with no external action [18]. This method fits progresses from Figure 2.3 as follows in Figure 3.4:

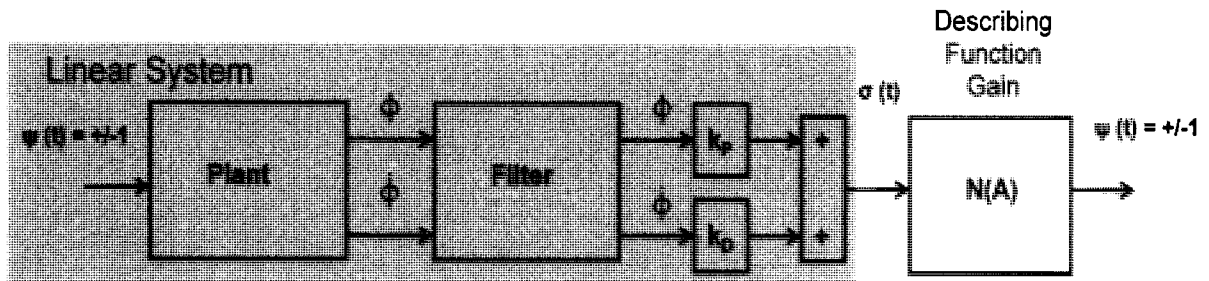


Figure 3.4: Phase Plane Control System with Describing Function

Describing functions are a natural choice for control system design because they are a frequency-based technique; therefore, they can be used in conjunction with classical control techniques. This result is because describing functions are largely based on the Nyquist criterion.

### 3.2.1 Describing Function Theory

The basic form for describing function analysis splits the nonlinear and linear portions of the system as seen in Figure 3.5:



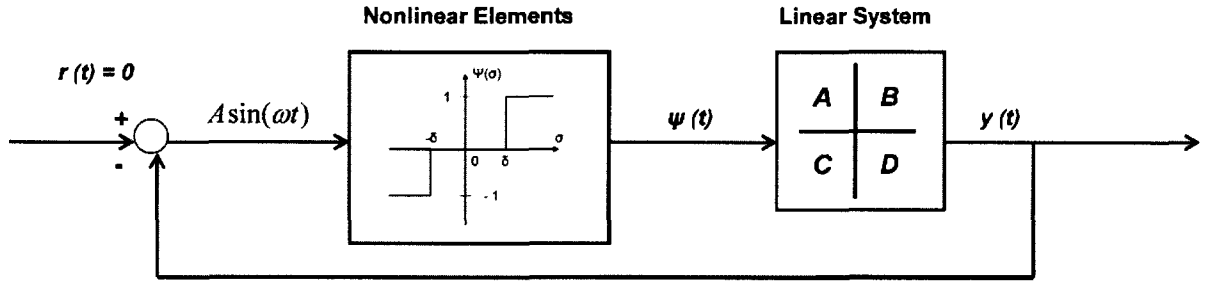


Figure 3.5: Describing Function Form

Since “describing function analysis...belongs to those methods of solving nonlinear differential equations which are based upon an assumed solution,” there must be an assumed input into the nonlinear element,  $N(A, \omega)$  [18]. When using describing function analysis, it is necessary to assume the input to be of the sinusoidal form:

$$f(t) = A \sin(\omega t) \quad (3.19)$$

Because the output is a signal, it can be modeled through the Fourier series [10]. It will be assumed that the nonlinearity is odd and the only the fundamental output,  $\psi_1(t)$ , of the nonlinear element will be of concern in the following analysis [10].

### 3.2.2 Derivation of an Odd Describing Function in General Form

As stated above, a describing function's output can be represented using the Fourier series as in Equation 3.20 [10]:

$$\psi(t) = \frac{a_0}{2} + \sum_{n=1}^{\infty} [a_n \cos(n\omega t) + b_n \sin(n\omega t)] \quad (3.20)$$

Where  $a_n$  and  $b_n$  are determined in Equations 3.21 and 3.22 [10]:

$$a_n = \frac{1}{\pi} \int_{-\pi}^{\pi} w(t) \cos(n\omega t) d(\omega t) \quad (3.21)$$

$$b_n = \frac{1}{\pi} \int_{-\pi}^{\pi} w(t) \sin(n\omega t) d(\omega t) \quad (3.22)$$

All nonlinearities discussed in this thesis will be odd, that is, they will “possess odd symmetry” which is manifested in Equation 3.23 [16]:

$$\psi(\sigma) = -\psi(-\sigma) \quad (3.23)$$

Odd symmetry will eliminate  $a_0$  from Equation 3.20; furthermore; since only the first output,  $\psi_1(t)$ , is being considered the following is true [10]:

$$\psi(t) = \psi_1(t) = a_1 \cos(\omega t) + b_1 \sin(\omega t) \quad (3.24)$$

Transforming  $\psi_1(t)$  into polar coordinates provides the result [10]:

$$\psi_1(t) = M \sin(\omega t + \theta) = M e^{j(\omega t + \theta)} \quad (3.25)$$

$M$  and  $\theta$  are defined [10]:

$$M(A, \omega) = \sqrt{a_1^2 + b_1^2} \quad (3.26)$$

$$\theta(A, \omega) = \tan^{-1} \left( \frac{b_1}{a_1} \right) \quad (3.27)$$

The goal of describing functions is to quasi-linearize a nonlinearity in the frequency domain [16]. To accomplish this feat it will be necessary to model to output over input of a generalized nonlinearity using the input,  $A \sin(\omega t)$ , and the output,  $\psi_1(t)$  [10].

$$N(A, \omega) = \frac{\psi_1(t)}{A \sin(\omega t)} = \frac{M e^{j(\omega t + \theta)}}{A e^{j\omega t}} = \frac{M}{A} e^{j\theta} \quad (3.28)$$

For the generalized describing function form, it is necessary to transform the equation from polar to Cartesian coordinates [10].

$$N(A, w) = \frac{1}{A} (b_1 + ja_1) \quad (3.29)$$

### 3.2.3 Dead Zone Describing Function Derivation

The dead zone nonlinearity is a key nonlinearity in the phase plane controller discussed above; therefore, it is of the utmost importance that dead zone is modeled as a describing function in order to fully explore the system's nonlinear dynamics. Figure 3.6 below depicts the input/output relationship for a dead zone nonlinearity. The symbol,  $\delta$ , represents the numerical value for the dead zone.

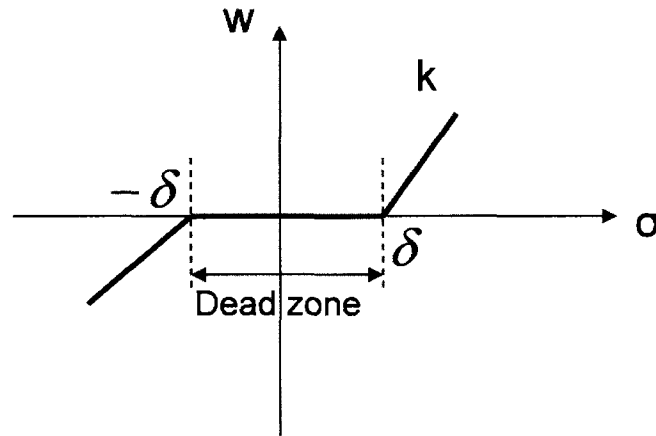


**Figure 3.6: Dead Zone Nonlinearity Input vs. Output**

For any nonlinearity which needs to be modeled with describing functions, it is always first required to start with the output function. The output function for dead zone is shown [10]:

$$\psi(t) = \begin{cases} 0, & 0 \leq \omega t \leq \gamma \\ k(A \sin(\omega t) - \delta), & \gamma \leq \omega t \leq \pi/2 \end{cases} \quad (3.30)$$

In Equation 3.30 above,  $\gamma$  is defined:

$$\gamma = \sin^{-1}(\delta/A) \quad (3.31)$$

For the dead zone nonlinearity the “quadrature gain” or  $a_I$  is always zero because this is true for any nonlinearity that is “static and single-valued” [16]. A static nonlinearity is defined by Equation 3.32:

$$\psi = \psi(\sigma) \quad (3.32)$$

This means the nonlinearity displays “no dependence upon the input derivatives” [16]. The generalized equation for a describing function can be reduced as such:

$$N(A) = \frac{b_1}{A} \quad (3.33)$$

In order to have a treatable equation, it is necessary to expand  $b_1$  in the preceding equation [10]:

$$b_1 = \frac{1}{\pi} \int_{-\pi}^{\pi} w(t) \sin(\omega t) d(\omega t) \quad (3.34)$$

$$b_1 = \frac{4}{\pi} \int_0^{\frac{\pi}{2}} w(t) \sin(\omega t) d(\omega t) \quad (3.35)$$

Dividing the equation into two integrals, one for each  $\psi(t)$  function gives [10]:

$$b_1 = \frac{4}{\pi} \left[ \int_0^{\delta} (0) \sin(\omega t) d(\omega t) + \int_{\delta}^{\frac{\pi}{2}} k(A \sin(\omega t) - \delta) \sin(\omega t) d(\omega t) \right] \quad (3.36)$$

Finally integrating  $b_1$  and placing it into the equation for  $N(A)$  yields [10]:

$$b_1 = \frac{2kA}{\pi} \left[ \frac{\pi}{2} - \sin^{-1} \left( \frac{\delta}{A} \right) - \frac{\delta}{A} \sqrt{1 - \frac{\delta^2}{A^2}} \right] \quad (3.37)$$

$$N(A) = \frac{b_1}{A} = \frac{2k}{\pi} \left[ \frac{\pi}{2} - \sin^{-1} \left( \frac{\delta}{A} \right) - \frac{\delta}{A} \sqrt{1 - \frac{\delta^2}{A^2}} \right] \quad (3.38)$$

It will be useful to know the describing function for other nonlinearities such as an ideal relay; therefore, the describing function for a relay element is given in the equation [16]:

$$N(A) = \frac{4D}{\pi A} \quad (3.39)$$

In the above expression,  $D$  is the magnitude of the relay's output which can be either positive or negative depending on the sign of the input.

### 3.2.4 Two Nonlinear Elements in Series

In many systems there will be more than one nonlinear element to consider. In this section, two nonlinear elements ( $N_1$  and  $N_2$ ) in series will be examined. The model below in Figure 3.7 illustrates the nonlinear element set up that will be discussed [16].

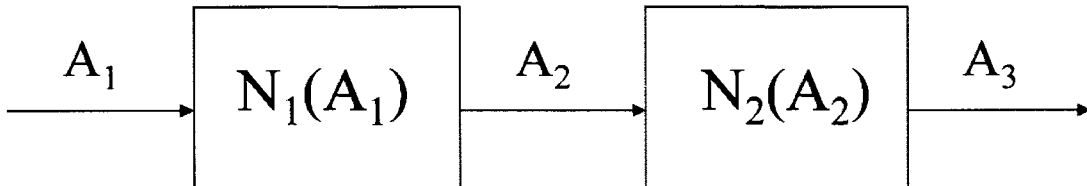


Figure 3.7: Two Nonlinear Elements in Series

The goal of this exercise is to create one describing function which captures the nonlinear behavior of both  $N_1$  and  $N_2$ . It is important to remember that single valued describing functions are considered to be linear gains in nonlinear control theory; therefore, the two nonlinearities need to be multiplied by each other in order to determine their combined gain value [16]. Before the combined gain can be determined it is necessary to more clearly define each of the input amplitudes  $A_n$ .  $A_1$  is the input amplitude to the nonlinear element series.  $A_2$  is the output of  $N_1$  and the input to  $N_2$  and is defined by the expression:

$$A_2 = N_1(A_1)A_1 \quad (3.40)$$

The symbol  $A_3$  denotes the output to  $N_2$  and is defined by the following expression:

$$A_3 = N_2(A_2)A_2 \quad (3.41)$$

Combining  $N_1$  and  $N_2$  to create a combined describing function  $N(A_1)$  requires multiplying the two gains together:

$$N(A_1) = N_1(A_1)N_2(A_2) = N_1(A_1)N_2(N_1(A_1)A_1) \quad (3.42)$$

The above process provides a method for combining two describing functions to approximate two nonlinear elements in series.

### 3.2.5 Nichols-Based Limit Cycle Prediction

The first method of predicting whether or not a system will experience limit cycling involves plotting  $-1/N(A)$  in a Nichols plot with the linear system response,  $G(j\omega)$ . Whenever the two plots intersect, limit cycling may occur [10]. For example; Penchuk, Hattis and Kubiak established modeling the space shuttle's phase plane controller's nonlinearities as hysteresis [1]. Hysteresis is different than dead zone because it has not only a real but an imaginary portion which means it has frequency content as can be seen below [1]:

$$N(A) = \begin{cases} \frac{2}{\pi A^2} (A + \sqrt{A^2 - 1} - j), & A \geq 0 \\ 0, & A < 0 \end{cases} \quad (3.43)$$

As a result of this frequency content, the Nichols plot of  $-1/N(A)$  is not just a vertical as would be the case for dead zone. Figure 3.8 below demonstrates how the hysteresis can predict limit cycling in a nonlinear system [2]:

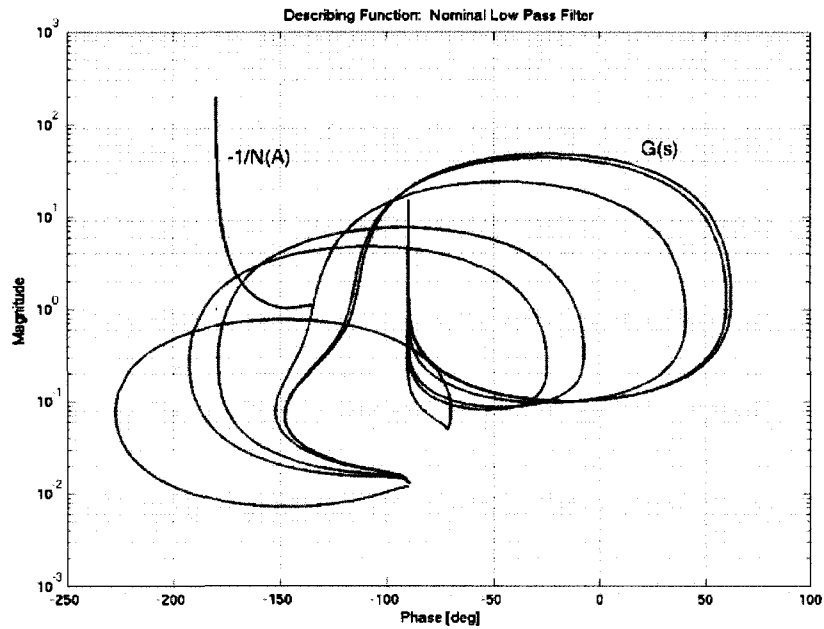


**Figure 3.8: Predicting Limit Cycling Through Intersections**

As can be seen in Figure 3.8, there are two frequencies at which the system in this example limit cycles. Such knowledge can be critical in ascertaining the overall stability and performance of a system. It must be noted that describing functions are conservative in nature and it takes experience to know whether or not limit cycling will actually occur even if there is an intersection [10]. Generally, it is the accepted practice to consider a system that does not intersect as non-limit cycling while one that does intersect needs to be examined more closely [10].

### 3.2.6 Gain and Phase Margin Tester

Wu and Perng establish a gain and phase margin testing technique which is based on examining the characteristic equation of the closed loop transfer function  $T(s)$  also



known as the complementary sensitivity function. The gain and phase margin tester is of the form [19]:

$$\text{Gain/Phase Margin Tester} = Ke^{-j\theta} \quad (3.44)$$

where  $K$  represents gain and  $\theta$  represents phase in the feedback loop. Consider the following figure [19]:

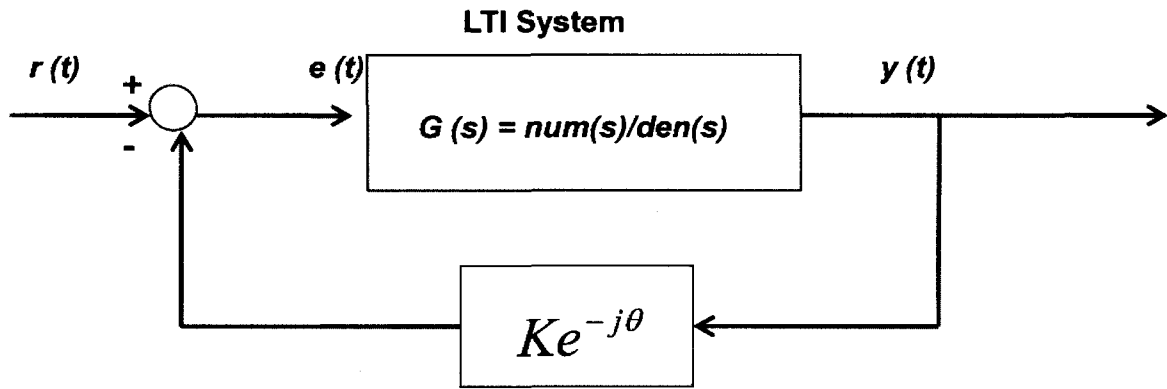


Figure 3.9: Gain/Phase Margin Tester Block Diagram

From the above figure it can be seen that  $T(s)$  is defined by Equation 3.45:

$$T(s) = \frac{G(s)}{1 + Ke^{-j\theta} G(s)} \quad (3.45)$$

It is important to note that  $G(s)$  includes the describing function for the nonlinearity as a complex gain or in the case of dead zone as a gain with no frequency content. To determine stability (in this case defined by limit cycle existence or lack thereof, it is necessary to examine the characteristic equation for  $T(s)$  [19].

$$1 + Ke^{-j\theta} G(s) = 1 + Ke^{-j\theta} \frac{\text{num}(s)}{\text{den}(s)} = \text{den}(s) + Ke^{-j\theta} \text{num}(s) = 0 \quad (3.46)$$

By substituting zero into the phase, Equation 3.47 is found:

$$den(s) + num(s)K = 0 \quad (3.47)$$

In this equation,  $K$  now functions as the gain margin seeing as phase has been set to zero. Gain margin can now be solved for by splitting the above equation into real and imaginary portions and solving for  $K$  [19]:

$$K' = \frac{-Re[den(s)]}{Re[num(s)]} \quad (3.48)$$

$$K'' = \frac{-Im[den(s)]}{Im[den(d)]} \quad (3.49)$$

It is necessary to vary the describing function in  $G(s)$ 's amplitude,  $A$ , from 0 to  $\infty$  while also varying  $\omega_i$  from 0 to  $\infty$ . Solve for  $K' = K''$  at every  $A_i$ . If  $K' = K'' = K_i$  for  $A = A_i$ , then  $K_i$  is the valid gain margin for that amplitude. The minimum gain margin is considered the actual gain margin in this technique. The result can be seen in Figure 3.10:

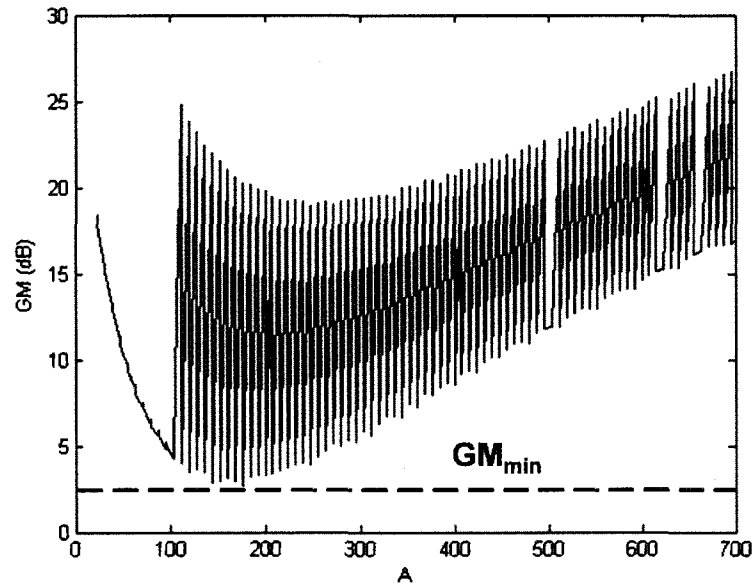


Figure 3.10: Gain Margin Test Results

The phase margin tester is constructed in a similar manner as the gain margin tester in that you begin with the characteristic equation for  $T(s)$  [19]:

$$1 + Ke^{-j\theta}G(s) = 1 + Ke^{-j\theta} \frac{\text{num}(s)}{\text{den}(s)} = \text{den}(s) + Ke^{-j\theta}\text{num}(s) = 0 \quad (3.50)$$

By substituting unity into  $K$  and applying Euler's method yields [19]:

$$W + U\cos(\theta) + V\sin(\theta) = 0 \quad (3.51)$$

Separating the equation into real and imaginary parts yields [19]:

$$W_R + U_R\cos(\theta) + V_R\sin(\theta) = 0 \quad (3.52)$$

$$W_I + U_I\cos(\theta) + V_I\sin(\theta) = 0 \quad (3.53)$$

Using the previous two equations,  $\theta$  is determined [19]:

$$\theta = \cos^{-1} \left( \frac{V_R W_I - V_I W_R}{U_R V_I - U_I V_R} \right) \triangleq \theta' \quad (3.54)$$

$$\theta = \cos^{-1} \left( \frac{U_R W_I - U_I W_R}{U_R V_I - U_I V_R} \right) \triangleq \theta'' \quad (3.55)$$

Again it is necessary to vary the describing function in  $G(s)$ 's  $A$  from 0 to  $\infty$  while also varying  $\omega_i$  from 0 to  $\infty$ . Solve for  $\theta' = \theta''$  at every  $A_i$ . If  $\theta' = \theta'' = \theta_i$  for  $A = A_i$ , then  $\theta_i$  is the valid phase margin for that amplitude. The minimum phase margin is considered the actual phase margin in this technique. The result can be seen in the following plot:

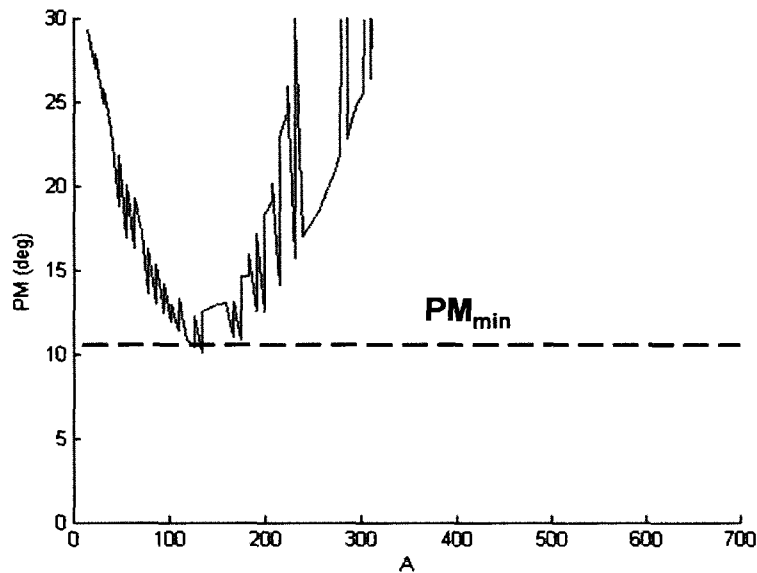


Figure 3.11: Phase Margin Test Results

The preceding method can be applied to any describing function both with and without frequency content.

### 3.3 PWM and Describing Function Conclusions

Both PWM and describing functions can be utilized to predict the existence of limit cycles in nonlinear systems. The prediction of unstable limit cycles is critical for

determining whether or not a nonlinear system will behave in a controllable and stable manner. These techniques will later be applied to spacecraft attitude control systems and compared to other nonlinear methods by means of their results.

## Chapter 4: Absolute Stability

The phase plane controller is a nonlinear control scheme which means it is necessary to take these nonlinearities into account when determining system stability. Absolute stability provides a method for guaranteeing asymptotic stability for a nonlinear system primarily through two techniques called the circle criterion and the Popov criterion. Both the circle criterion and the Popov criterion were developed in the 1960's by theorists such as Zames, Aizermann, Gantmacher and Popov who applied Lyapunov's second method to the frequency domain [15] [20] [21].

### 4.1 Lur'e Problem and Background

For systems with nonlinearities such as dead zone and ideal relay, standard linear control methodologies such as Bode and Nichols cannot be applied. These nonlinear aspects must be taken into account. The Lur'e Problem accomplishes this task by separating the linear and nonlinear elements as in the Figure 4.1 [22]:

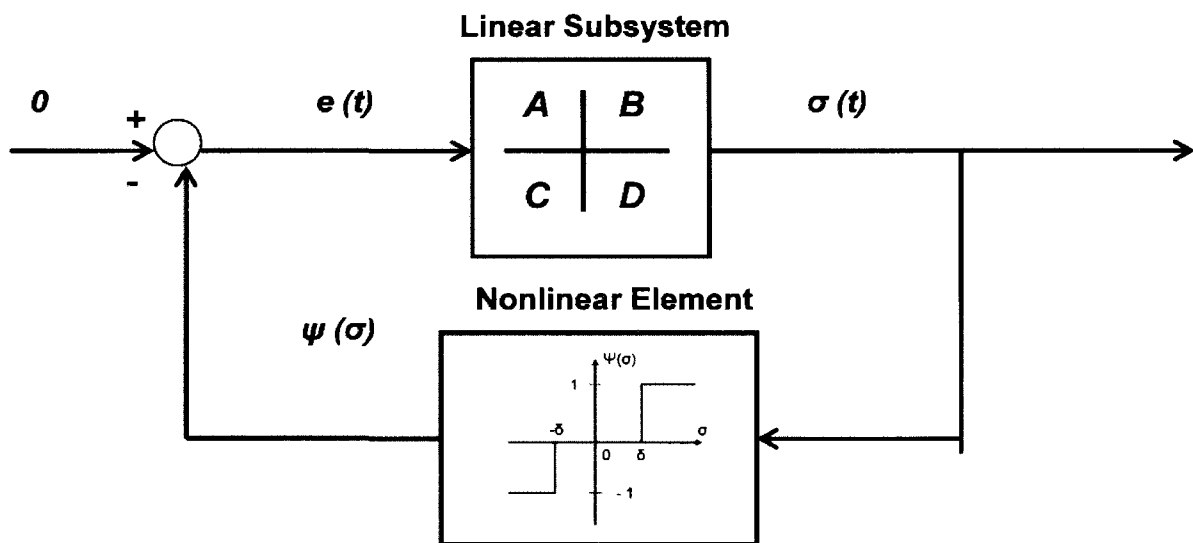


Figure 4.1: Lur'e Problem System Model

Figure 4.1 corresponds to the following system of equations [22]:

$$\dot{x}(t) = Ax(t) + B\psi(\sigma) \quad (4.1)$$

$$\sigma(t) = Cx(t) \quad (4.2)$$

Using this model, it is possible to evaluate the sector bounds for the nonlinear element. A nonlinearity belongs to a sector  $[\alpha, \beta]$ , where  $\beta$  and  $\alpha$  are the upper and lower sector bounds respectively, if the inequality

$$\alpha\sigma^2 \leq \psi(\sigma)\sigma \leq \beta\sigma^2 \quad (4.3)$$

holds true [23]:. Sector bounds define the regions where a nonlinearity can dwell when plotting the input,  $\sigma(t)$ , versus the output,  $\psi(\sigma)$  as in Figure 4.2 [26].

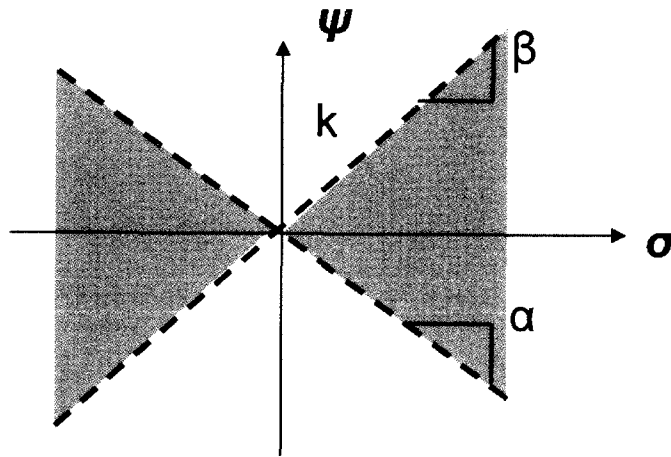


**Figure 4.2: Input/Output Sector Bounds**

These sector bounds allow for nonlinear stability to be ascertained by way of frequency-based methods such as the circle criterion and Popov criterion.

## 4.2 Circle Criterion

A system with nonlinearities enclosed within the sector bound is guaranteed to be asymptotically stable provided the system is a minimal realization of  $G(s)$ . This means that the **A** and **C** matrices must be observable while the **A** and **B** matrices must be controllable when the system is in state space form [22]. Determining  $\beta$  and  $\alpha$  can be accomplished through one of the following three cases, collectively known as the Circle Criterion.

*Case One:*  $[0 < \alpha < \beta]$

For this case the “Nyquist plot of  $G(s)$  does not enter the disk  $D(\alpha, \beta)$  and encircles it  $m$  times in the counterclockwise direction, where  $m$  is the number of poles of  $G(s)$  with positive real parts” [23]. For the expression:

$$G(s) = \frac{4}{(s-1)\left(\frac{s}{2}+1\right)\left(\frac{s}{3}+1\right)} \quad (4.4)$$

The accompanying Nyquist plot can be seen below:



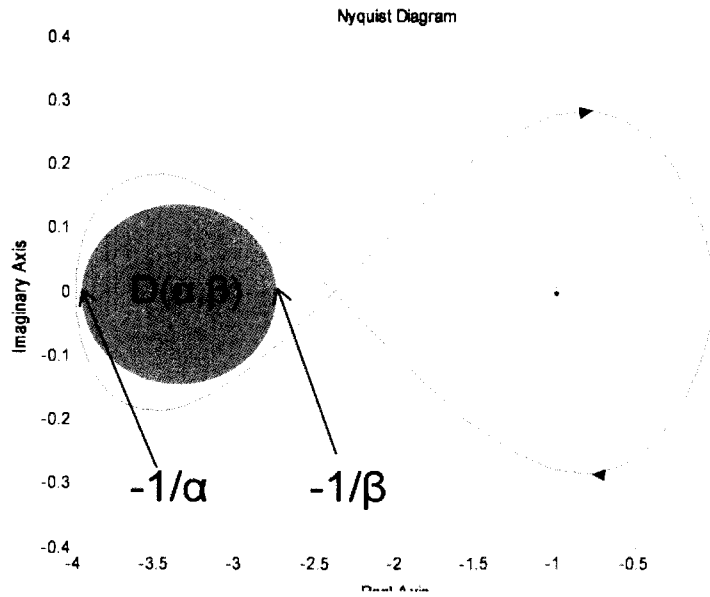


Figure 4.3: Circle Criterion (Case 1) Example

*Case Two:*  $[\alpha = 0, \beta > 0]$

For the second condition, the linear portion,  $G(s)$ , must be strictly Hurwitz which means all poles are in the open left hand side of the s-plane. The Nyquist plot of  $G(s)$  must lie to the “right of the vertical line defined by  $\text{Re}[s] = -1/\beta$ ” [22]. Khalil includes the following example [23]:

$$G(s) = \frac{1}{(s+1)(s+2)(s+3)} \quad (4.5)$$

Which when plotted appears as below:

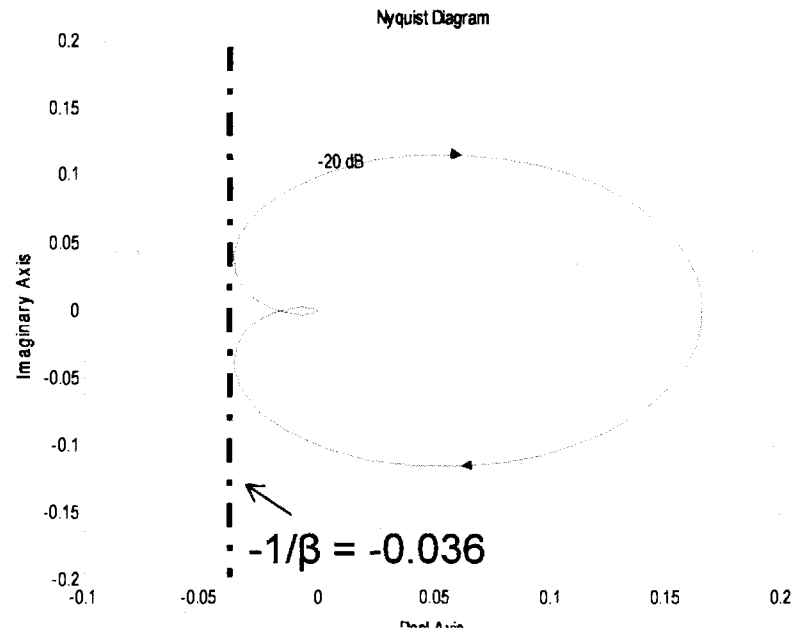


Figure 4.4: Circle Criterion (Case 2) Example

This above chart shows that for this particular transfer function,  $\beta$  will be equal to 27.8 which is large enough for both dead band and ideal relay nonlinearities.

*Condition Three:*  $[\alpha < 0, \beta > 0]$

This case also requires  $G(s)$  to be Hurwitz; however, the Nyquist response of  $G(s)$  must be completely inside the disk,  $D(\alpha, \beta)$  [23]. The same example function can be taken from condition two; however, condition three will be applied.

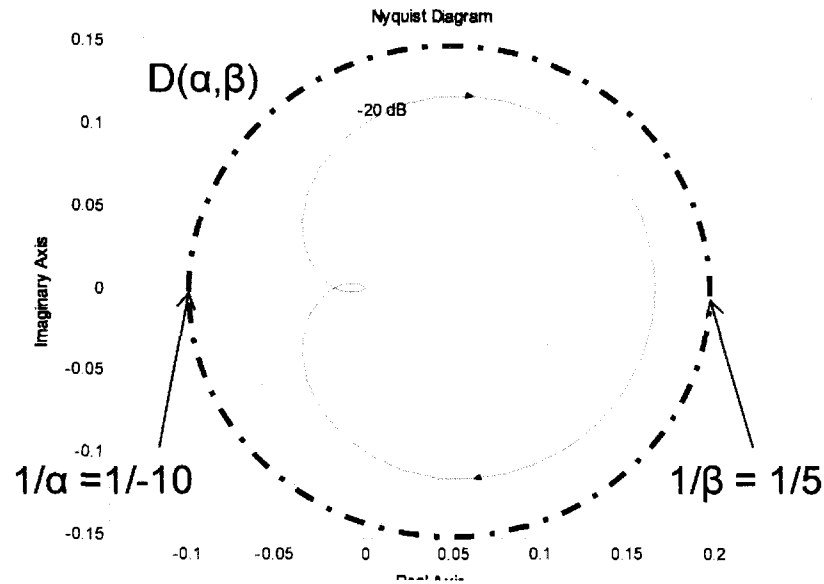


Figure 4.5: Circle Criterion (Case 3) Example

Condition three leads to an  $\alpha$  of -10 and a  $\beta$  equal to 5 which means there are regions of absolute stability in both the second and fourth quadrants of the input/output nonlinearity chart.

The dead zone and ideal relay nonlinearities cannot fit inside the sector as defined by condition one, so that means condition one is ruled out as an option. Sector conditions are more difficult to derive for condition three than for condition two. Condition three requires the disk,  $D(\alpha, \beta)$ , to be generated while condition two implements a vertical line placed at the minimum real value of the Nyquist response to  $G(s)$ . That minimum real Nyquist value is then compared to  $-1/\beta$  in order to determine if a system possesses absolute stability. For these reasons, condition two will be explored for the remainder of this paper rather than condition one or condition three.

It is important to note that circle criterion is only a sufficient condition for absolute stability [10]. In other words, a system is guaranteed asymptotic stability if the system meets circle criterion conditions, but if the system fails to satisfy those conditions, it is not necessarily unstable.

### 4.3 Popov Criterion

The Popov criterion is an additional method for determining whether or not a nonlinear system possesses absolute stability. As in the circle criterion, it is necessary to begin with the Lur'e problem system setup in Figure 4.1. There are limitations to the particular type of system that can use the Popov criterion to ensure absolute stability. Vidyasagar notes “unlike the circle criterion, the Popov criterion is applicable only to *autonomous* systems” [22]. An autonomous system is defined as autonomous if  $f$  in the following expression “does not depend explicitly on time” [10]. That is:

$$\dot{x} = f(x) \tag{4.6}$$

A system that is non-autonomous would have behavior that could be described by Equation 4.7 [10]:

$$\dot{x} = f(x, t) \tag{4.7}$$

As in the circle criterion, it is necessary that the **A** and **B** matrices are controllable and the **A** and **C** matrices are observable, therefore, ensuring the open loop transfer function for the system is a minimal realization of the system [22]. Similar to conditions two and three of the circle criterion, it is necessary for the system to be strictly Hurwitz to

satisfy the Popov criterion [10]. Popov's criterion is similar to condition two of the circle criterion in that the lower sector bound,  $\alpha$ , is set equal to zero while the upper sector bound,  $\beta$ , is determined through a graphical-frequency based technique [10]. From here it is necessary to examine the following inequality. The inequality must be satisfied in order for absolute stability to exist [10]:

$$\operatorname{Re}[(1 + j\omega r)G(j\omega)] + \frac{1}{\beta} \geq \epsilon, \quad \forall \omega \geq 0 \quad (4.8)$$

In Equation 4.7, the value  $c$  should be an arbitrarily small value while  $r$  is required to be non-negative [10]. Applying constrained minimization to minimize  $1/\beta$  in the above expression results in a solution for  $\beta$  for a particular transfer function. Using a sample transfer function from Vidyasagar along with MATLAB code created to perform the above constrained minimization generates results which are best seen in a Popov plot [22]. The Popov plot only considers positive frequencies (unlike circle criterion plots) and is similar to the s-plane except that the Popov plot graphs  $\operatorname{Re}[G(j\omega)]$  vs.  $\omega \operatorname{Im}[G(j\omega)]$  as opposed to  $\operatorname{Re}[G(j\omega)]$  vs.  $\operatorname{Im}[G(j\omega)]$  as in the circle criterion [22]. A sample transfer function from Vidyasagar will be used for demonstration purposes [22]:

$$G(s) = \frac{1}{s(s+1)^2} \quad (4.9)$$

Plotting the positive frequencies for the above transfer function (blue line) as well as performing the constrained minimization which generates the red line in Figure 4.6 below:

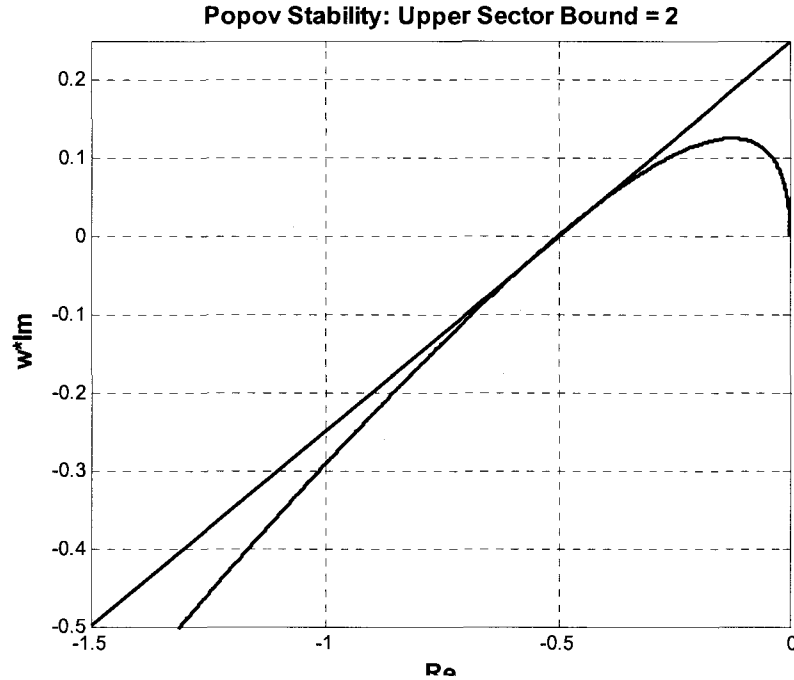


Figure 4.6: Popov Criterion Example

Figure 4.6 shows that the upper sector bound for the given transfer function is equal to two. It is important to note that sector bounds generated for a given transfer function using the Popov criterion will be less conservative than those generated utilizing the circle criterion. Another significant difference between the two absolute stability criteria is that the circle criterion proves global exponential stability while the Popov criterion only guarantees global asymptotic stability [22].

## 4.4 The Siljak Transformation

### 4.4.1 Siljak Transformation Theory

As stated earlier, the circle criterion (case 2) and the Popov criterion require the system A matrix to be strictly Hurwitz. Siljak's transformation method circumvents this requirement by introducing a feedback gain which creates a transformed Hurwitz system [5]. Starting with the Lur'e system shown in Figure 4.1, the linear time-invariant (LTI) system's minimal realization transfer function leads to the following loop transformation model when Siljak's method is applied [22]:

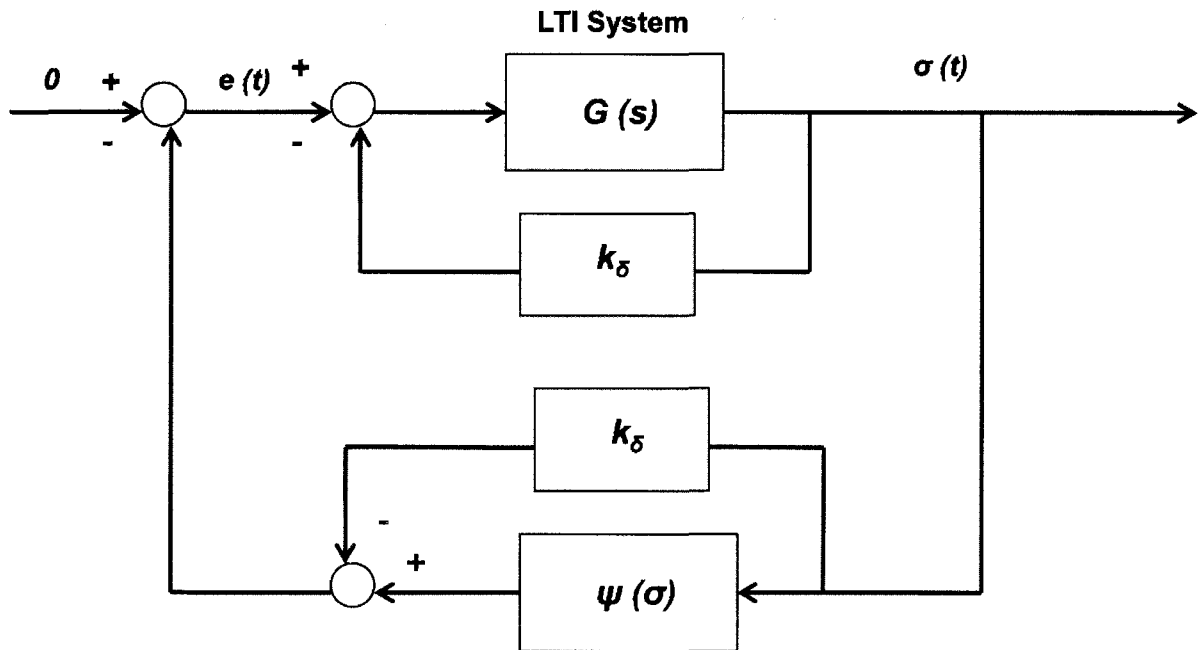


Figure 4.7: Loop Transformation

The above loop transformation results in the following expression for the transformed system [5]:

$$G_{tr}(s) = \frac{G(s)}{1+k_\delta G(s)} \quad (4.10)$$

Using Equation 4.9,  $k_\delta$  should be varied until  $G_{tr}(s)$  is strictly Hurwitz. The transformed  $\mathbf{A}$  matrix can be seen in the equation [5]:

$$A_{tr} = A + k_\delta BC \quad (4.11)$$

The transformed nonlinearity can be seen in the expression [5]:

$$\psi_{tr}(\sigma) = \psi(\sigma(t)) - k_\delta \sigma(t) \quad (4.12)$$

Because of the subtracted portion in the above equation, there will be a limit on  $\sigma(t)$ , denoted as  $v$ , where any input greater than that limit will lead to a sector violation. This means a system with an input greater than  $v$  will not be guaranteed absolute stability. The new transformed state space system is seen in the form [5]:

$$\dot{x}(t) = A_{tr}x(t) + B\psi_{tr}(\sigma) \quad (4.13)$$

$$\sigma(t) = Cx(t) \quad (4.14)$$

The sector limits ( $\alpha = 0, \beta$ ) are still determined by applying condition two of the circle criterion or the Popov criterion to the non-transformed system. These sectors can be shown in the following inequality [5]:

$$0 \leq \sigma\psi_{tr}(\sigma) \leq \beta\sigma^2, \text{ where } |\sigma| < \sigma_{\max} \text{ and } \psi_{tr}(0) = 0 \quad (4.15)$$

The Siljak transformation's main benefit is it allows the control designer to establish absolute stability over a finite domain. Whether or not a region possesses



asymptotic stability depends on the type of nonlinearity which needs to be accounted for through absolute stability. Because of the negative portion in the nonlinear function equation, dead zone regions do not possess guaranteed absolute stability over a finite domain even using the Siljak transformation. This is because the sector bounds would be immediately violated as soon a  $\sigma(t)$  was greater than zero, but ideal relay nonlinearities do not suffer from the same handicap. Ideal relays result in asymptotic stability because the nonlinearity has a positive slope at the origin; therefore,  $\sigma_{max} > 0$  for saturation nonlinearities and a finite domain of absolute stability exists. The figure below helps demonstrate this concept that dead zone regions do not possess absolute stability while ideal relay regions possess absolute stability over a finite domain. In the figure below the transformed system is not guaranteed to be absolutely stable when the transformed nonlinearity enters the second or fourth quadrant.

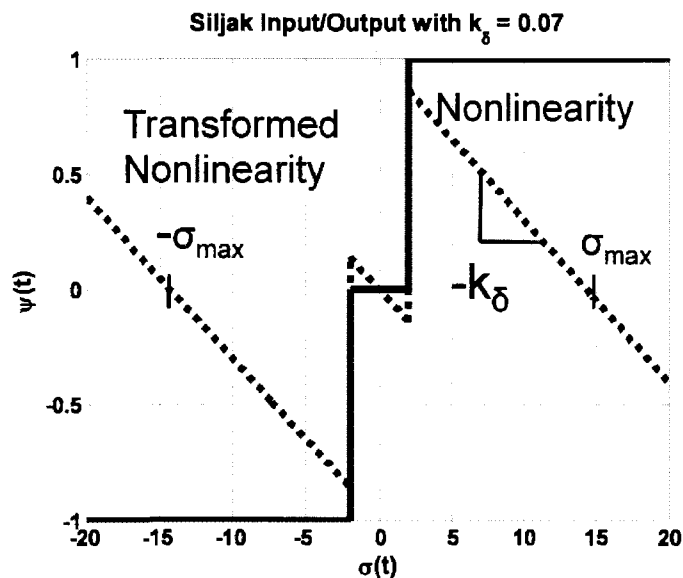


Figure 4.8: Siljak Transformed Input/Output

The result of the Siljak transformation with respect to dead zone and ideal relay match how the phase plane controller is designed to operate. When in the dead zone region there is no firing only drifting compared to when the system is in the ideal relay portion it is firing and asymptotically stable.

#### 4.4.2 Siljak Transformation Example

Violating the finite domain of absolute stability will result in an unstable system as can be seen in the following example. To demonstrate how the finite domain of absolute stability functions, a pitch control system will be analyzed at  $t = 60$  seconds. This is important because the pitch plant is open loop unstable in the pitch axis at this frozen-time without closed loop control because the system is not Hurwitz and has a maximum, real eigenvalue greater than zero. The first step is to perform a linear analysis to find the minimum  $k_\delta$  value necessary to transform the pitch plant into a Hurwitz system.

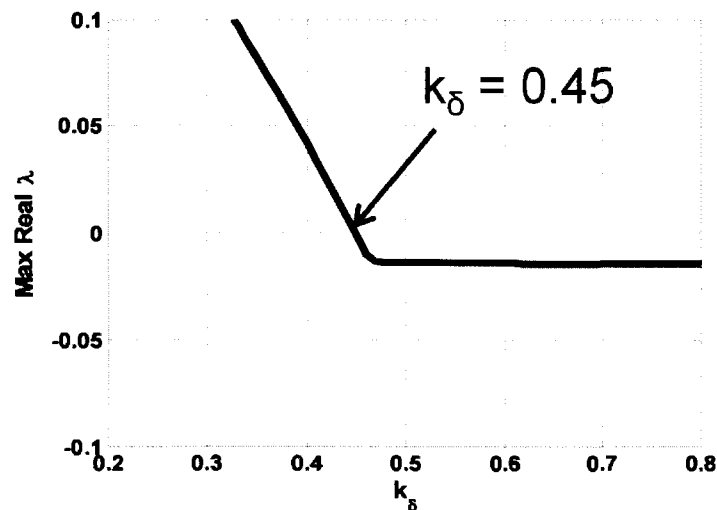


Figure 4.9: Linear  $k_\delta$  Analysis

Once  $k_\delta$  has been determined, it is now possible to plot the transformed nonlinearity in order to determine  $v$  which will define the maximum input amplitude the nonlinear element can sustain before it becomes unstable.

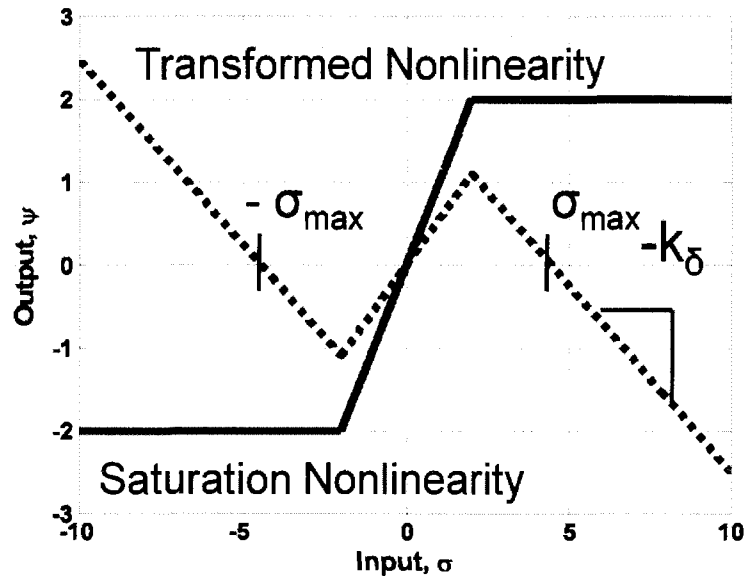


Figure 4.10: Pitch Control Transformed Nonlinearity

It can be seen in Figure 4.10 that  $\sigma_{max} = 4.5$ , thereby, defining the limit to the nonlinear element input amplitude,  $\sigma$ . Time domain simulation confirms this  $\sigma_{max}$  value to be a conservative estimate. Figure 4.11 demonstrates the system maintains stability with  $\sigma = 5.0$  input into the system:

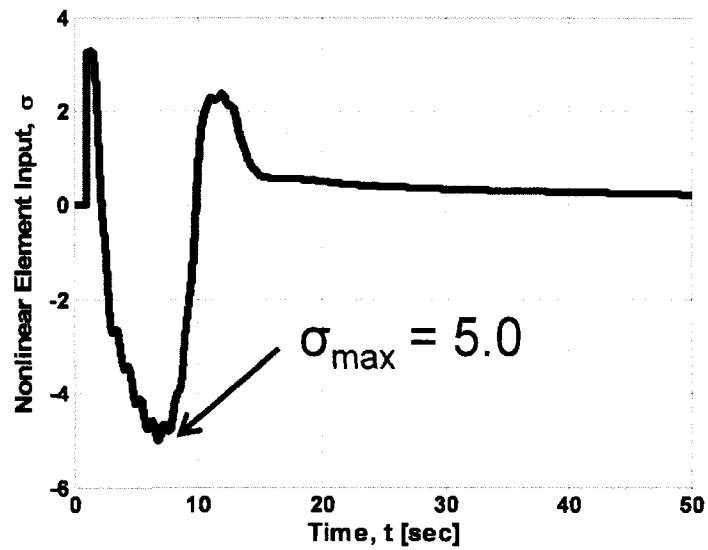


Figure 4.11: Time Domain Simulation for Pitch Example ( $\sigma = 5.0$ )

However, when inputs greater than 5.0 are encountered, the system response diverges, indicating an unstable system.

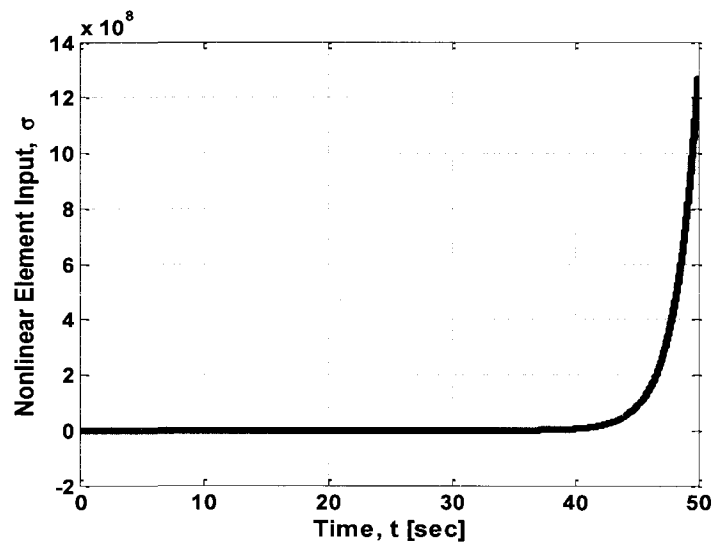


Figure 4.12: Time Domain Simulation for Pitch Example ( $\sigma > 5.0$ )

These results indicate that  $\sigma_{max} = 4.5$  is a serviceable estimate for the maximum nonlinear input amplitude for the Pitch Control System. The finite domain of absolute stability can be utilized in nonlinear systems as an abort condition. If  $\sigma > \sigma_{max}$ , the current maneuver should be aborted.

#### 4.5 Kharitonov's Theorem

Determining stability for a particular nominal set of parameters at a particular time is useful to the control engineer; however, in order to fully establish a full spectrum picture of a system's stability, it is desirable to explore a system's parametric uncertainty. This can be accomplished through several different techniques both analytical and probabilistic. Dobra and Trusca established a method for combining Kharitonov's theorem with absolute stability based on the Popov criterion [25]. Using this method, it will be possible to prove absolute stability for a system with uncertain parameters.

Kharitonov's theorem establishes an interval plant family with minima and maxima for each uncertain parameter. From here, the theory builds four polynomials for the interval plant's numerator and four polynomials for the interval plant's denominator. Combining these sets of numerators and denominators results in sixteen boundary plants that define the limits of a system's parametric uncertainty [26]. The interval plant takes the form [25]:

$$G(s, p, q) = \frac{N(s, q)}{D(s, p)} \quad (4.16)$$

The numerators and denominators in the above interval plant are defined by the expressions [25]:

$$N(s, q) = q_0 + q_1 s + q_2 s^2 + q_3 s^3 + \dots \quad (4.17)$$

$$D(s, p) = p_0 + p_1 s + p_2 s^2 + p_3 s^3 + \dots \quad (4.18)$$

Each value of  $q_i$  and  $p_i$  above represents a value which is governed by one of the two expressions [25]:

$$q_i \in [\underline{q_i} \quad \overline{q_i}] \quad (4.19)$$

$$p_i \in [\underline{p_i} \quad \overline{p_i}] \quad (4.20)$$

For both the numerator and denominator, it is necessary to compute the Kharitonov polynomials in order to map out the parametric space. The numerator Kharitonov polynomials are determined through the family of expressions where the negative and positive superscripts denote minima and maxima respectively [25]:

$$N_{k1}(s) = q_0^- + q_1^- s + q_2^+ s^2 + q_3^+ s^3 + \dots \quad (4.21)$$

$$N_{k2}(s) = q_0^+ + q_1^- s + q_2^- s^2 + q_3^+ s^3 + \dots$$

$$N_{k3}(s) = q_0^+ + q_1^+ s + q_2^- s^2 + q_3^- s^3 + \dots$$

$$N_{k4}(s) = q_0^- + q_1^+ s + q_2^+ s^2 + q_3^- s^3 + \dots$$

The denominator Kharitonov polynomials are similarly computed using the family of expressions:

$$D_{k1}(s) = p_0^- + p_1^- s + p_2^+ s^2 + p_3^+ s^3 + \dots \quad (4.22)$$

$$D_{k2}(s) = p_0^+ + p_1^- s + p_2^- s^2 + p_3^+ s^3 + \dots$$

$$D_{k3}(s) = p_0^+ + p_1^+ s + p_2^- s^2 + p_3^- s^3 + \dots$$

$$D_{k4}(s) = p_0^- + p_1^+ s + p_2^+ s^2 + p_3^- s^3 + \dots$$

The combination of the above family of expressions creates sixteen Kharitonov systems which can each be analyzed via an absolute stability criterion. Starting with the interval plant similar to one in Dobra and Trusca [25]:

$$G(s, p, q) = \frac{q_1 s + q_0}{s^4 + q_3 s^3 + q_2 s^2 + q_1 s + q_0} \quad (4.23)$$

Defining the parameter space:

$$q_1 \in [1 \ 2], q_0 \in [2 \ 3] \quad (4.24)$$

$$p_3 \in [9 \ 10], p_2 \in [10 \ 13], p_1 \in [7 \ 9], p_0 \in [1 \ 2] \quad (4.25)$$

These values result in the Kharitonov polynomials:

$$N_{k1}(s) = 1 + 2s \quad (4.26)$$

$$N_{k2}(s) = 2 + 2s$$

$$N_{k3}(s) = 2 + 3s$$

$$N_{k4}(s) = 1 + 3s$$

$$D_{k1}(s) = 1 + 7s + 13s^2 + 10s^3 + s^4 \quad (4.27)$$

$$D_{k2}(s) = 2 + 7s + 10s^2 + 10s^3 + s^4$$

$$D_{k3}(s) = 2 + 9s + 10s^2 + 9s^3 + s^4$$

$$D_{k4}(s) = 1 + 9s + 13s^2 + 9s^3 + s^4$$

These Kharitonov polynomials create sixteen transfer functions which can be evaluated using absolute stability techniques such as circle criterion and the Popov Criterion. Although Dobra and Trusca only discuss using Kharitonov's theorem in their paper, it is also possible to apply condition two of the circle criterion because all sixteen Kharitonov plants will be strictly Hurwitz. Below is a graph displaying the results of a condition two circle criterion test for the upper sector limit,  $\beta$ :

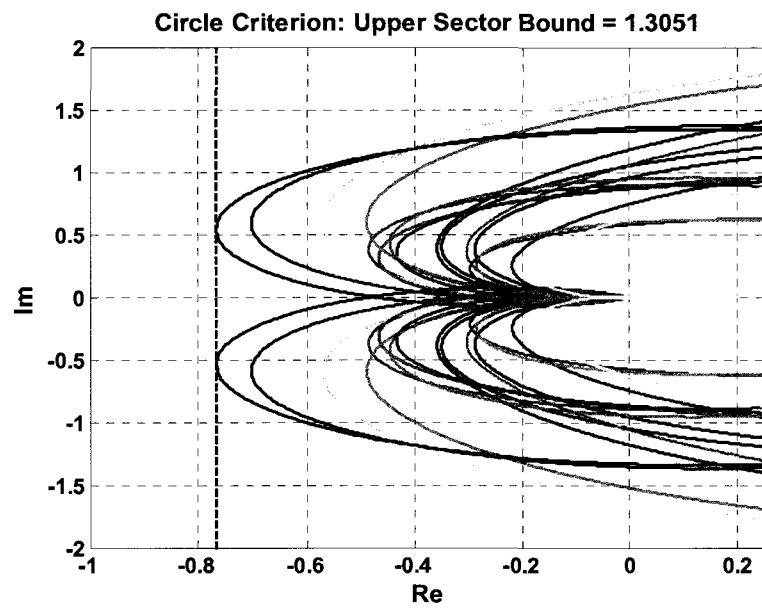


Figure 4.13: Kharitonov Based Circle Criterion (Case 2) Example

It is also useful to examine the Popov plot of the same sixteen Kharitonov plants and determine the worst case condition:

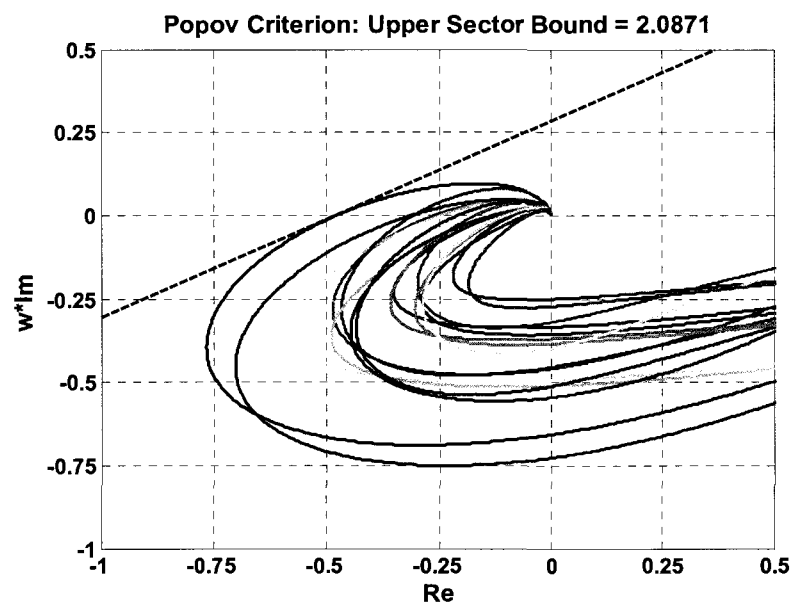


Figure 4.14: Kharitonov Based Popov Criterion Example



As can be seen in the above two plots, the Popov criterion is less conservative than the circle criterion which means it will provide more accurate stability margins predictions and a wider variety of nonlinear elements can be utilized in a system while still maintaining absolute stability.

#### 4.6 Stability Margin Prediction

To effectively compare nonlinear stability techniques, it is necessary to develop a method for determining stability margins. With absolute stability it is possible to predict gain margins through the following process. This method will be valid for absolute stability techniques such as circle criterion (case 2) or the Popov criterion. First, it is necessary to review the Lur'e model:

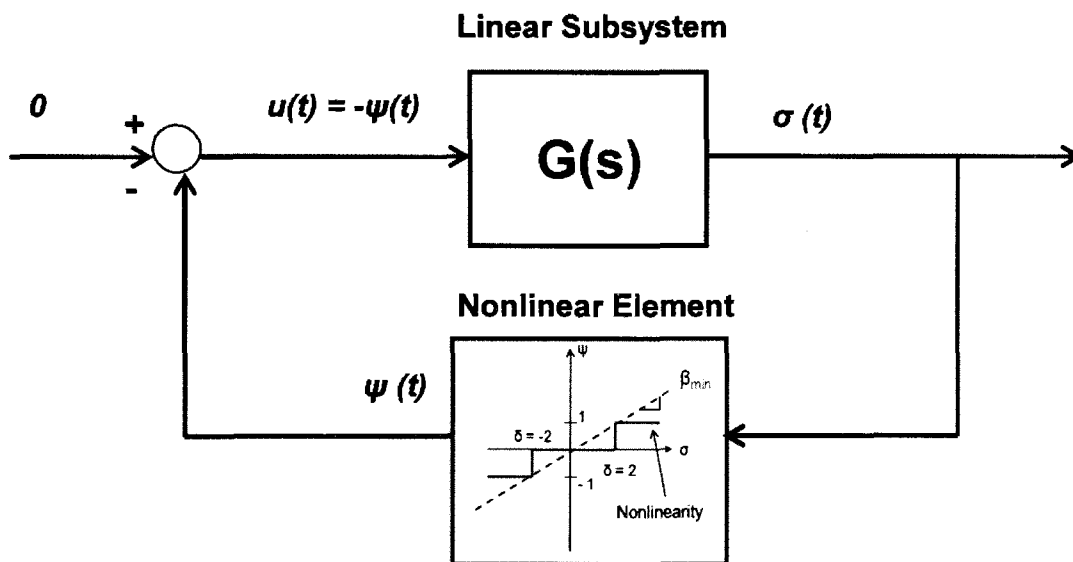
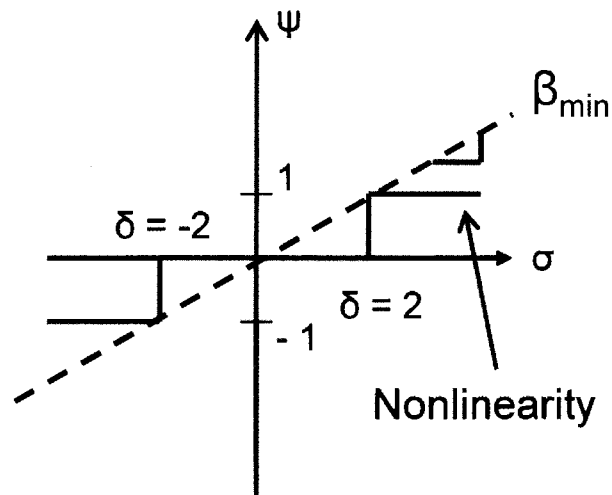


Figure 4.12: Lur'e Model

From the above linear system, it is possible to determine the actual upper sector limit,  $\beta$ , using either the circle criterion (case 2) or the Popov criterion. Next, it is

necessary to determine from the nonlinear element the required upper sector limit,  $\beta_{min}$ , as is demonstrated in Figure 4.14:



**Figure 4.13: Determining the Required Upper Sector Limit,  $\kappa$**

The difference between  $\beta$  and  $\beta_{min}$  results in a gain margin region, in which the system is absolutely stable. As long as  $\beta \geq \beta_{min}$ , the system is considered to be stable. This region is depicted for circle criterion in Figure 4.13:

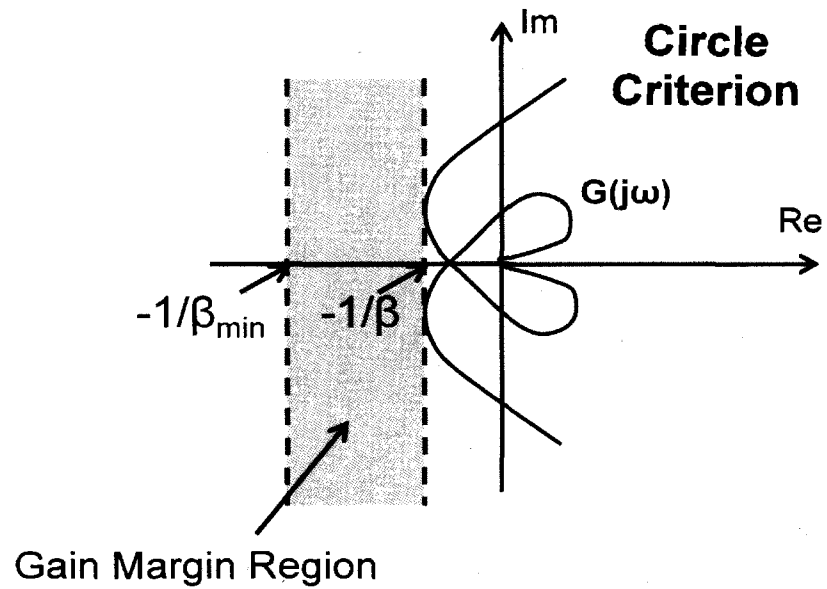


Figure 4.14: Gain Margin Region for Circle Criterion

The same region is illustrated for the Popov criterion in Figure 4.15:

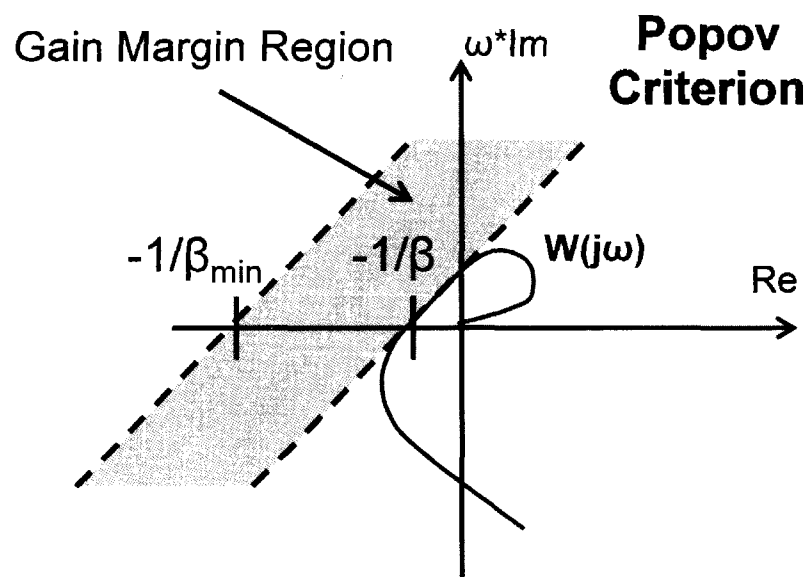


Figure 4.15: Gain Margin Region for Popov Criterion

Taking advantage of this gain margin region, Equation 4.28 is developed to determine the gain margin for a particular system.

$$\text{Gain Margin} = dB \left( \beta / \beta_{\min} \right) \quad (4.28)$$

The gain margin prediction method developed in this section will be tested later in Chapter 5 with regards to a phase plane controlled roll system. Its effectiveness and conservatism will be compared to other nonlinear stability analysis techniques.

#### **4.7 Absolute Stability Conclusions**

Absolute stability includes useful techniques such as the circle criterion and the Popov criterion. These techniques are critical in determining sector bounds for which systems with nonlinear elements can be considered stable. In general, circle criterion (case two) is the easiest both conceptually and computationally to implement; however, the Popov criterion does have an advantage. The Popov criterion is less conservative than the circle criterion (as will be demonstrated in Chapter 5) which means that a more accurate picture of how the system operates is achieved. Siljak's transformation offers obvious benefits with its ability to allow for absolute stability even with non-Hurwitz poles while conveniently helping to explain the phase plane controller's stable and neutrally stable regions. Finally, a method for harnessing absolute stability for predicting gain margins is developed.

## Chapter 5: Application to a Phase Plane Control System

In the following section techniques such as PWM analysis, describing functions, circle criterion, Popov criterion, and Kharitonov's theorem discussed in the previous chapters will be applied to a roll control system. Additionally, the SIMULINK tool will be utilized to simulate the nonlinear system in order to verify the results obtained from the analytical techniques. The primary concern of this analysis is to determine whether or not the system meets the design criteria of 6 dB gain margin and 10 dB flex dynamics attenuation.

### 5.1 Flex Filter

Many aerospace systems currently employ elliptic filters for low pass filtering to stabilize the spacecraft by attenuating high-frequency noise while allowing the low-frequency spacecraft dynamics to be fed back to the controller. An elliptic filter is unique in that it is "equiripple in both the passband and the stopband" which is in contrast to Butterworth filters which are "monotonic in the passband and in the stopband" and Chebyshev filters which contain an "equiripple characteristic in the passband and monotonic in the stopband [27]. Using a filter with equiripple provides the advantage of being able to use a smaller order filter and additionally for a given cutoff frequency, "the transition band is small as possible" [27]. The latter advantage means that an elliptic filter "yields the sharpest cutoff frequency selective filter" for a filter of a given order [27]. When designing elliptic functions, it is important to keep in mind "elliptic filters must have both poles and zeros" in order "to obtain equiripple error in both the passband

and stopband” [27]. The current filter was designed using MATLAB’s “ellip” function in which the engineer specifies the filter order, the ripple, the stopband minimum attenuation, and the cutoff frequency [28]. Figure 5.1 shows the Bode plot for the current filter.

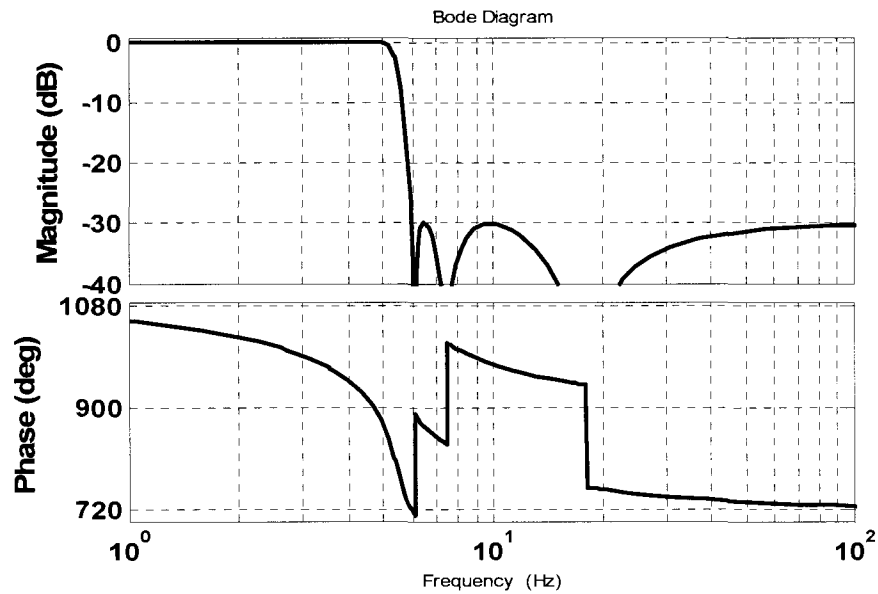


**Figure 5.1: Current Flex Filter**

The current filter above in Figure 5.1 is a sixth order filter with a ripple of 0.01, a stopband attenuation of -30 dB, and a cutoff frequency of 5 Hz. Using the current filter, roll stability will be analyzed and simulated:

## 5.2 PWM Results

The PWM method provides a method for linearly approximating a nonlinear roll control system. This linear approximation is necessary for classical control tools to be applied to the system. In the following section, nonlinear elements will be linearly approximated, the Nichols plot of the linearized system will be examined, and the

singular value decomposition (SVD) will be analyzed in order to determine if the current system satisfies the design criteria.

### 5.2.1 PWM Linear Approximation

Because the phase plane controller exhibits nonlinear behavior, linear approximation is required before classical techniques such as the Nichols Chart and SVD can be applied. As discussed in Chapter 2, linear approximation is accomplished by cutting the closed loop system at the dead zone nonlinearity to create an open loop system. This system is then scaled by the dead zone value in order to approximate the nonlinear behavior of the phase plane controller. It is worth noting that this method does not account for the ideal relay nonlinearity. In the following two subsections, the PWM-based analysis technique will be utilized to generate the Nichols Chart and the SVD of the flex dynamics.

### 5.2.2 Nichols Chart Results

After performing PWM linear approximation on the nonlinear elements by scaling the system response by  $1/\delta = 0.5$  degrees, it is now possible to evaluate the stability and performance of the system. The Nichols chart allows the control engineer to see both magnitude and phase information on one chart. In order to fully understand the spacecraft stability, it is desirable to examine both the rigid and flex dynamics. The Nichols chart will allow for the gain margin to be easily determined visually while, simultaneously, providing a means for examining each filter's performance with respect to high-frequency flex dynamics. A gain margin of 6 dB and a high-frequency peak of

less than -10 dB will be desired in a design. Figure 5.2 contains a Nichols chart depicting the frequency response.

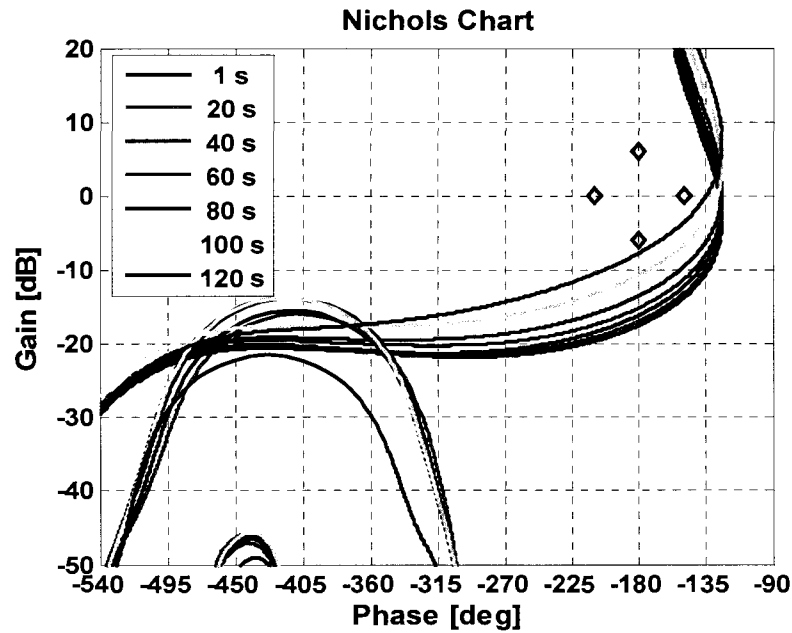


Figure 5.2: PWM Nichols Chart

The current flex filter fulfills the requirement for 6 dB rigid margin and 10 dB attenuation for high-frequency peaks. The table below again summarizes the gain margin results from the Nichols chart.

Time [sec]	Gain Margin [dB]
1	17.5
20	17.0
40	16.2
60	15.1
80	13.5
100	10.7
120	7.7

Table 5.1: PWM Results



The table above demonstrates that with the current flex filter, the system meets the gain margin requirements of 6 dB, even with flex dynamics.

### 5.2.3 Flex Dynamics Results

It is now necessary to consider the SVD response for the flex dynamics in order to determine to what extent the current filter attenuates high-frequency noise in the system's dynamic response. This is a relatively simple process and the result can be seen below in Figure 5.3.

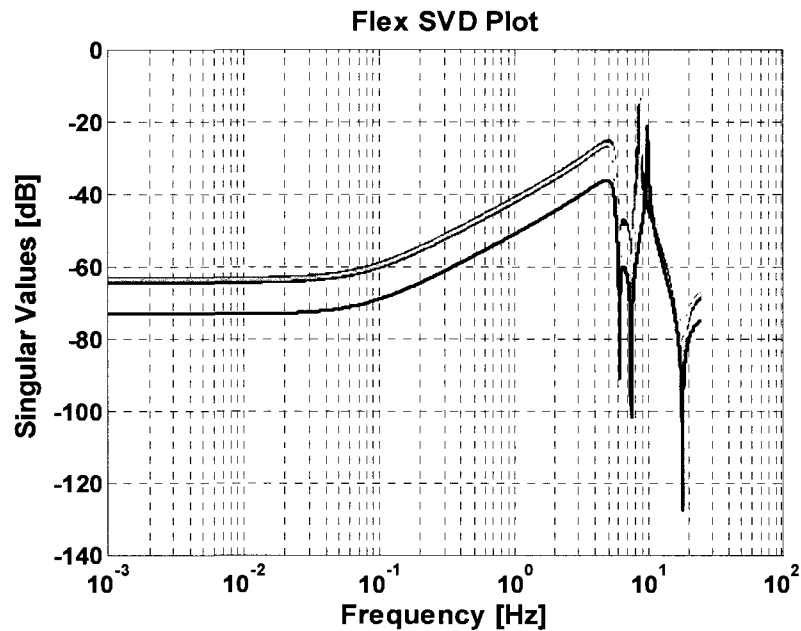


Figure 5.3: PWM SVD Plot

Examining the SVD plot in Figure 5.3 above, it can be seen that the maximum flex response is at approximately -15 dB. The SVD plot agrees with the Nichols chart for the high-frequency flex dynamics. This result satisfies the design criterion for 10 dB flex dynamics attenuation.

### 5.3 Describing Function Results

The phase plane controller's nonlinearity can primarily be modeled as a dead zone combined with an ideal relay. The describing function for dead zone was shown earlier [16]:

$$N_1(A_1) = \frac{2k}{\pi} \left[ \frac{\pi}{2} - \sin^{-1} \left( \frac{\delta}{A_1} \right) - \frac{\delta}{A_1} \sqrt{1 - \frac{\delta^2}{A_1^2}} \right] \quad (5.1)$$

On the other hand, the describing function for an ideal relay was shown [16]:

$$N_2(A_2) = \frac{4D}{\pi A_2} \quad (5.2)$$

Using the procedure developed in Section 3.2.3 to create a combined describing function for these two nonlinear elements in series results in the expression.

$$N(A_1) = \frac{4D}{\pi N_1(A_1) A_1} \quad (5.3)$$

In the above expressions,  $D$  is the saturation output,  $\delta$  is the dead zone width, and  $A_I$  is the input amplitude. This describing function will be used in both describing function techniques that determine whether or not the nonlinear system will limit cycle.

#### 5.3.1 Nichols-Based Intersection Analysis

By plotting the linear portion of the system for first stage times ranging from 1 to 120 seconds and comparing those results to a plot of  $-1/N(A)$ , it is possible to discover whether or not the nonlinear system will encounter unstable limit cycling. If the linear plots intersect with the  $-1/N(A)$  plot, then a limit cycle may occur. This is by no means an

exact method for limit cycle determination; whereas, not every intersection will result in a limit cycle. It is important to remember, however, that if no intersection occurs, it is guaranteed there will be no unstable limit cycling in the nonlinear system. For the analysis below both rigid dynamics and flex dynamics are considered.

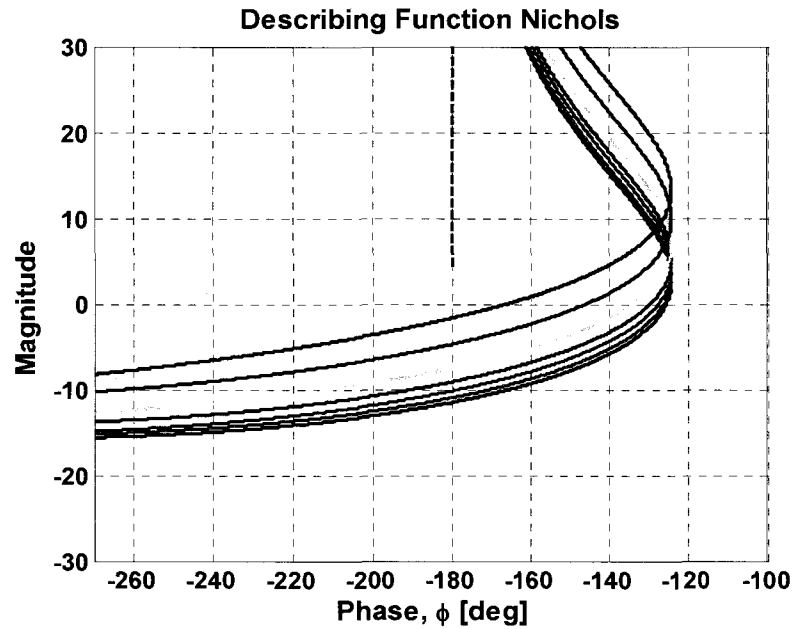


Figure 5.4: Describing Function Nichols Chart

Figure 5.4 above indicates that the linear frequency responses for the system at varying times do not intersect the negative, inverse describing function plot. Table 5.2 below summarizes the amount of gain that can be introduced into the system before limit cycling will occur.

<b>Time [sec]</b>	<b>Gain Margin [dB]</b>
1	15.4
20	14.9
40	14.1
60	13.0
80	11.4
100	8.6
120	5.6

**Table 5.2: Describing Function Nichols Chart Results**

Such a result is favorable because it demonstrates the filter successfully avoids additional limit cycling which would decrease system stability while increasing the amount of propellant consumed during roll maneuvers.

### **5.3.2 Gain Margin Tester**

Wu and Perng's method for determining the stability margins for limit cycles is a natural extension of the classical intersection method applied above for analysis. Using the gain margin tester developed in Chapter 3, it is possible to detect how much gain can be introduced into the nonlinear phase plane controlled roll axis before the system begins to undergo limit cycling. The gain margin will be analyzed versus amplitude as is necessary with describing functions.

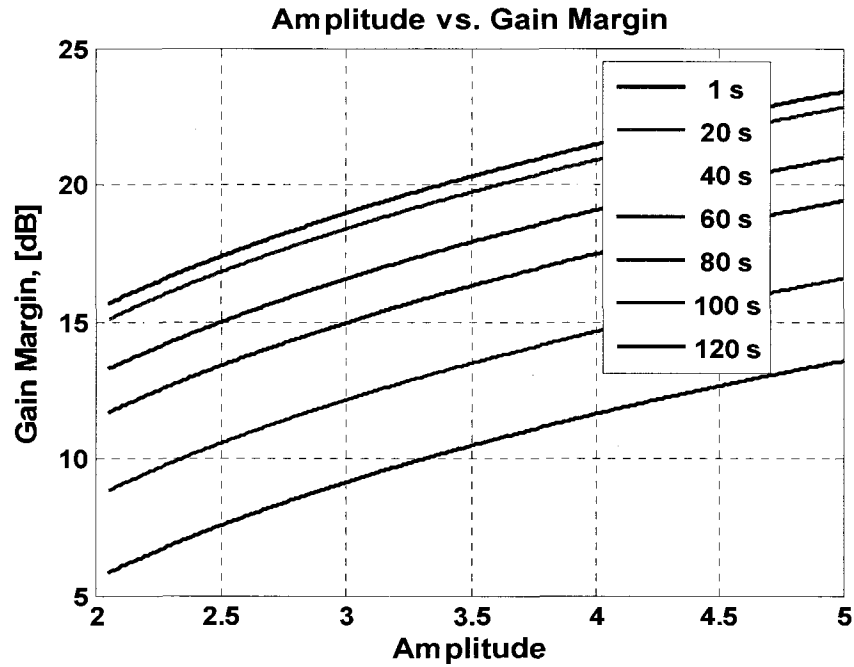


Figure 5.5: Describing Function Margin Tester Results

Gain margin is determined from the lowest value for each time. The most critical time is at  $t = 120$  seconds, and from the figure above it can be seen that the gain margin is 5.6 dB. It is important to note that the amplitude begins at  $A = 2$  because amplitudes less than this fall within the dead zone of the nonlinearity. For the purposes of this thesis, only limit cycling outside the dead zone will be of concern because they are the only limit cycles that will lead to excessive propellant usage. For each time, the minimum gain margin is selected as the critical and overall gain margin for the system. This result matches the results previously analyzed through the intersection method. The gain margin is clear because the plot of  $-1/N(A)$  is all at one phase while  $-1/N(A)$  exists across a range of magnitudes. The results are summarized in the table below:

Time [sec]	Gain Margin [dB]
1	15.4
20	14.9
40	14.1
60	13.0
80	11.4
100	8.6
120	5.6

**Table 5.3: Describing Function Margin Tester**

It is worth noting that the results obtained here using the margin tester directly match the results obtained by using the Nichols intersection method above. This demonstrates that both approach the same information from different viewpoints.

## 5.4 Absolute Stability Results

In this section, the absolute stability will be examined through the application of the circle criterion and the Popov criterion. First, it will be necessary to determine the sector requirement for the phase plane controller's nonlinearities. After that exercise, the  $k_\delta$  values for Siljak's transformation will be optimized in order to provide the largest upper sector limit,  $\beta$ , possible for the system. This will ensure the proper (and least conservative) gain margin is calculated using the circle criterion and the Popov criterion. After values for  $k_\delta$  have been obtained through the optimization, the circle criterion and the Popov criterion will be employed to determine  $\beta$  for each major frozen-time. Finally, robust, absolute stability will be examined by using Kharitonov's theorem.

### 5.4.1 Sector Requirements

Before absolute stability analysis techniques such as circle criterion and the Popov criterion can be applied to the system, it is necessary to determine the minimum  $\beta$  required for the phase plane controller's nonlinearities defined earlier as  $\kappa$ . As previously discussed in Chapter 3 and in Section 5.3, the phase plane controller incorporates a dead zone nonlinearity in series with an ideal relay as can be seen in Figure 5.6.

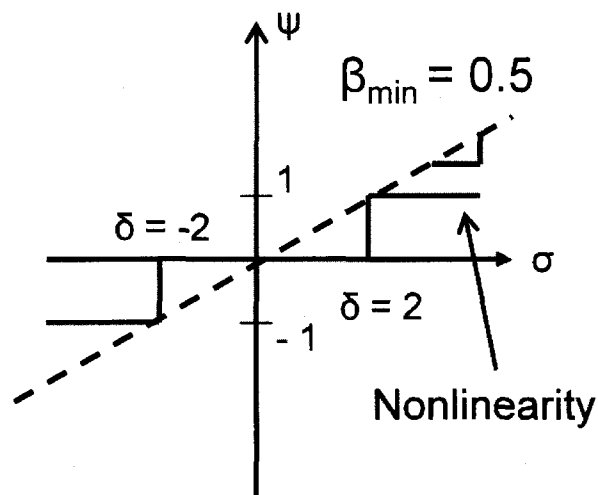


Figure 5.6: Nonlinear Element with Sector Requirements

The dead zone is equal to 2 degrees while the relay outputs a simple  $\pm 1$  depending on the sign of the input  $\sigma$ . A positive ideal relay output corresponds to a positive thruster firing in the phase plane while a negative relay output indicates a negative thruster firing. These values create a nonlinear element as shown by the red line in Figure 5.6. The nonlinearity requires a  $\kappa$  equal to 0.5 because that is the minimum slope necessary for the nonlinearity to fit inside the sector. When the circle criterion or Popov criterion is utilized to determine the linear system's  $\beta$ , it is critical that  $\beta$  is greater

than or equal to 0.5 to guarantee absolute stability. In order to determine the gain margin with regards to absolute stability, it is necessary to consider how much gain could be added to the linear system before  $\beta = 0.5$ , therefore, violating the sector condition. It can be seen that the following expression can be utilized to determine the gain margin once  $\beta$  is known for a given system.

$$\text{Gain Margin} = dB\left(\beta/\kappa\right) = dB\left(\beta/0.5\right) \quad (5.4)$$

#### 5.4.2 $k_\delta$ Optimization

When applying the circle criterion and the Popov criterion for absolute stability, it is necessary to consider the linear system's poles. Particularly, the designer must know whether or not the linear system is strictly Hurwitz. For circle criterion, both case two and case three require all poles to be strictly Hurwitz while the Popov criterion requires strictly Hurwitz poles as well [10]. Performing eigenanalysis upon the linear system results in three poles at  $s = 0$  for all times in the first stage. This result indicates neither the circle criterion nor the Popov criterion can be utilized to guarantee absolute stability without a modification to the system. The modification required is the Siljak transformation which allows for the linear system to be modified by closing the loop on the linear system with negative feedback and gain,  $k_\delta$ . Siljak's transformation makes the system absolutely stable; however, optimized values for  $k_\delta$  should be selected in order to increase stability by maximizing  $\beta$ . The first critical step in determining optimal  $k_\delta$  values is ensuring all values being considered will lead to a Hurwitz system.



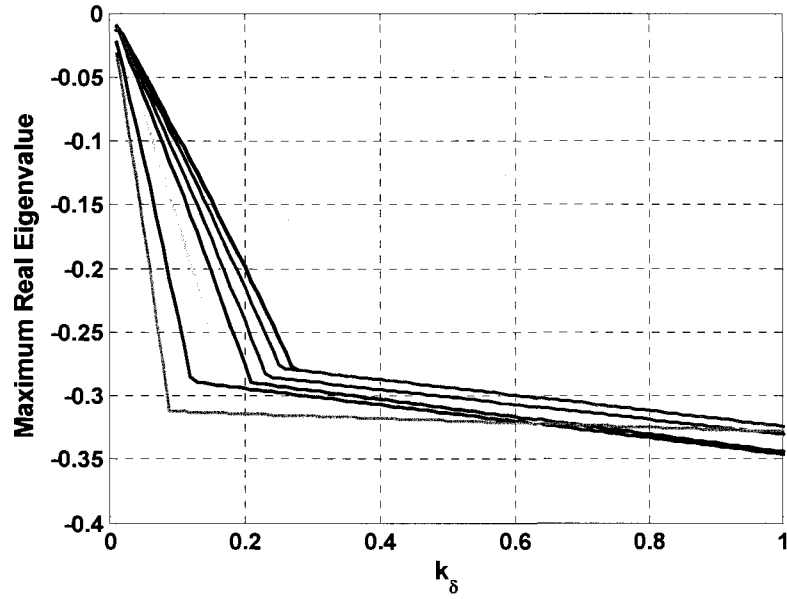


Figure 5.7:  $k_\delta$  versus Maximum Real Eigenvalues

Figure 5.7 above shows that any value satisfying the following inequality in Equation 5.5 will guarantee a Hurwitz system.

$$0 < k_\delta \leq 1 \quad (5.5)$$

Smaller values for  $k_\delta$  decrease the slope for the transformed nonlinearity in the following chart which results in a larger finite domain of absolute stability:

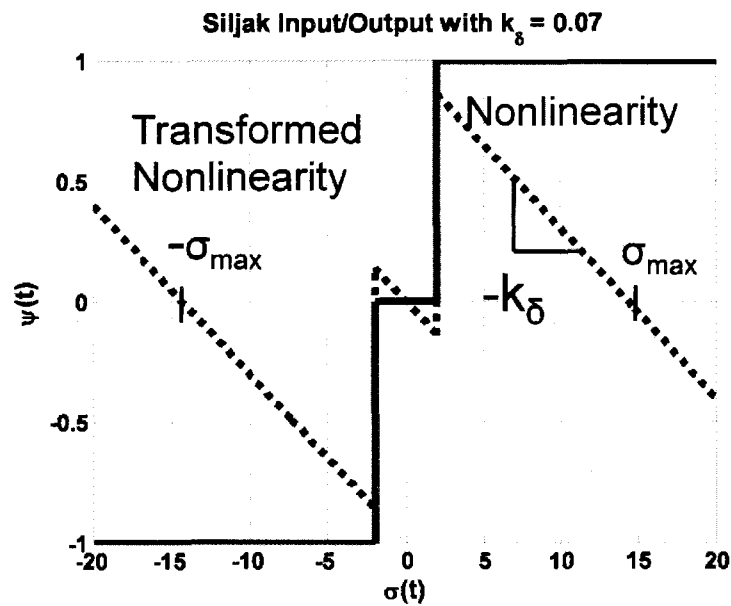


Figure 5.8: Siljak Transformed Input/Output Chart

Figure 5.8 illustrates how smaller  $k_\delta$  values increase the value for  $\sigma_{max}$ , the limit to the finite domain of absolute stability which increases the overall absolute stability of the system. For the phase plane control system, there is a  $k_\delta$  value which results in the largest  $\beta$  value. Graphical optimization is employed by way of charts plotting  $k_\delta$  versus  $\beta$  in order to select  $k_\delta$  with the maximum  $\beta$ . Using the current filter, a  $k_\delta$  set is determined using circle criterion and Popov criterion based graphical optimization. The circle criterion results can be seen in Figure 5.9:

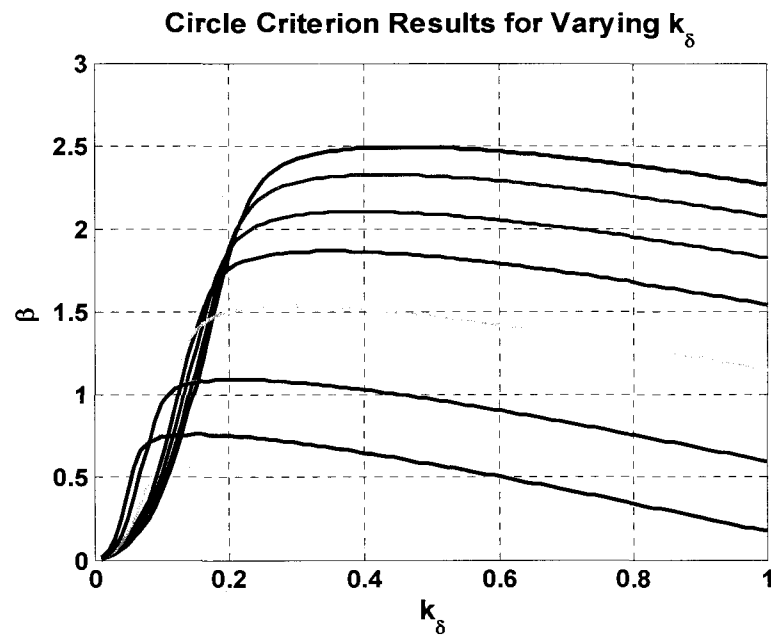


Figure 5.9: Circle Criterion  $k_\delta$  Graphical Optimization

The Popov results below provide less conservative  $\beta$  values:

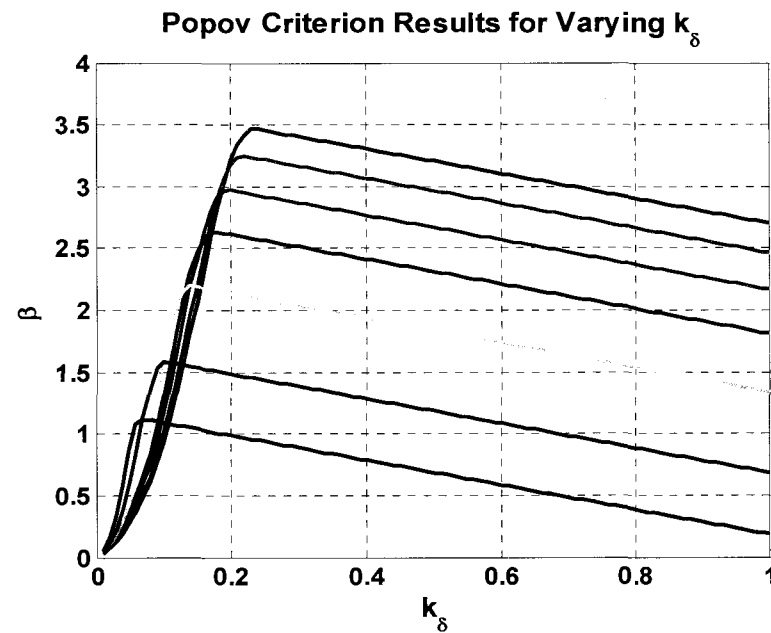


Figure 5.10: Popov Criterion  $k_\delta$  Graphical Optimization

The results from the two charts above are condensed in Table 5.4:

Time [sec]	$k_\delta$ Value		$\beta_{\max}$	
	Circle Criterion	Popov	Circle Criterion	Popov
1	0.45	0.24	2.5	3.5
20	0.42	0.22	2.4	3.3
40	0.39	0.20	2.1	3.0
60	0.34	0.17	1.9	2.7
80	0.29	0.14	1.6	2.2
100	0.22	0.10	1.1	1.6
120	0.15	0.07	0.8	1.1

**Table 5.4:  $k_\delta$  Graphical Optimization**

It can be seen in the results above that the Popov criterion results in smaller  $k_\delta$  values which means the system will possess a larger finite domain of absolute stability. In addition to this fact, it can also be seen that the Popov criterion should have larger  $\beta$  values which indicates the Popov criterion is a less conservative absolute stability technique than the circle criterion.

### 5.4.3 Circle Criterion and Popov Criterion Results

First, the results for the circle criterion (case two) for the current flex filter will be examined in Figure 5.11.

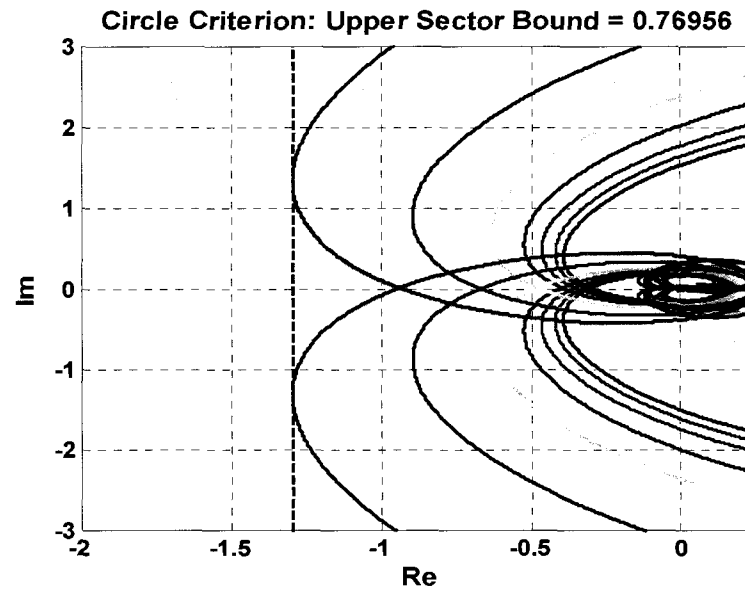


Figure 5.11: Circle Criterion Plot Results

While the current system meets the nominal requirement for  $\beta = 0.5$  with its  $\beta = 0.76956$ , it does not meet the 6 dB criteria of  $\beta = 1$  which we defined earlier. The Popov criterion supplies a less conservative absolute stability requirement as can be seen in the Popov plot in Figure 5.12:

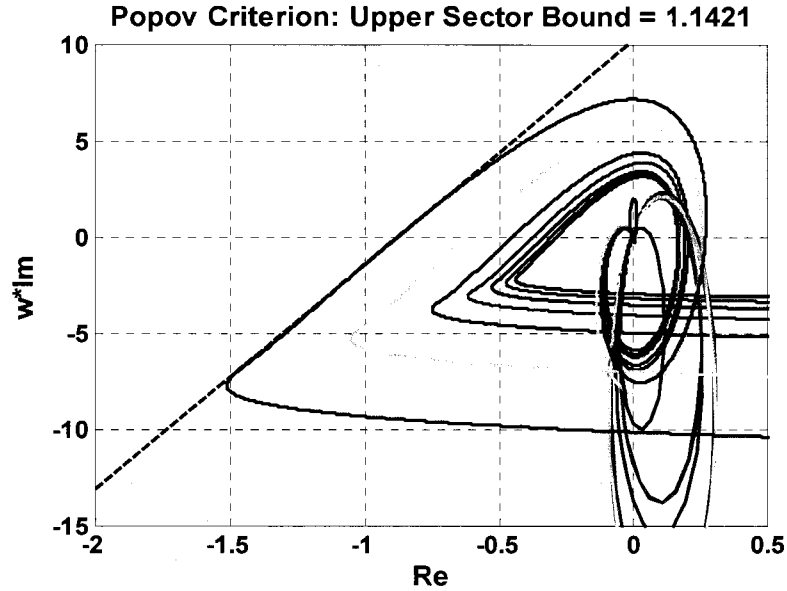


Figure 5.12: Popov Criterion Plot Results

In contrast to the circle criterion chart for the initial filter designed system, the Popov plot results in  $\beta = 1.1421$  which fulfills both the design criteria  $\beta$  requirements.

The results from the circle criterion and the Popov criterion are summarized in Table 5.5:

Time [sec]	Gain Margin [dB]	
	Circle Criterion	Popov Criterion
1	14.1	17.0
20	13.5	16.4
40	12.6	15.6
60	11.6	14.6
80	9.9	13.0
100	6.9	10.2
120	3.7	7.2

Table 5.5: Absolute Stability Gain Margin Comparison

As in Section 5.4.2, the above results show that the Popov criterion proves to be a less conservative technique than the circle criterion which is as predicted in the literature [13, 24].

#### 5.4.4 Finite Domain of Absolute Stability Determination

Because the Siljak transformation is used in the absolute stability analysis during Section 5.4.3, it is necessary to determine the finite domain of absolute stability. The first step is to perform a linear analysis to find the minimum  $k_\delta$  value necessary to transform the phase plane control system into a Hurwitz system.

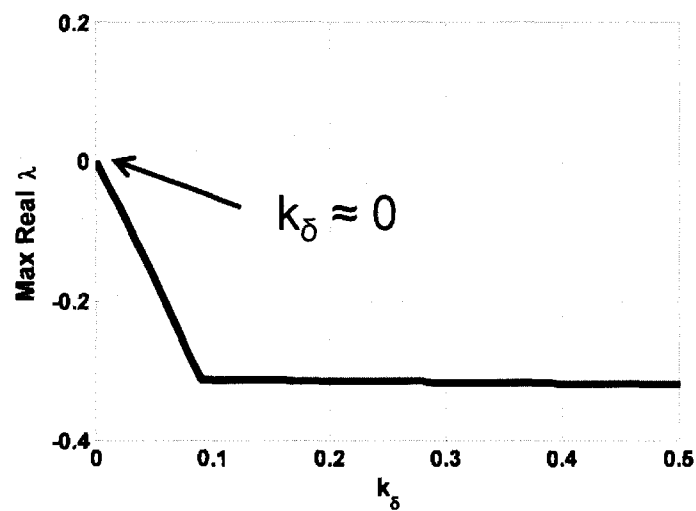


Figure 5.13: Linear  $k_\delta$  Analysis

For this particular case, the  $k_\delta$  required is so small that it can be considered to be zero. Now that  $k_\delta$  has been determined, it is now necessary to plot the transformed nonlinearity to find the  $v$  which defines the maximum input amplitude the nonlinear element can sustain before it becomes unstable.

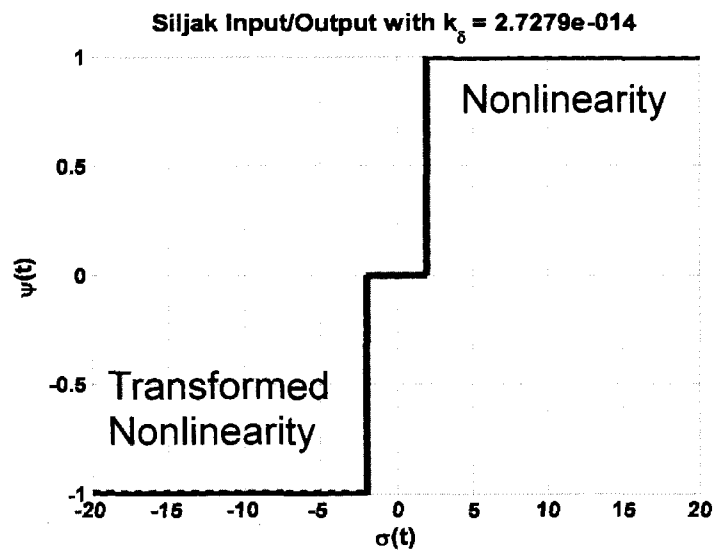


Figure 5.14: Input/Output Plot for Finite Domain Determination

From the plot above it can be noted that  $\sigma_{max} = \infty$  which means that there will be no practical finite domain of absolute stability for the nominal case. Using time domain simulation, it should be noted the system maintains stability an extremely large input,  $\sigma = 287.2$ , in the nominal case.

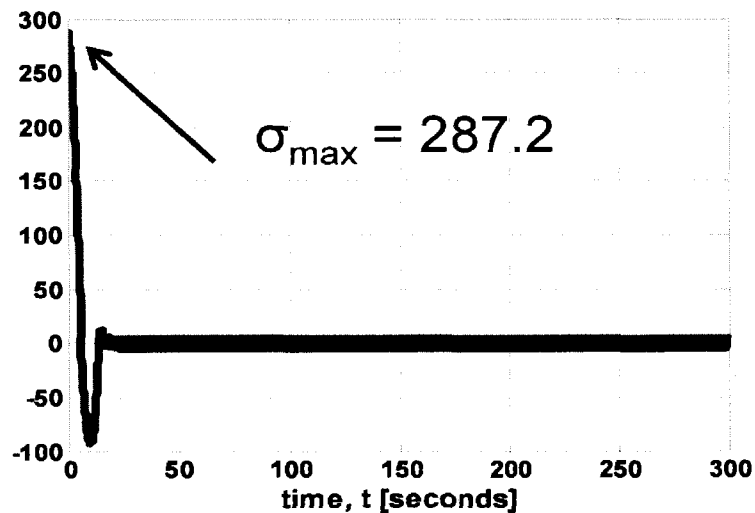


Figure 5.15: Time Domain Test for Finite Domain of Absolute Stability



This result indicates  $v \approx \infty$  for the roll control system; therefore, the finite domain of absolute stability does not need to be utilized as an abort condition for the system in this case.

#### 5.4.5 Kharitonov Theorem Results

Kharitonov's theorem of robust control was discussed earlier in Chapter 4, and now it will be applied to the phase plane controller. As a reminder, Kharitonov's theorem involves finding the minima and maxima for each element of the numerator and denominator polynomials from the transfer function. Kharitonov polynomials are used to construct sixteen new transfer functions with outline a system's robust boundaries. These boundaries can then be tested against the circle criterion and the Popov criterion. Ideally, all the first stage frozen times could be inputted into the Kharitonov algorithm and the outputted sixteen systems would all fulfill the circle criterion and Popov criterion. Unfortunately this is not the case. Transfer functions representing the system at 5 seconds were inputted into the system for the entire first stage and the results can be seen below in the circle criterion. It is important to note that because the Kharitonov theorem accounts for robustness,  $\beta$  is only required to be greater than or equal to 0.5 as opposed to the previous test where the 6 dB gain margin requirement necessitated a  $\beta$  greater than or equal to 1.

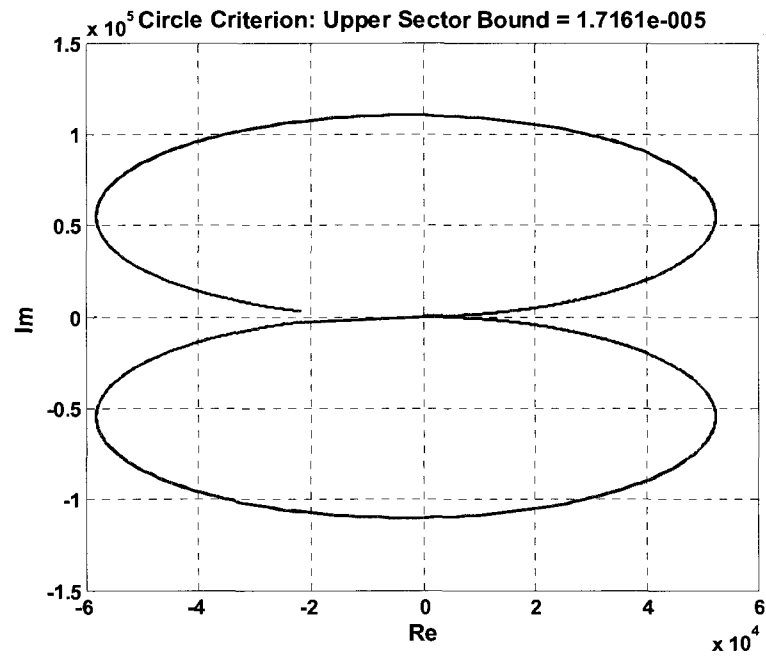


**Figure 5.16: Kharitonov Circle Criterion Plot**

With  $\beta = 1.7161 \text{ E-}5$ , it is clear the absolute stability requirement of  $\beta = 0.5$  cannot be met for circle criterion; furthermore, the Popov criterion cannot be met also ( $\beta = 0.00010225$ ) as can be seen Figure 5.14:

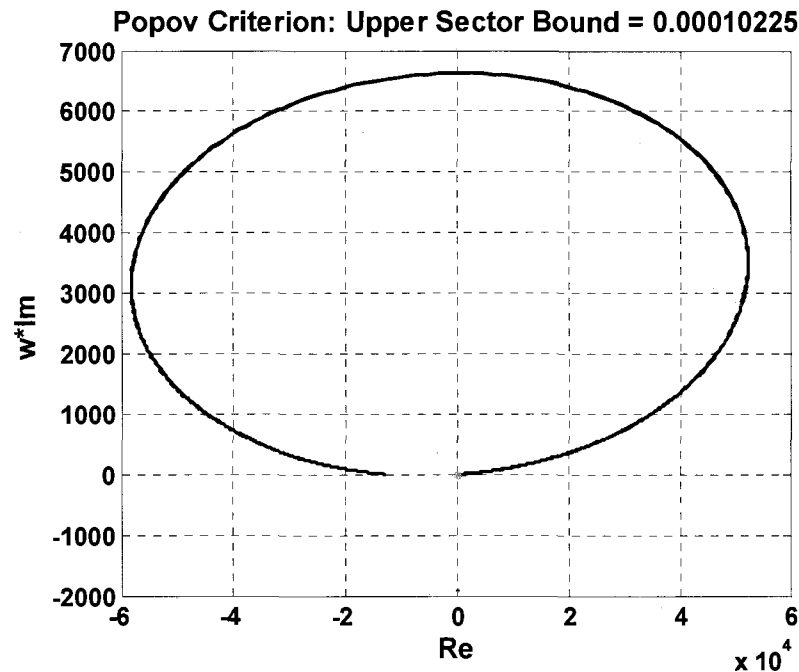


Figure 5.17: Kharitonov Popov Criterion Plot

Since considering all the first stage at once does not result in Kharitonov systems which pass the circle criterion and the Popov criterion, it is necessary to break the time varying system into twenty overlapping ten second intervals, thereby, creating a less conservative robustness criterion. The problem is that for the phase plane control system these intervals would have to be so small that they would practically be the same as frozen time analysis. Kharitonov theorem-based results become increasingly unreliable as the order of the system increases due to the technique's reliance on varying transfer function coefficients instead of the parameters themselves. For this reason, Kharitonov's theorem is too conservative for the purpose of phase plane control.

## 5.5 Time Domain Simulation

plane controlled system because the dead zone and ideal relay nonlinearities ensure the system's response will never diverge for a system featuring a stable plant and filter; however, with enough gain added to the system, it will eventually experience limit cycles with no dead zone drift. Penchuk, Hattis, and Kubiak define this stability condition as when the system will "periodically exceed angular rate limits before it is excited enough to cause forced attitude deadband oscillations," [1]. The phase plane controller will essentially become a bang-bang controller, thereby, invalidating the entire purpose of using a phase plane controller and resulting in a much greater amount of propellant consumed due to dramatically increased thruster on-times. Simulations considered were performed at the least stable time ( $t = 120$  second) in the first stage in order to achieve a worst case time scenario. Each simulation is run for 300 seconds with varying initial attitude errors between  $\pm 2$  degrees and initial rate errors between  $\pm 1$  degree per second. Additional simulations at varying times can be examined in Appendix A. The graph below shows energy as compared to the amount of gain introduced into the system.

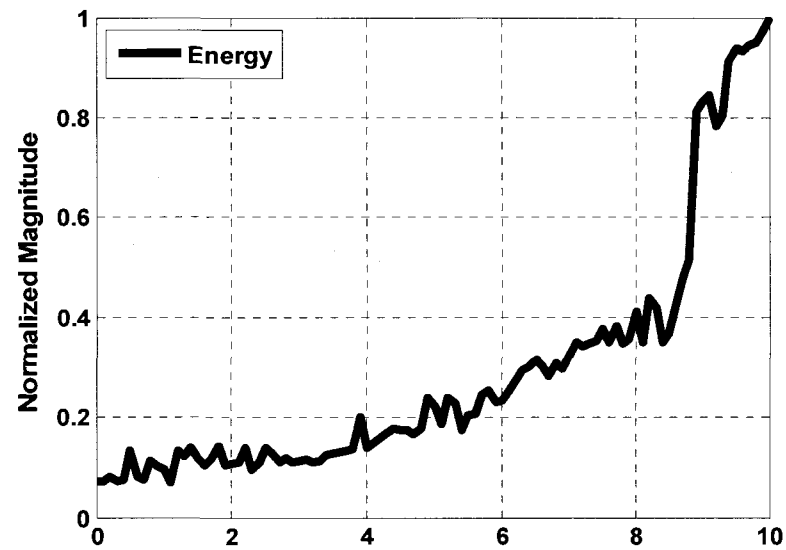


Figure 5.19: Gain vs. Energy (t = 120 sec)

Figure 5.16 demonstrates that there is a dramatic increase in energy at 8.3 dB indicating that as the gain margin point. The gradual development of unrestrained thruster firings and high-frequency limit cycles can be observed in the phase plane charts:

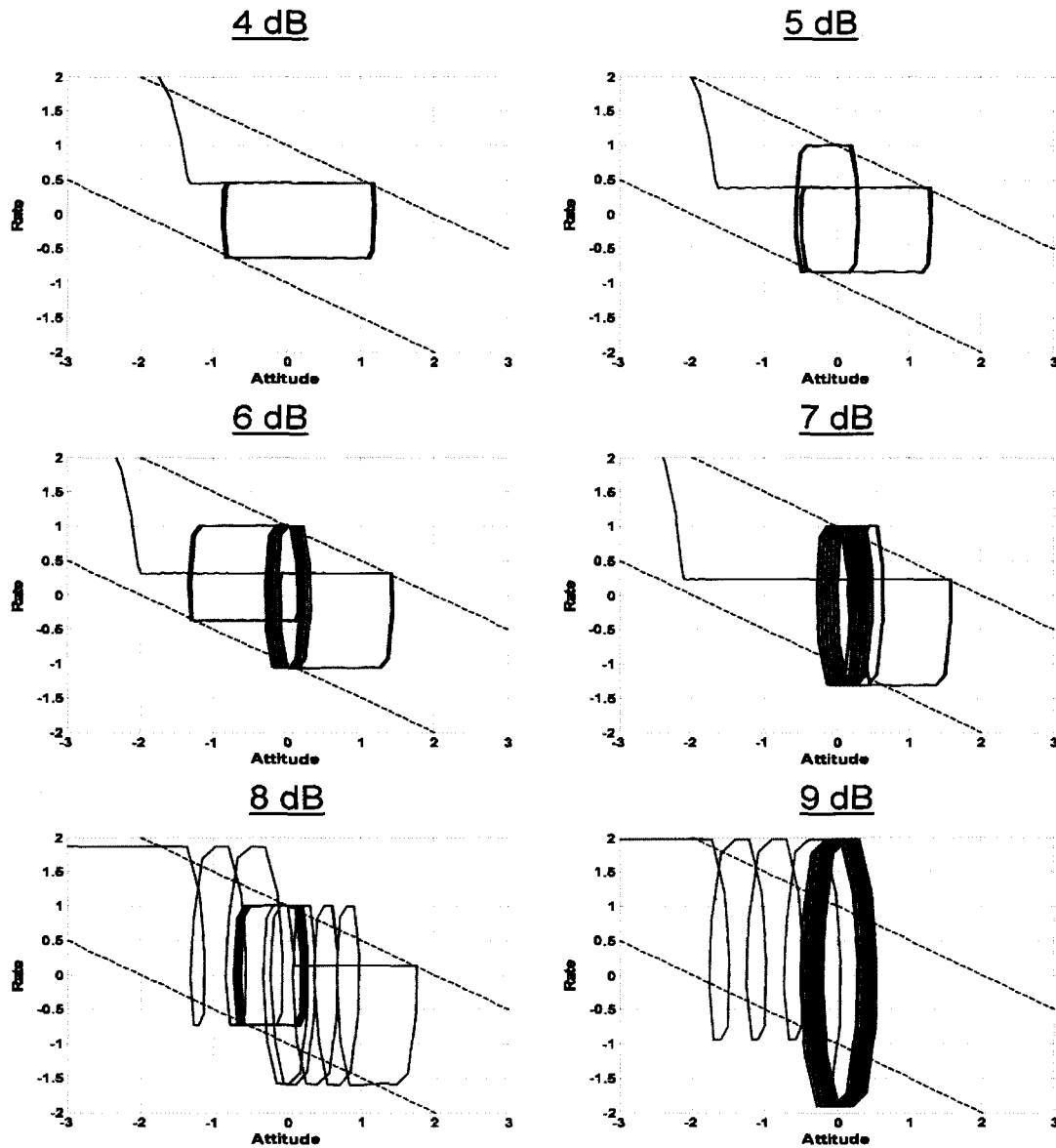


Figure 5.20: Phase Plane Plots with Gain Added ( $t = 120$  sec)

As more and more gain is introduced into the system, the phase plane response develops a primary and then secondary limit cycles. Referring back to Figure 5.17, it can be noticed that the system transitions to fully bang-bang behavior between 8 dB and 9 dB which agrees with the 8.3 dB gain margin determined from the energy plot.

The above analysis was performed for the entire first stage of flight; Table 5.6 below includes the gain margins at twenty second intervals which were gleaned from this process.

<b>Time [sec]</b>	<b>Gain Margin [dB]</b>
1	18.9
20	18.3
40	17.2
60	16.2
80	14.5
100	11.7
120	8.3

**Table 5.6: Simulation Results**

The results in Table 5.6 indicate that the system gradually decreases in stability as the time within the first stage progresses.

## 5.6 Method Comparison

Table 5.7 below summarizes all of the gain margins for the various analytical techniques and the simulation discussed in this chapter.

<b>Time [sec]</b>	<b>1</b>	<b>20</b>	<b>40</b>	<b>60</b>	<b>80</b>	<b>100</b>	<b>120</b>
PWM	17.5	17.0	16.2	15.1	13.5	10.7	7.7
Describing Function (Nichols)	15.4	14.9	14.1	13.0	11.4	8.6	5.6
Describing Function (Margin Tester)	15.4	14.9	14.1	13.0	11.4	8.6	5.6
Circle Criterion	14.1	13.5	12.6	11.6	9.9	6.9	3.7
Popov Criterion	17.0	16.4	15.6	14.6	13.0	10.2	7.2
Time Simulation	18.9	18.3	17.2	16.2	14.5	11.7	8.3

**Table 5.7: Gain Margin Comparison [dB]**

Comparing the analytical techniques such as PWM, describing functions, the circle criterion and the Popov criterion to the time domain simulation provides a method



for judging each analytical technique's effectiveness at predicting the gain margin for the system. PWM, describing functions, the circle criterion, and the Popov criterion are all conservative, but PWM and the Popov criterion are the least conservative of these methods for predicting nonlinear gain margins.

## **5.7 Analysis Conclusions**

After reviewing the gain margin results for analytical techniques such as PWM, describing functions, circle criterion, and the Popov criterion and comparing those to the time domain simulation results, certain conclusions can be drawn. PWM, describing functions, the circle criterion, and the Popov criterion all yielded conservative gain margin results, but PWM and the Popov criterion results were the least conservative. PWM does not fully model ideal relay; however, the Popov criterion can be utilized with most nonlinear elements.

## Chapter 6: Filter Design for a Phase Plane Control System

While the current filter resulted in stable gain margins of a spacecraft attitude control system, the filter was not designed to maximize fuel-consumption performance. The nonlinear control analysis techniques demonstrated in Chapter 5 are useful for determining the roll stability margins, but these methods can also be applied towards designing a better filter that is optimized for performance but still guarantees stability margins. The current elliptic filter was not optimized for the best performance by means of maximum bandwidth; therefore, new 6<sup>th</sup> order flex filters specifically designed to guarantee PWM and absolute stability while optimizing performance are created. Equation 6.1 shows the design concept for an optimized filter.

$$Flex\ Filter(s) = \prod_{i=0}^2 \frac{\frac{s^2}{\omega_{4i+1}^2} + \frac{2\zeta_{4i+1}s}{\omega_{4i+1}} + 1}{\frac{s^2}{\omega_{4i+2}^2} + \frac{2\zeta_{4i+2}s}{\omega_{4i+2}} + 1} \quad (6.1)$$

This chapter will detail the flex filter optimizations and then compare their performance to that of the current filter, thereby, demonstrating the optimized filters' improved performance over the current filter.

### 6.1 Flex Filter Optimization

The purpose of flex filter optimization is to maximize the performance of the system while ensuring that all constraints imposed by stability and flex margin requirements are still met. An approach similar to that followed by Jang, Hall and Bedrossian will be taken in this thesis [24]. A numerical optimization code is developed utilizing MATLAB's 'fmincon' function to perform a constrained minimization [30].

Before optimization is performed, it is necessary to design an initial filter to feed into the system. Ideally, any values could be selected and the optimization code would still work, but experience has shown that providing a good initial estimate improves the optimization's performance. The optimization is performed with the goal being to maximize the bandwidth of the system. This is accomplished by minimizing to following equation.

$$f = -\text{bandwidth}[G(s)] \quad (6.2)$$

This minimization is constrained by the need for the system to be Hurwitz, the frequencies and damping ratios must be positive, and the flex filter must achieve 30 dB of attenuation at frequencies within the stopband. The flex filter must possess 30 dB of high-frequency attenuation because the unfiltered system exhibits 16 dB of high-frequency gain as can be seen in Figure 6.1:

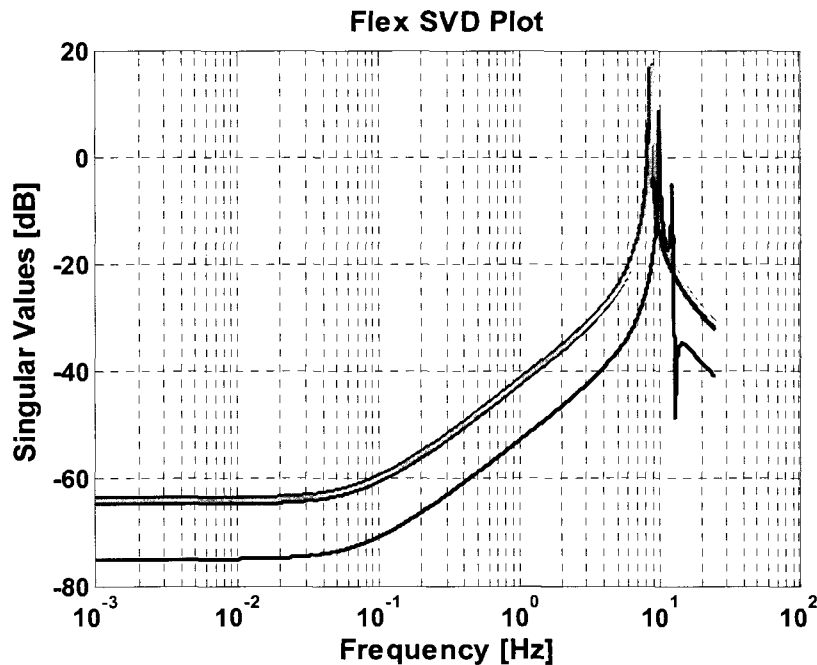


Figure 6.1: Unfiltered SVD Flex Response

The high-frequency flex dynamics must have 10 dB attenuation with 4 dB gain robustness added. The total from these three sources adds up to 30 dB high-frequency attenuation in the sop band. For stability, PWM, 6 dB can be guaranteed by simply using Bode or Nichols analysis to determine the linearly approximated system's gain margin. Additionally, absolute stability is guaranteed by ensuring that the system passes the circle criterion with 6 dB of gain margin at each time step. Once all the constraints have been outlined, it is now possible to perform the optimizations described above which can be seen in the proceeding sections.

## **6.2 PWM-Based Flex Filter**

A PWM-based filter will be designed to maximize bandwidth while ensuring system stability in terms of 6 dB rigid gain margin and 10 dB high-frequency flex dynamics attenuation. The requirements for the PWM-based filter are condensed and summed up in Figure 6.2.

$\text{minimize} \quad -\text{bandwidth}[F(s)]$   
 $\text{subject to}$

$ G(s)  \geq 6 \text{ dB}$	$\forall \angle G(s) = \pm 180 \text{ deg}$	Gain Margin
$ F(s)  < 0 \text{ dB}$	$\forall \omega < \omega_c$	Rigid Gain Stability
$ F(s)  < -30 \text{ dB}$	$\forall \omega > \omega_c$	Flex Gain Stability
$\omega_i > 0$	$i = 1, 2, 3, \dots$	Filter Stability
$\zeta_i > 0$	$i = 1, 2, 3, \dots$	

where  
 $F(s)$  = Flex Filter  
 $G(s)$  = Linear System Transfer Function  
 $\omega_c$  = Crossover Frequency (rad/sec)

Figure 6.2: Optimization Criteria (PWM Filter)

The 6<sup>th</sup> order PWM flex filter obtained from the above described optimization can be seen below in Figure 6.3.

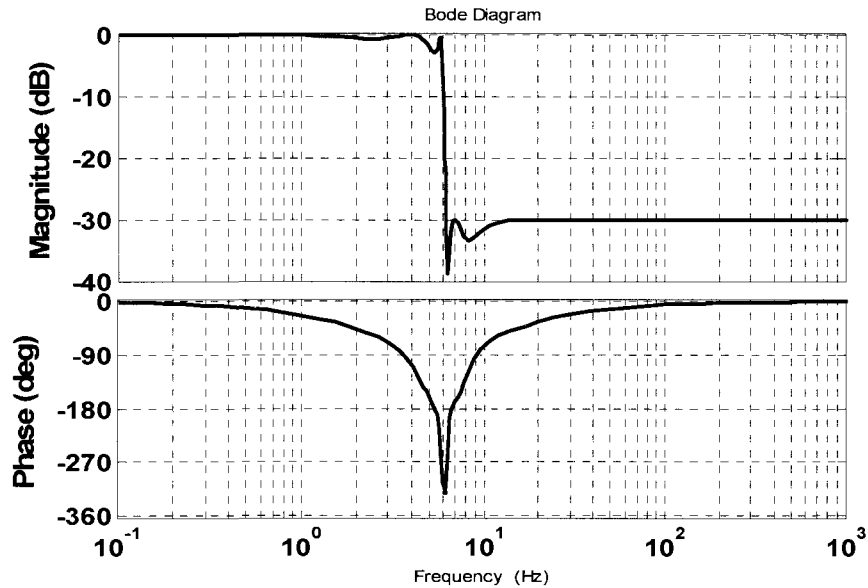


Figure 6.3: PWM Optimized Flex Filter

The above filter has a bandwidth of 5.37 Hz and it can be seen in the above figure that it possesses 30 dB of stopband attenuation. The following section will confirm the PWM filter's stability. PWM stability relies on two plots, the Nichols chart to check rigid and flex margins and the SVD plot to ensure the high-frequency flex dynamics are sufficiently attenuated. First, the Nichols chart can be observed in Figure 6.4:

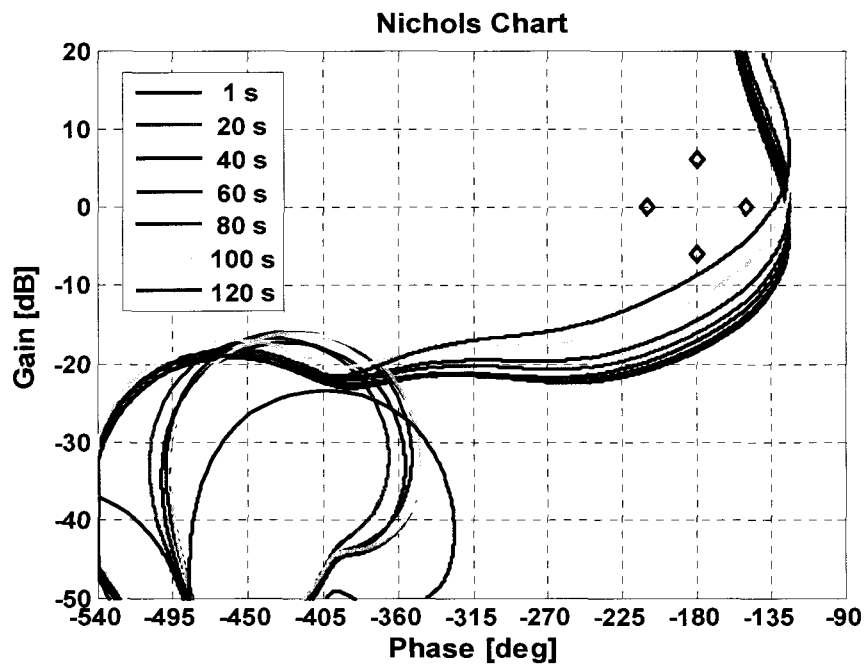


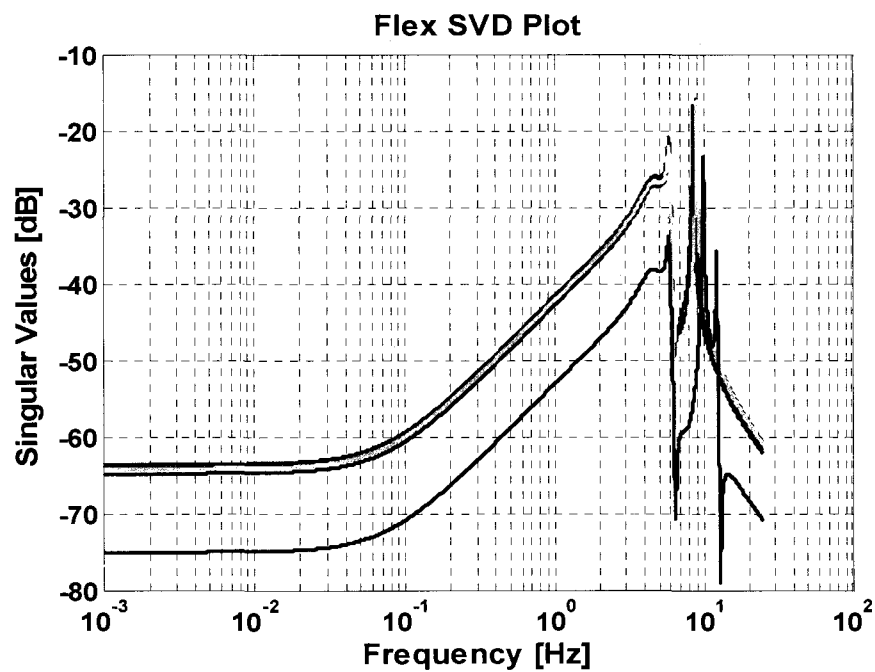
Figure 6.4: PWM Nichols Chart (PWM Filter)

Figure 6.4 demonstrates that the system with the optimized filter meets the 6 dB rigid dynamics gain margin requirement and also the 10 dB high-frequency flex dynamics margin. The PWM Nichols Chart results are summarized in Table 6.1.

Time [sec]	Gain Margin [dB]
1	18.4
20	17.8
40	17.0
60	16.0
80	14.4
100	11.6
120	8.6

**Table 6.1: Gain Margin Results (PWM Filter)**

The 10 dB margin for high-frequency flex dynamics is also confirmed in the SVD chart in Figure 6.5.



**Figure 6.5: Filtered SVD Response (PWM Filter)**

These two plots confirm the PWM-optimized filter meets the stability constraints set forth previously for the system. There is 6 dB rigid gain margin and more than 10 dB high-frequency flex attenuation.

### 6.3 Absolute Stability-Based Flex Filter

An absolute stability-based filter will also be designed to maximize bandwidth while ensuring system stability in terms of 6 dB rigid gain margin and 10 dB high-frequency flex dynamics attenuation. For the filter designed using absolute stability, gain margin can be guaranteed through the constraint.

$$\min Re[G_{tr}(s)] = \min Re \left[ \frac{G(s)}{1+k_\delta G(s)} \right] \geq 1 \quad (6.3)$$

The circle criterion is used for this calculation instead of the Popov criterion for several reasons. The first reason is that the circle criterion requires less computational resources than the Popov criterion due to the Popov criterion's use of 'fmincon'. An additional motive for using the circle criterion is that using a 'fmincon' function within another 'fmincon' function appears to create inaccuracies in the numerical optimization code and output. The requirements and design criteria are condensed in Figure 6.6:



$$\begin{array}{ll}
\text{minimize} & -\text{bandwidth}[F(s)] \\
\text{subject to} & \\
& \min \operatorname{Re}[G_{tr}(s)] \geq 1 \quad \forall \omega \quad \text{Absolute Stability} \\
& |F(s)| < 0 \text{ dB} \quad \forall \omega < \omega_c \quad \text{Rigid Gain Stability} \\
& |F(s)| < -30 \text{ dB} \quad \forall \omega > \omega_c \quad \text{Flex Gain Stability} \\
& \omega_i > 0 \quad i = 1, 2, 3, \dots \quad \text{Filter Stability} \\
& \zeta_i > 0 \quad i = 1, 2, 3, \dots
\end{array}$$

where

$F(s)$  = Flex Filter

$G(s)$  = Linear System Transfer Function

$$G_{tr}(s) = \frac{G(s)}{1 + k_\delta G(s)}$$

$k_\delta$  = Siljak Gain

$\omega_c$  = Crossover Frequency (rad/sec)

**Figure 6.6: Optimization Criteria (Absolute Stability Filter)**

Again, a 6<sup>th</sup> order flex filter was obtained through constrained minimization and the resulting figure can be seen below in Figure 6.7.

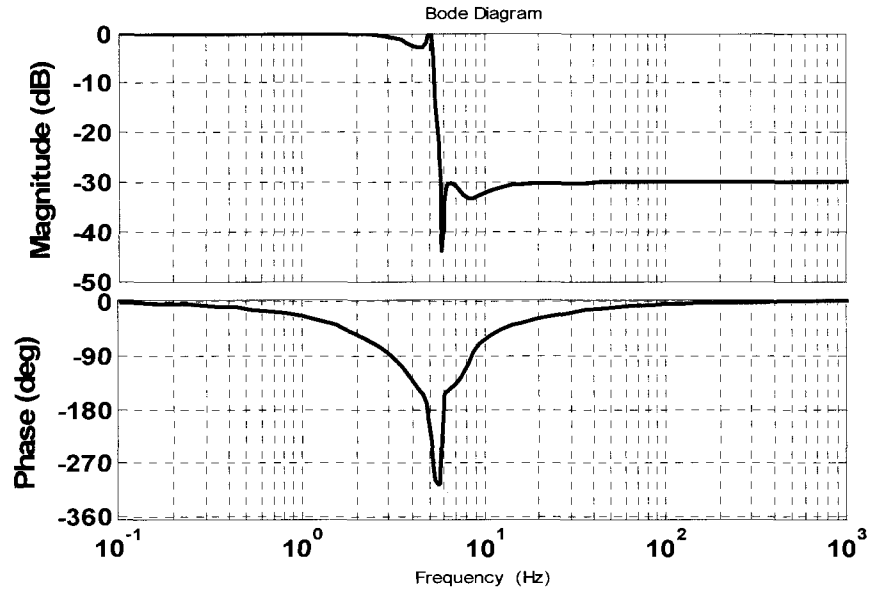


Figure 6.7: Absolute Stability Optimized Flex Filter

The absolute stability filter has a bandwidth of 5.17 Hz; furthermore, Figure 6.7 demonstrates that the filter successfully achieves 30 dB of stopband attenuation. The following sections will graphically optimize  $k_\delta$  and confirm the filter's stability.

### 6.3.1 Optimizing $k_\delta$ for the New Filter

It is now necessary to graphically optimize the values for  $k_\delta$  for the optimized flex filter. The values are selected on the basis of obtaining the maximum value for the upper sector limit,  $\beta$ . Below the circle criterion results can be seen:

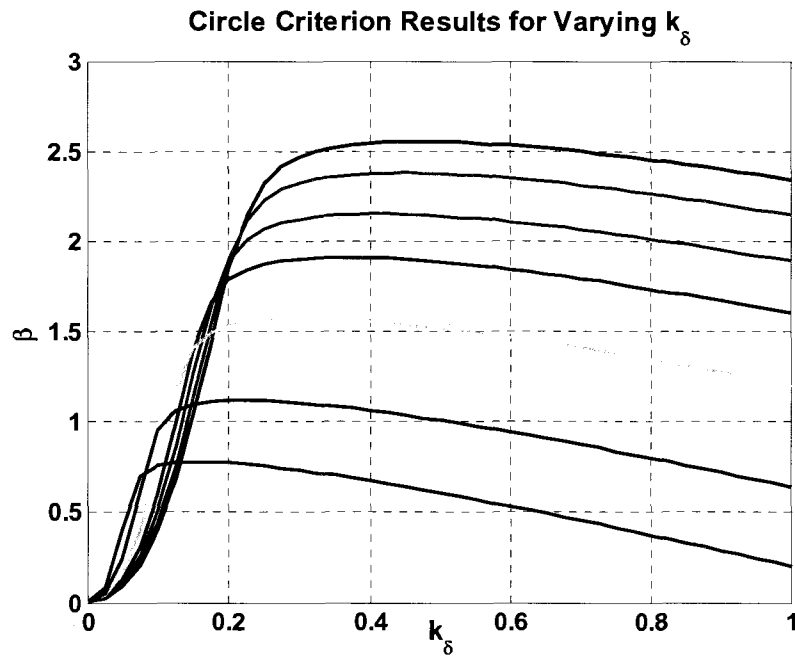


Figure 6.8: Circle Criterion  $k_\delta$  Graphical Optimization (Absolute Stability Filter)

The Popov results below provide less conservative  $\beta$  values:

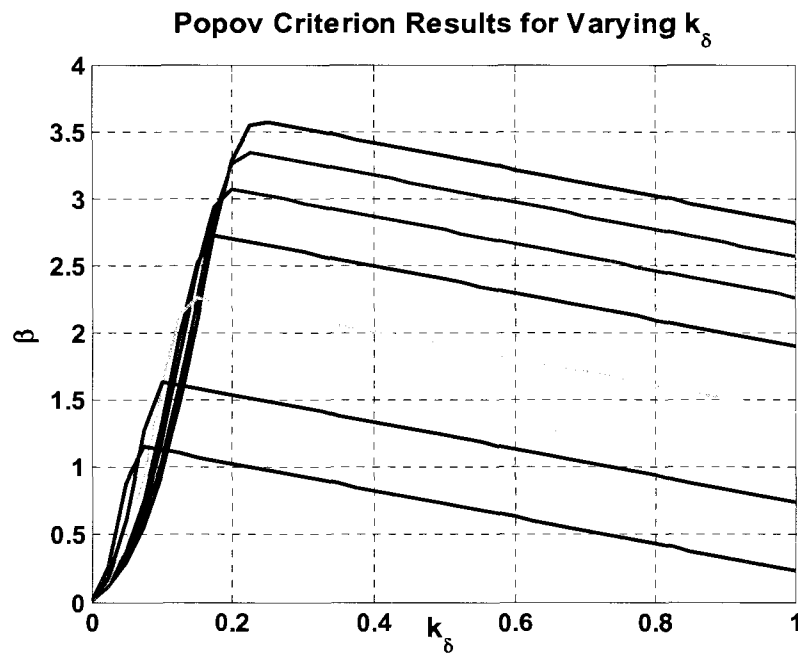


Figure 6.9: Popov Criterion  $k_\delta$  Graphical Optimization (Absolute Stability Filter)

The results from the two charts above are condensed in Table 6.2:

Time [sec]	$k_\delta$ Value		$\beta_{\max}$	
	Circle Criterion	Popov	Circle Criterion	Popov
1	0.475	0.250	2.5	3.6
20	0.450	0.225	2.4	3.3
40	0.400	0.200	2.1	3.1
60	0.350	0.175	1.9	2.7
80	0.300	0.150	1.6	2.3
100	0.225	0.100	1.1	1.6
120	0.150	0.075	0.8	1.2

**Table 6.2:  $k_\delta$  Graphical Optimization (Absolute Stability Filter)**

The table indicates that Popov criterion-based  $k_\delta$  values not only provide less conservative  $\beta$  values, they also lead to smaller  $k_\delta$  values which mean a larger finite domain of absolute stability.

### 6.3.2 Stability Confirmation

Confirming absolute stability is important for the optimized filter. Figure 6.10 displays the Popov plot showing the results for the optimized filter.

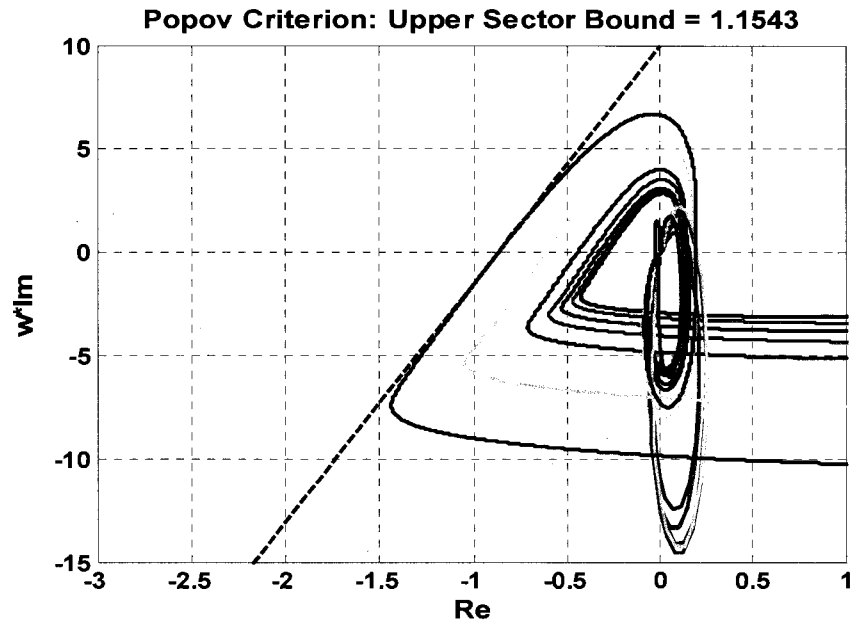


**Figure 6.10: Popov Criterion (Absolute Stability Filter)**

The Popov plot above shows the worst case scenario for Popov stability, and it can be seen for this instance the worst case upper sector limit,  $\beta = 1.1543$  which corresponds to 7.6 dB. The remainder of the gain margins can be seen below in Table 6.3.

Time [sec]	Gain Margin
	Popov Criterion [dB]
1	17.0
20	16.5
40	15.7
60	14.7
80	13.1
100	10.3
120	7.3

**Table 6.3: Gain Margin Results (Absolute Stability Filter)**

Table 6.3 above clearly shows that the absolute stability-based filter results in a fully stable system according to the Popov criterion. It is also critical to ensure the

absolute stability-based filter ensures 10 dB high-frequency flex dynamics attenuation as can be seen in Figure 6.11:

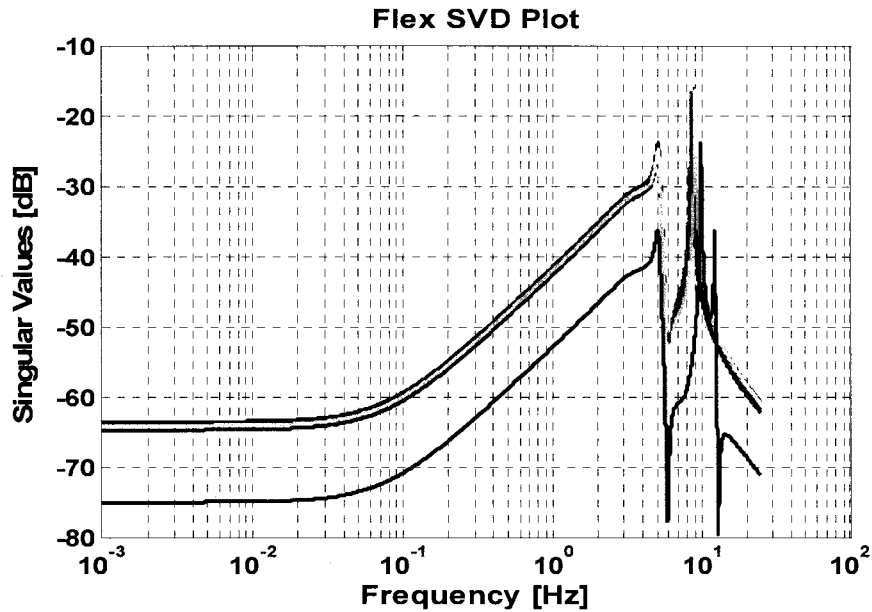


Figure 6.11: Filtered SVD Response (Absolute Stability Filter)

The SVD plot above indicates the absolute stability-based filter successfully attenuates the high-frequency flex dynamics 10 dB, thereby, fulfilling the design criteria.

## 6.4 Performance-Measuring Time Simulation

At this point it is necessary to compare the performance of the optimized filters to that of the GNC 6 filter which involves utilizing the Monte Carlo to generate random initial conditions for attitude error and rate error. Once these initial conditions have been generated, it is possible to perform simulations which record key performance metrics and then to evaluate those numbers statistically.

#### 6.4.1 The Monte Carlo Method

Monte Carlo analysis is the natural choice to probabilistically determine flex filter performance [31]. Monte Carlo is “a numerical method of solving mathematical problems by the simulation of random variables” [32]. The first critical step in generating random values of a particular distribution is to generate a random number  $n$  in the open interval  $(0, 1)$ . Computational methods cannot generate truly random numbers, so “random” numbers generated by a computer, as will be used in this paper, are actually called “pseudo-random” numbers [33]. Using MATLAB to compute  $n$  of a desired size, it is now possible to generate uniformly distributed numbers in the interval  $(a, b)$  with the expression:

$$u = a + (b - a)n \quad (6.4)$$

Sample size is an important issue when performing Monte Carlo simulations. This is because “the larger the number of the simulated records is, the smaller the expected deviation of the obtained numerical values from the theoretical values of the response statistics should be” [34]. Based on Dr. Roberts and Dr. Spanos’s recommendations, distributions with 3,000 samples were generated in this paper [34].

#### 6.4.2 Random Initial Condition Generation

As mentioned above, uniformly distributed initial attitude and rate errors must be generated; furthermore, to ensure an accurate simulation, three thousand random samples will be generated for each variable. First, a random uniform distribution for attitude error

will be generated. It can be seen below in Figure 6.12 that initial attitude errors range from  $\pm 1$  degree.

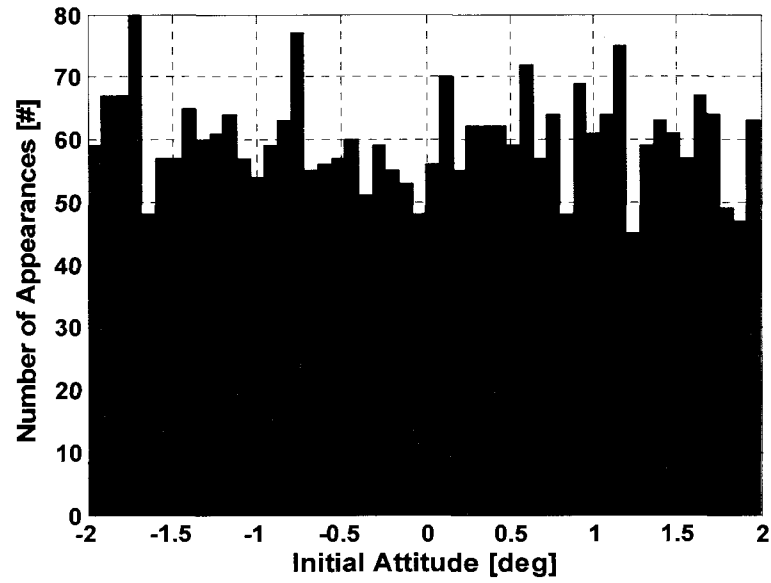


Figure 6.12: Uniformly Distributed Initial Attitude Error

In Figure 6.13, the probability distribution for the initial rate error can be observed.



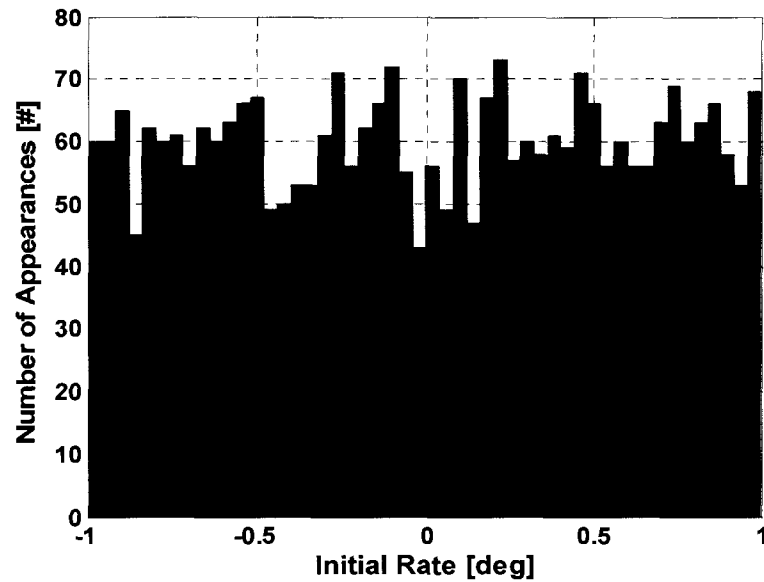
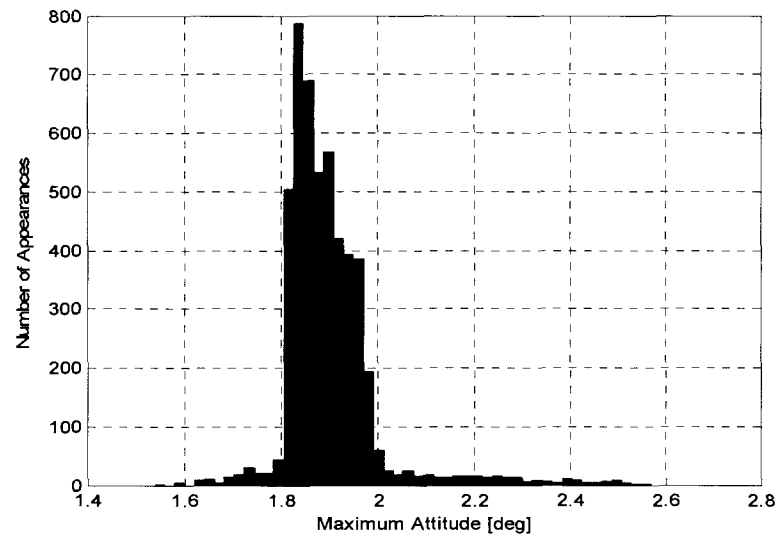


Figure 6.13: Uniformly Distributed Initial Rate Error

### 6.4.3 Performance Results

The distributions generated above were used for both current filter and optimized filter simulations. The SIMULINK model from Figure 5.15 was again used for simulation; however, a 5000 ft-lbf disturbance torque was introduced at  $t = 20$  seconds. With regards to performance, there are two main criteria by which both filters: maximum attitude and number of on-times. The maximum attitude distribution for the current filter can be seen in Figure 6.14:



**Figure 6.14: Maximum Attitude Distribution (Current Filter)**

Figure 6.14 demonstrates the maximum attitude distribution with mean equal to 1.9 degrees and standard deviation equal to 0.1 degrees. Figure 6.15 includes the distribution for the PWM stability filter.

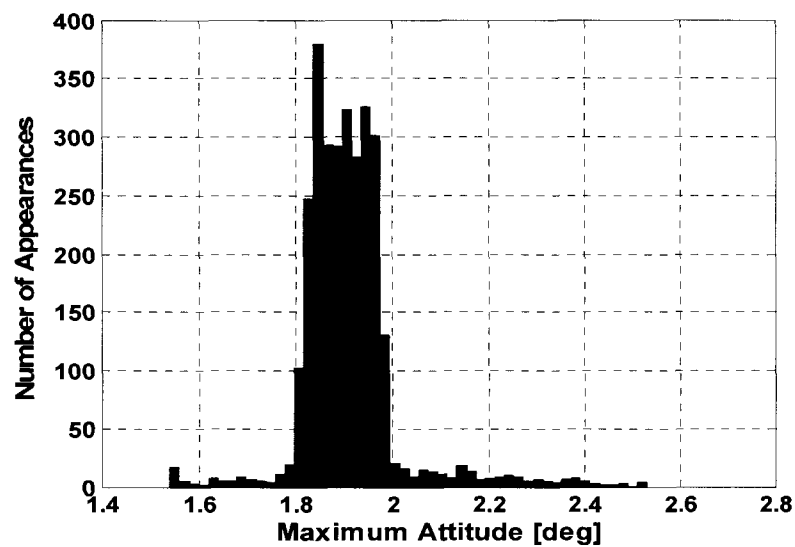


**Figure 6.15: Maximum Attitude Distribution (PWM Filter)**

For the PWM-based filter, the mean maximum attitude distribution is 1.9 degrees while the standard deviation is 0.1 degrees. This is somewhat larger maximum attitude than the current filter, but not significantly so. Figure 6.16 below illustrates the results for the absolute stability filter.

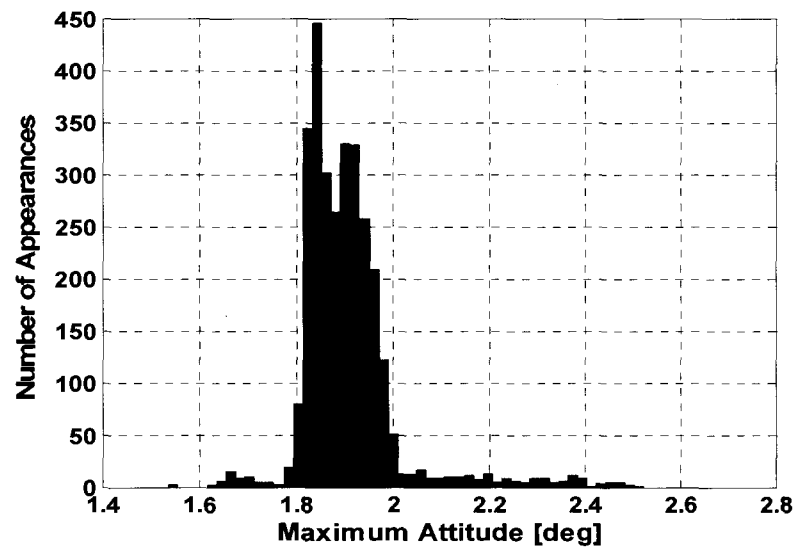
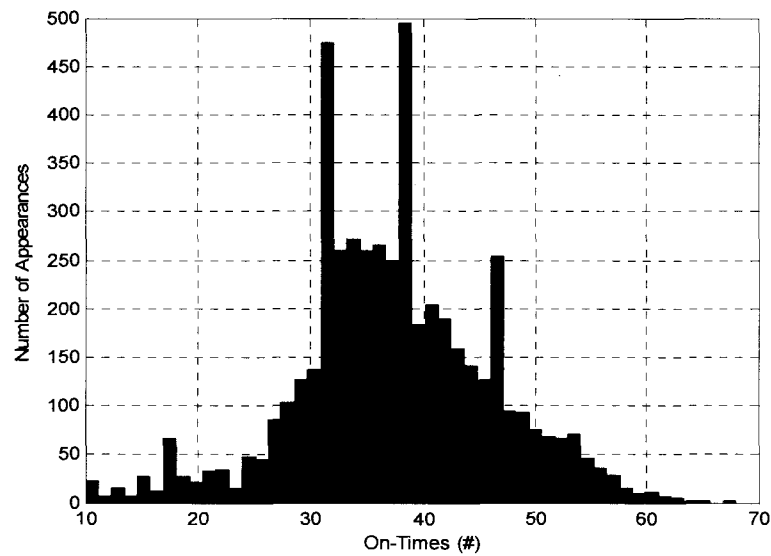


Figure 6.16: Maximum Attitude Distribution (Absolute Stability Filter)

For the optimized filter, the mean maximum attitude is equal to 1.9 degrees and standard deviation of 0.1 degrees. Next, the number of on-times will be examined for both the current filter and the optimized filter. The number of on-times distribution for the current filter is shown in Figure 6.17:



**Figure 6.17: Number of On-Times Distribution (Current Filter)**

It can be seen in Figure 6.17 that the number of on-times for the current filter has a mean equal to 37.4 times and standard deviation equal to 8.6 times. Figure 6.18 includes the distribution for the PWM filter.

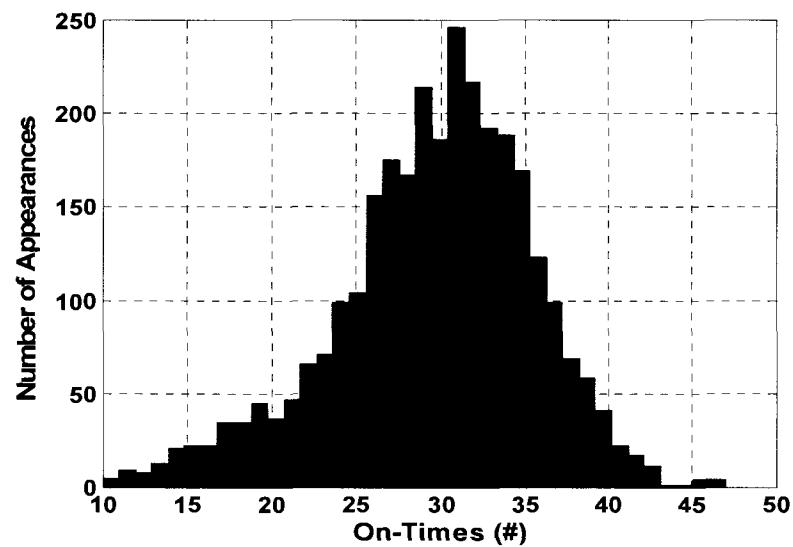


**Figure 6.18: Number of On-Times Distribution (PWM Filter)**

The PWM filter results indicate that the mean number of on-times is 29.6 times which is the smallest value out of any of the filters; furthermore, the standard deviation for the on-times is 6.1 times. The results for the absolute stability-based filter can be observed in Figure 6.19:

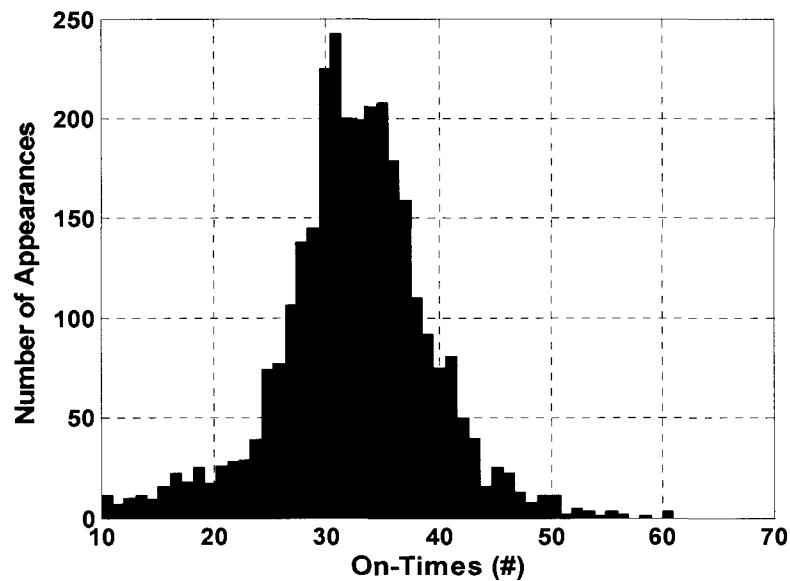


Figure 6.19: Number of On-Times Distribution (Absolute Stability Filter)

For the above distribution, the mean number of on-times is equal to 32.6 times and a standard deviation equal to 6.7 times. Table 6.4 summarizes the results of the Monte Carlo analysis.

	Maximum Attitude [deg]			# of On-Times		
	Current Filter	PWM Filter	Absolute Stability Filter	Current Filter	PWM Filter	Absolute Stability Filter
Mean	1.9	1.9	1.9	37.4	29.6	32.6
Standard Deviation	0.1	0.1	0.1	8.6	6.1	6.7

Table 6.4: Statistical Performance Comparison

The optimized filters have a significantly lower number of on-times which is a function of their improved bandwidth. This propellant performance increase does not come at a decrease in maximum attitude performance, thereby, creating an overall improvement in system performance.

## **6.5 Performance Conclusions**

Two optimized 6<sup>th</sup> order filters were designed to maximize performance with regards to propellant consumption. The filters were optimized to maximize bandwidth in order to acquire the greatest level of performance for the phase plane controller. This optimization included constraints requiring the system to have 30 dB attenuation in the stopband, 0 dB gain in the passband, 6 dB gain margin for the rigid dynamics, and 10 dB attenuation of high-frequency flex dynamics. These constraints were shown to have been met through PWM and Popov criterion analysis. Finally, Monte Carlo simulation was utilized to demonstrate the two optimized filters' improved performance over the current filter which could be seen in the new filters' reduced number of on-times. The PWM-based filter resulted in a smaller number of on-times than the absolute stability-based filter. This result is likely due to PWM being a less conservative analysis technique than absolute stability.

## Chapter 7: Closure

The phase plane controller offers an idealized method for optimizing time and fuel performance while ensuring stability and attitude tracking. As seen in Chapter 5, the phase plane controller becomes unstable when it no longer functions with a dead zone drift; more specifically, the phase plane controller behaves like a ‘bang-bang’ controller. This behavior consumes an unacceptable amount of propellant while leading to high rate errors which can cause structural damage or guidance failure.

Nonlinear control techniques such as PWM, describing functions, the circle criterion, and the Popov criterion all offer methods for determining not only the stability of a system but also how much gain robustness the system contains. The nonlinear techniques discussed above all resulted in conservative gain margins, but PWM proved to be the least conservative. It must be noted, however, that PWM does not model the ideal relay nonlinearity which is an important part of the phase plane controller. The Popov criterion combined with Siljak’s loop transformation accounts for both the dead zone and ideal relay nonlinearities and the gain margin yielded from the criterion is the second most conservative. This necessitates the conclusion that both PWM and the Popov criterion should be utilized in predicting a system’s gain margin. The PWM is less conservative and allows the designer to consider both rigid and flex dynamics while the Popov criterion fully accounts for any type of nonlinearity that may fit into the sector bounds. This attribute makes the Popov criterion more universally applicable while the PWM is more closely tailored to roll control system.

The nonlinear analysis techniques discussed above can also be used to design optimized filters with improved performance over the current filter. In Chapter 6, two 6<sup>th</sup> order filters were designed to maximize bandwidth while ensuring adequate stability. The first filter used PWM analysis to ensure stability while the second filter used absolute stability to define the stability constraints. The primary constraints for the filter design were 30 dB attenuation in the stopband, 0 dB gain in the passband, 6 dB gain margin for the rigid dynamics, and 10 dB attenuation of high-frequency flex dynamics. Monte Carlo simulation verified the optimized filters' improved performance over the current filter which could be seen in their reduced number of on-times while the maximum attitude performance metric showed no significant increase in value. The PWM-based filter resulted in a smaller number of on-times than the absolute stability-based filter though it possessed a worse maximum attitude distribution. Both techniques created filters that utilized nonlinear control gain margins while ensuring maximized performance.

With regards to future research into nonlinear analysis techniques for the phase plane controller, several avenues are particularly interesting in the area of absolute stability-based control. These developments include time-varying stability, necessary and sufficient conditions for absolute stability, and robust absolute stability.

Molchanov and Liu developed a technique which effectively determines a nonlinear discrete-time system's robustness towards the parametric uncertainty, which develops in a time-varying system such as aerospace systems [35]. The method's primary drawback is that it is necessary to confirm that the system's  $A$  matrix at each time step belongs to a convex set [35].



In Chapter 4 it was noted that absolute stability being derived from Lyapunov's second method is a sufficient condition for asymptotic stability. G. A. Leonov has developed a method for guaranteeing absolute stability for two-dimensional time-varying systems [36]. Leonov accomplishes this task by "the method of comparison systems" in which regions of attraction in the phase plane are computed [36]. The technique developed would be based on a necessary condition; thereby, it would be less conservative than the strictly sufficient condition based absolute stability criterions. The method also has the added advantage of being time-varying which would allow for more accurate modeling of aerospace systems.

There have been several cases where researchers such as Tsytkin, Polyak, Impram, Munro, Yang, Duan, and Huang have explored robust, absolute stability [37] [38] [39]. Tsytkin and Polyak utilized the circle criterion and the Popov criterion where the linear subsystem is subjected to a  $H_\infty$  norm-bound multiplicative or additive perturbation while Impram and Munro approach absolute stability with both "structured and unstructured" perturbations in the linear subsystem [37] [38]. Finally, Yang, Duan, and Huang apply a " $H_\infty$  sub-optimal controller by using a loop transformation" and solving a linear matrix inequality (LMI) to guarantee robust, absolute stability for a system [39].

Implementing a time-varying solution through Molchanov and Liu's discrete-time method or through Leonov's necessary conditions would result in a higher fidelity solution than what is currently offered by the methods detailed in this thesis. Furthermore, the application of robust perturbations could ensure that a phase plane

controlled system would have a fully trustworthy stability envelope which would greatly increase its reliability.

## Bibliography

- [1] Penchuk, A., P. Hattis, and E. Kubiak, "A Frequency Domain Stability Analysis of a Phase Plane Control System," *Journal of Guidance*, Vol. 8, No. 1, 1984.
- [2] Hall, R., Barrington, R., K. Kirchwey, A. Alaniz, and K. Grigoriadis, "Shuttle Stability and Control During the Orbiter Repair Maneuver," *AIAA Guidance, Navigation, and Control Conference and Exhibit*, San Francisco, CA, August 2005, AIAA 2005-5852.
- [3] Bedrossian, N., J. Jang, A. Alaniz, M. Johnson, K. Sebelius, and Y. Mesfin, "International Space Station US GN&C Attitude Hold Controller Design for Orbiter Repair Maneuver," *AIAA GNC Conference*, Monterrey, CA, 2005.
- [4] Elgersma, M., G. Stein, M. Jackson, R. Matulenko, and B. Caldwell, "Space Station Attitude Control Using Reaction Control Jets," *Proceedings of the 31st Conference on Decision and Control*, Tucson, AZ, 1992.
- [5] Siljak D. and S. M. Setzer, "Absolute Stability Analysis of Attitude Control Systems for Large Boosters," *Journal of Spacecraft and Rockets*, Vol. 9, No. 7, July 1972.
- [6] Greensite, A., *Analysis and Design of Space Vehicle Flight Control Systems*, United States: Spartan Books, 1970.
- [7] Jang, J., Van Tassell, C., and Bedrossian, N., "Evaluation of Ares-I Control System Robustness to Uncertain Aerodynamics and Flex Dynamics," *AIAA GN&C Conference*, Honolulu, HI, 2008, AIAA-2008-6621.

- [8] Frosch, James A., and Donald P. Vallely, "Saturn AS-501/S-IC Flight Control System Design," *Journal of Spacecraft*, Vol. 4, No. 8, August 1967.
- [9] Wertz, J., *Spacecraft Attitude Determination and Control*, Boston, MS: D. Reidel Publishing Company, 1995.
- [10] Slotine, J. and W. Li, *Applied Nonlinear Control*, Upper Saddle River, NJ: Prentice-Hall, Inc., 1969.
- [11] Martin, E., Evangelos Papadopoulos, Jorge Angeles, "A Novel Approach to Reduce Dynamic Interactions in Space Robots," IASTED Conference, Santa Barbara, CA, 1999.
- [12] Ogata, Katsuhiko, *Discrete-Time Control Systems*, Englewood Cliffs, NJ: Prentice-Hall, Inc., 1995.
- [13] Trefethen, L., and D. Bau II, *Numerical Linear Algebra*, Philadelphia, PA: Society for Industrial and Applied Mathematics, 1997.
- [14] Leon, S., *Linear Algebra with Applications*, Second Edition, New York, NY: Macmillan Publishing Company, 1986.
- [15] Zames, G., "On the Input-Output Stability of Time-Varying Nonlinear Feedback Systems Part I and II," *IEEE Transactions on Automatic Control*, Vol. AC-11, No. 2-3, April-July 1966.
- [16] Gelb, A., and W. Vander Velde, *Multiple-Input Describing Functions and Nonlinear System Design*, New York, NY: McGraw-Hill Book Co., 1968.
- [17] Lim, S., R. Pileggi, and G. Barton, "MIMO Adaptive Bank-to-Steer Control Algorithms for Guided Reentry Vehicles," *The Draper Technology Digest*, Vol. 12, 2008, CSDL-R-3010.

- [18] Siljak, D., *Nonlinear Systems: The Parameter Analysis and Design*, New York, NY: John Wiley and Sons, Inc., 1969.
- [19] Wu, B. and J. Perng, "Gain-Phase Margin Analysis of Pilot-Induced Oscillations for Limit-Cycle Prediction," *Journal of Guidance, Control, and Dynamics*, Vol. 15, No. 4, July-August 1992.
- [20] Popov, V.M., "Absolute Stability of Nonlinear Systems of Automatic Control," *Automation and Remote Control*, 22, 1961.
- [21] Aizerman M. A., and F. R. Gantmacher, *Absolute Stability of Regulator Systems*. San Francisco, CA: Holden-Day, 1964.
- [22] Vidyasagar, M., *Nonlinear Systems Analysis, 2nd Edition*, Englewood Cliffs, NJ: Prentice-Hall, Inc., 2002.
- [23] Khalil, H., *Nonlinear Systems, 3rd Edition*, Upper Saddle River, NJ: Prentice-Hall, Inc., 2001.
- [24] Jang, J., Hall, R., and Bedrossian, N., "Ares-I Bending Filter Design Using a Constrained Optimization Approach," AIAA GN&C Conference, Honolulu, HI, 2008, AIAA-2008-6289.
- [25] Dobra, P., and M. Trusca, "Analysis of Stability Nonlinear Systems with Varying Parameters using the Popov Criterion," *Proceedings of the 2006 IEEE Conference on Computer Aided Control Systems Design*, Munich, Germany, 2006.
- [26] Chapellat, H., and S. P. Bhattacharyya, "A Generalization of Kharitonov's Theorem: Robust Stability of Interval Plants," *IEEE Transactions on Automatic Control*, Vol. 34, No. 3, March 1989.

- [27] Oppenheim, A., and R. Schaffer, *Digital Signal Processing*, Englewood Cliffs, NJ: Prentice-Hall, Inc., 1975.
- [28] The Math Works, Inc., *Signal Processing Toolbox*, Natick, MA: The Math Works, Inc., 2000.
- [29] The Math Works, Inc., *SIMULINK Dynamic System Simulation for MATLAB Modeling, Simulation, Implementation*, Natick, MA: The Math Works, Inc., 2007.
- [30] The Math Works, Inc., *Optimization Toolbox*, Natick, MA: The Math Works, Inc., 1999.
- [31] Spanos, P. and B. Zeldin, "Monte Carlo treatment of random fields: A broad perspective," *Applied Mechanics Reviews*, Vol. 51, No. 3, March 1988, pp 219-237.
- [32] Sobol', Ilya M., *A Primer for the Monte Carlo Method*, Boca Raton, FL: CRC Press, 1994.
- [33] Elishakoff, I., *Probabilistic Theory of Structures*, Second Edition, Mineola, NY: Dover Publications, Inc., 1999.
- [34] Roberts, J. and Spanos, P., *Random Vibration and Statistical Linearization*, Mineola, NY: Dover Publications, Inc., 1999.
- [35] Molchanov, A., and D. Liu, "Robust Absolute Stability of Time-Varying Nonlinear Discrete-Time Systems," *IEEE Transactions on Circuits and Systems-I: Fundamental Theory and Applications*, Vol. 49, No. 8, August 2002.

[36] Leonov, G. A., "Necessary and Sufficient Conditions for the Absolute Stability of Two-Dimensional Time-Varying Systems," Automation and Remote Control, Vol. 66, No. 7, 2005.

[37] Tsypkin, Y. Z., and B. T. Polyak, "Robust Absolute Stability of Continuous Systems," International Journal of Robust and Nonlinear Control, Vol. 3, 231-239, 1993.

[38] Impram, S., and N. Munro, "A note on absolute stability of uncertain systems," Automatica, 37, 2001.

[39] Yang, Y., Z. Duan, and L. Huang, "Absolute Stabilization Based on Circle Criterion:  $H_\infty$  and LMI Approach," 2004 5th Asian Control Conference, Melbourne, Australia, July 2004.